Engineering

Journal of Research

of the

U.S. National Bureau of Standards

MAY 1954

VOLUME 52 NUMBER 5

U. S. DEPARTMENT OF COMMERCE
Sinclair Weeks, Secretary
NATIONAL BUREAU OF STANDARDS
A. V. Astin, Director

MAY • 1954
VOLUME • 52
NUMBER • 5

JOURNAL OF RESEARCH

of the

NATIONAL BUREAU OF STANDARDS

PERIODICALS OF THE NATIONAL BUREAU OF STANDARDS

The National Bureau of Standards is engaged in fundamental and applied research in physics, chemistry, mathematics, and engineering. Projects are conducted in thirteen fields: electricity, optics and metrology, heat and power, atomic and radiation physics, chemistry, mechanics, organic and fibrous materials, metallurgy, mineral products, building technology, applied mathematics, electronics, and radio propagation. The Bureau has custody of the national standards of measurement and conducts research leading to the improvement of scientific and engineering standards and of techniques and methods of measurement. Testing methods and instruments are developed; physical constants and properties of materials are determined; and technical processes are investigated.

JOURNAL OF RESEARCH

Internationally known as a leading scientific periodical, the Journal presents research papers by authorities in the specialized fields of physics, mathematics, chemistry, and engineering. Complete details of the work are presented, including laboratory data, experimental procedures, and theoretical and mathematical analyses. Annual subscription: domestic, $5.50; foreign, $6.75.

TECHNICAL NEWS BULLETIN

Summaries of current research at the National Bureau of Standards are published each month in the Technical News Bulletin. The articles are brief, with emphasis on the results of research, chosen on the basis of their scientific or technologic importance. Lists of all Bureau publications during the preceding month are given, including Research Papers, Handbooks, Applied Mathematics Series, Building Materials and Structures Reports, Miscellaneous Publications, and Circulars. Each issue contains 12 or more two-column pages; illustrated. Annual subscription: domestic, $1.00; foreign, $1.35.

BASIC RADIO PROPAGATION PREDICTIONS

The Predictions provide the information necessary for calculating the best frequencies for communication between any two points in the world at any time during the given month. The data are important to all users of long-range radio communications and navigation, including broadcasting, airline, steamship, and wireless services, as well as to investigators of radio propagation and ionosphere. Each issue, covering a period of one month, is released three months in advance and contains 16 large pages, including pertinent charts, drawings, and tables. Annual subscription: domestic, $1.00; foreign, $1.25.

Order all publications from the Superintendent of Documents
U. S. Government Printing Office, Washington 25, D. C.

The printing of this publication has been approved by the Director of the Bureau of the Budget, May 12, 1953.

Journal of Research of the National Bureau of Standards Vol. 52, No. 5, May 1954 Research Paper 2493

A Cryoscopic Study of the Solubility of Uranium in Liquid Sodium at 97.8° C

Thomas B. Douglas

The equilibrium temperatures, at various stages of melting, of three samples of sodium were measured with a standard deviation of 0.001 degree. One sample contained uranium in compact form, and one contained finely divided uranium. Impurities lowered the freezing points of all the samples by approximately 0.035 degree, but the sodium containing finely divided uranium was found to have a freezing point higher than those of the other two samples by 0.005 degree, an effect that may be due to a partial purification of the sodium by the uranium. After extrapolation to no impurity, the freezing points of the three samples agree within 0.001 degree. Allowing for errors, it is concluded that the solubility of uranium in liquid sodium at 97.8° C probably does not exceed 0.05 percent by weight and may actually be many times smaller.

1. Introduction

One of the most sensitive and convenient methods commonly used to estimate the concentration of a dilute solution is the comparison of its liquidus temperatures (freezing points) with that of the pure solvent, if the solid phases are immiscible. This method was applied in an attempt to estimate the solubility of uranium in liquid sodium at 97.8° C, the triple point of the latter element. The equilibrium temperatures at intervals from 70- to 100-percent completion of fusion of the sodium were observed.

2. Experimental Procedure

Three samples were prepared, each containing 6½ g of sodium from a batch that had been purified by distillation. In addition to the sodium, the sample designated as A contained no uranium, sample B contained 2 g of a solid section of uranium, and sample C contained 2 g of finely divided uranium prepared by hydride decomposition. The samples were sealed, by induction welding in an oxygen-free inert atmosphere, in small cylinders of stainless steel type 347. Subsequent tests at room temperature and at 150° C indicated leakage through the seals to be no greater than 4×10^{-12} cm³ of helium per second, a rate not taken to indicate a real leak.

The apparatus for the cryoscopic measurements is shown in figure 1. Each sample was suspended by a No. 32 nichrome wire in air inside a vertical furnace, whose core maintained a highly uniform environmental temperature because it was surrounded by a silver pipe 10 in. long and of ½-in. wall thickness. The temperature of the silver was measured by a platinum resistance thermometer whose ice point remained constant to within an amount equivalent to ±0.0005 deg throughout the measurements. Heat was supplied to the sample at will by a constantan heater imbedded in a gold-plated copper jacket that surrounded the sample container at an average distance of 0.002 in. A four-junction differential thermocouple (chromel P versus constantan), calibrated in place against freezing sodium, enabled precise measurement of the temperature difference between the silver pipe of the furnace and the sample.

A detailed systematic procedure was followed in an effort to make the systematic errors constant and thereby to secure accurate differences in temperature among the three samples. With the individual runs numbered chronologically, runs 1, 5, and 9 were on sample A; runs 2, 3, and 4 were on sample C; and runs 6, 7, and 8 were on sample B. Run 10 was on a fourth sample of sodium, taken from a different batch prepared 2 years earlier. Each run was made on a different day.

With the sample in place, the furnace was heated to a temperature at which melting of the sodium would just begin, and was then held at approximately this temperature for the next 3 hr. The sample was then heated for separated intervals of time until fusion was clearly complete. Thus at any stage of the fusion process the fraction of the total fusion heat that had entered the sample could be taken as a measure of the fraction of the sodium then present as liquid. After each such interval of heating, the equilibrium temperature was measured in the following way. The temperature of the furnace was held constant (within ±0.0005 deg) at a temperature no more than 0.003 deg higher or lower than the prevailing sample equilibrium temperature,[1] until the thermocouple reading appeared to be changing by less than 0.0001 deg/min. This furnace control was accomplished by means of a 0.7-w variable auxiliary heater inside the silver. When the sodium was all crystalline or all molten, the difference between its temperature and that of the furnace decreased by 15 percent per minute owing to heat conduction through the intervening air spaces. However, during melting the error introduced in this way was negligible because of the large magnitude of the heat of fusion and the ease of maintaining then a small temperature difference.

To each equilibrium temperature found was added 0.012 deg, as the thermocouple reading was found to approach −0.012 deg when the temperatures of its junctions were known to be rapidly approaching

[1] Reversal of the sign of this temperature difference was used to prove that the thermocouple read the unbiased relative temperature of the sample.

290819—54——1

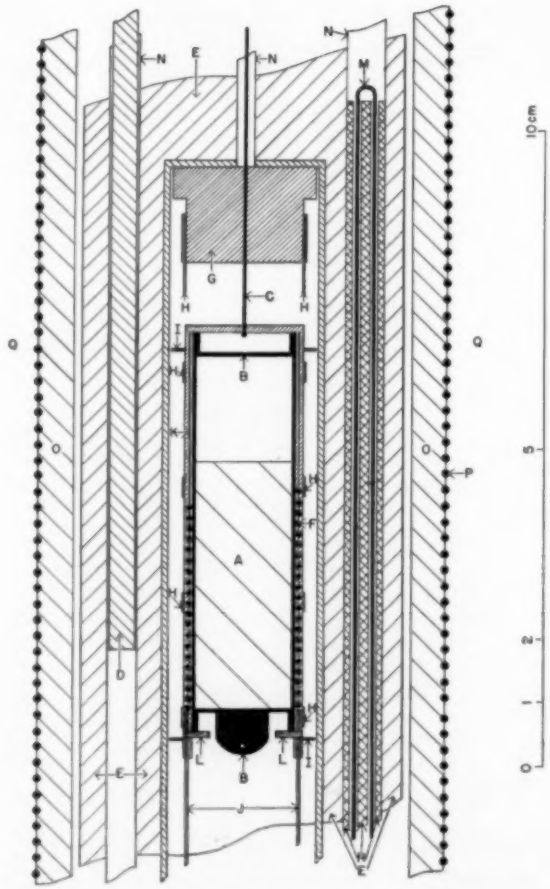

FIGURE 1. *Apparatus for cryoscopic measurements.*

A, Sodium sample (with or without uranium); B, sealed container for sample (stainless steel type 347); C, suspension wire (Nichrome V); D, platinum resistance thermometer; E, isothermal jacket (silver); F, heater for sample (glass-covered constantan); G, thermocouple reference block (gold-plated copper); H, thermocouple junctions (copper bands or tabs); I, spacers (nichrome V wire); J, heater leads (copper); K, jacket for sample container and heater cover (gold-plated copper); L, pins for supporting sample container; M, auxiliary heater for silver jacket (platinum); N, Inconel tubing; O, alundum tube; P, main furnace heater (platinum); Q, furnace insulation (silica powder); R, porcelain tube.

equality. In addition, 0.003 deg also was added to correct for the error due to the estimated azimuthal temperature gradient in the silver pipe.

3. Results and Conclusions

The variation of temperature as the impure sodium melts may be predicted from Raoult's law. For very small proportions of impurities entirely insoluble in the solid solvent (sodium), this law may be written in the approximate form

$$t=t_0-(RT_0^2/L_f)(x_1+x_2). \qquad (1)$$

In this equation the total mole fraction of all solutes in solution in the liquid sodium has been divided into two parts. x_1 designates that part due to solute that, if present at all, is sufficient in amount to maintain the liquid sodium saturated with it. (This solute will be assumed to be uranium only.) x_2 designates that part due to any solute at all times entirely in solution in whatever liquid sodium is present; t is the equilibrium temperature (in deg C); t_0 is the freezing (triple) point of pure sodium (also in deg C, the corresponding value in deg K being T_0); R is the gas constant; and L_f is the molal heat of fusion of sodium.

It is evident that as fusion of the sodium progresses, the increasing amount of liquid available as solvent leads to a decrease of x_2 but not of x_1. x_2 may be replaced by its equivalent, x_2'/f, where f is the fraction of the sodium present as liquid when the temperature is t, and x_2' is then the value of x_2 when f is unity. Equation (1) then becomes

$$t=t_0-RT_0^2x_1/L_f-(RT_0^2x_2'/L_f)(1/f). \qquad (2)$$

Substituting numerical values for the known constants (R=8.314 j mole^{-1} deg K^{-1}, T_0=371.0° K, and L_f=2603 j mole^{-1}),[2] eq (2) may be written in the present specific case as follows:

$$t=t_0-440x_1-440x_2'(1/f). \qquad (3)$$

The points in figure 2 show for various stages of fusion the individual observed equilibrium temperatures. The chronological number of each run is shown beside its respective points. It may be seen that for the same sample there is, in general, more variation from one run to another than in the systematic deviations from linearity of the points of one run. This is due partly to the errors in the calculated fractions melted, these errors arising chiefly from the difficulty of determining accurately when in each run fusion began and ended. The solubility of the steel container in the liquid sodium [3] should have caused a constant error of less than 0.001 deg. This error has been ignored. Temperatures recorded when fusion was less than 70 or more than 98 percent complete were always decidedly too high to be in line with the others and were discarded. It seems likely that these latter discrepancies resulted partly from lack of the expected thermal and composition equilibrium, under these less favorable conditions, as the samples were neither shaken nor stirred. Also, the solubility of unidentified impurity may have been exceeded until a large fraction of the sodium had become molten.

Equation (3) predicts that as fusion progresses, the temperature will increase linearly with the decrease in $1/f$. In figure 2 the straight line for each sample was obtained from the observed points by the method of least squares. The corresponding numerical values of the coefficients of eq (3), together with their standard deviations (precision), are shown in table 1. Several conclusions may be drawn from these values.

TABLE 1. *Coefficients of equation (3) for three samples*

Sample	t_0-440x_1	$440x_2'$
	°C	°C
A	97.8199 (±0.0056)	0.0349 (±0.0048)
B	97.8208 (±0.0033)	.0379 (±0.0028)
C	97.8202 (±0.0025)	.0297 (±0.0021)

[2] D. C. Ginnings, T. B. Douglas, and A. F. Ball, J. Research NBS **45**, 23 (1950) RP2110.
[3] L. F. Epstein (private communication).

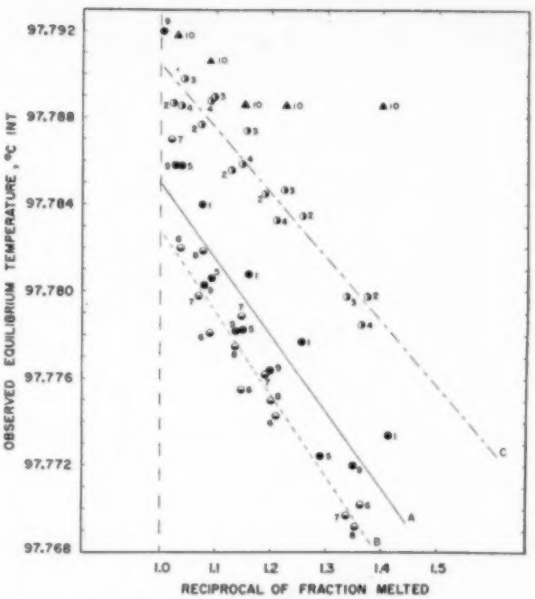

FIGURE 2. *Observed equilibrium temperatures.*

●————, sample A (sodium); ◒– – – – – – – –, sample B (sodium plus bulk uranium); ◑– · – · – · –, sample C (sodium plus finely divided uranium); ▲, sample D (an earlier sodium sample).
The run numbers given with the points are in chronological order.

From consideration of the details of purification of the sodium, it appears that the impurity with respect to which the liquid sodium was unsaturated may well have been largely sodium oxide, Na_2O. The values of the third column of table 1 give immediately the corresponding values of x_2', the mole fraction of this type of impurity in the whole sample. This averages 8×10^{-5} for samples A and B. This value corresponds to 0.02 percent of Na_2O by weight,[4] a reasonable amount of impurity from this source as it corresponds to the order of magnitude of the solubility of Na_2O in liquid sodium at this temperature. The corresponding quantity for sample C is somewhat lower than that for sample A, the difference having a standard deviation equal to the difference itself. It is possible that sample C actually contained substantially less impurity of this type, for the large surface of the finely divided uranium in this sample may have led to the removal of a considerable amount of the original impurity. Such a hypothesis is supported by the known ability of uranium to remove oxygen from Na_2O at higher temperatures.

If it be assumed that sample A, into which no uranium had been introduced, was free of all other "saturated" solutes, the value of t_0-440x_1 for this sample from table 1 gives 97.82° C as the triple point of pure sodium, and from a consideration of the

[4] If the effective molecular weight of Na_2O be taken equal to its formula weight.

various likely instrumental errors, this value is estimated to have an absolute accuracy of ± 0.02 deg. Earlier measurements on another sample of sodium, using a less stable copper resistance thermometer, had similarly yielded $97.80 \pm 0.03°$ C (see footnote 2).

The differences among the three values of the second column of table 1 will now be examined. Unless the uranium in samples B and C was completely protected from the sodium by some insoluble surface film, the values for these two samples should be lower than that for sample A by amounts $(440x_1)$ corresponding to the solubility of uranium in liquid sodium at this temperature.[5] These differences, with their standard deviations, are as follows: For sample B, $440x_1 = -0.0009° \pm 0.0067°$; and for sample C, $440x_1 = -0.0003° \pm 0.0058°$. These differences are thus zero within the precision of their measurement. The probability that the real differences exceed 0.02 deg is very small. This figure would correspond to a value of x_1 of 5×10^{-5}, equivalent to 0.05 percent by weight of uranium dissolved in the liquid sodium if the dissolved uranium is monatomic. It is accordingly concluded from these measurements that the solubility of uranium in liquid sodium at 97.8° C probably lies between 0.00 and 0.05 percent.

It seems likely that a radioactive tracer method would furnish a more definite value for this solubility.

[5] It seems very unlikely that uranium is appreciably soluble in solid sodium.

This work was supported by the Atomic Energy Commission. The author thanks C. E. Weber, of the Knolls Atomic Power Laboratory, Schenectady, N. Y., for supplying the sealed samples, and D. C. Ginnings, of the Bureau, for advice in designing part of the apparatus.

WASHINGTON, December 31, 1953.

Journal of Research of the National Bureau of Standards Vol. 52, No. 5, May 1954 Research Paper 2494

Multirange, Audiofrequency Thermocouple Instruments of High Accuracy

F. L. Hermach and E. S. Williams

Two new types of thermocouple instruments developed at the National Bureau of Standards are described. The first, called a volt-ampere converter, is used with a direct-current potentiometer to make measurements of alternating-current voltage and current over wide ranges with an accuracy of 0.05 percent at frequencies up to 20 kc/s. The second is a 0.5-percent multirange thermocouple volt-ammeter incorporating simple circuits so that the thermal converter may be checked with the indicating instrument normally connected to it.

1. Introduction

There have been increasing needs for convenient portable instruments for measuring voltage and current over wide ranges with high accuracy at audiofrequencies. Instruments of better than 0.1-percent accuracy are needed for standardizing or testing other instruments for precise laboratory measurements, and instruments accurate to one-fourth or one-half percent, and with low temperature coefficients, are needed for the more routine measurements. For the first type of instrument (0.1% or better), accuracy and stability are important requirements. Such an instrument need not be direct-reading, but should be portable and reasonably convenient to use. The second type of instrument (0.5% or better) must be direct-reading and should have many ranges.

For the applications mentioned above, thermocouple instruments are best suited because of their inherent wide frequency range and high sensitivity, and because multiple ranges are easily possible. The generally poor stability, large temperature influence (up to 0.3%/deg C), and low overload factor have in the past severely limited the accuracy of conventional instruments of this type and have deterred their use. However, recent work at the National Bureau of Standards [1] [1] has shown that these disadvantages may be overcome by using selected thermal converters [2] (often called thermoelements or thermocouples) as a-c–d-c transfer standards. Methods and equipment have been devised at the National Bureau of Standards for standardizing instruments with an accuracy approaching 0.01 percent at audiofrequencies. The equipment was designed to make a-c–d-c difference tests of instruments quickly and easily, and with the highest accuracy. Unfortunately, the equipment is not portable, and the methods for making ordinary a-c measurements are neither rapid nor convenient. This paper describes two new types of portable thermocouple instruments developed at the Bureau for a-c measurements where rapidity and convenience of operation are of greater importance than the high order of accuracy required in primary standardization work. The first is called a volt-ampere converter and the second a thermocouple volt-ammeter.

[1] Figure in brackets indicate literature references at the end of this paper.

[2] Proposed AIEE definition 30.89.040: A thermal converter is a device that consists of one or more thermojunctions in thermal contact with an electric heater or integral therewith, so that the electromotive force developed at its output terminals by thermoelectric action gives a measure of the input current in its heater.

2. Volt-Ampere Converter

2.1. Principle

The first instrument is a multirange volt-ampere converter to be used with a d-c potentiometer for measurements with 0.05-percent accuracy at frequencies from 20 c/s to 20 kc/s. Its basic principle may be seen in the elementary diagram of figure 1.[3] In this instrument the heater of a single thermal converter is connected in series with appropriate resistors for voltage measurements and is connected in parallel with appropriate shunts for current measurements. The resulting output electromotive force of the thermocouple is balanced against the voltage from an internal d-c "bucking circuit", B. Balance is indicated by the null reading of a built-in galvanometer, G. The heater is then switched to an internal d-c circuit, which is adjusted to give the same output emf and therefore equivalent heater current and voltage drop. The voltage, V_p, across a portion of this circuit is then measured with an external potentiometer and is multiplied by a simple factor to obtain the unknown alternating voltage or current.

From figure 1, under ideal conditions of negligible ac-dc differences, we have, for voltage measurements, since $I_a=I_d$, $V_a=I_aR_s=I_dR_s=V_p(R_s/R_p)$, where $R_s=R_m+R_h$. From figure 1,b, we have, for current measurements, since $V_a=V_p$, $I_a=V_aR'_s=V_p/R'_s$ where $R'_s=(R_sR_h)/(R_s+R_h)$.

A consideration of the circuits and these formulas shows that the measured alternating quantities are not dependent upon the conversion characteristics $E=f(I)$ of the thermal converter. They are dependent only on the potentiometer reading and the internal resistors, which can be made highly stable and whose values can be determined with great accuracy.

[3] The principle of this instrument is briefly described in section 9 of reference [1].

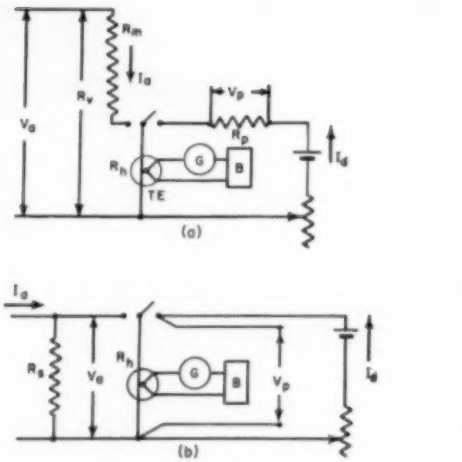

FIGURE 1. *Elementary diagram of volt-ampere converter.*

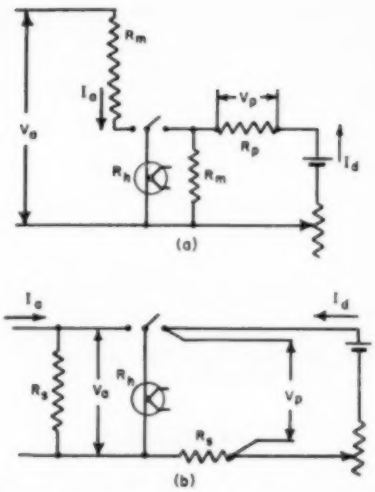

FIGURE 2. *Compensating circuits for volt-ampere converter.*

To realize this accuracy, however, the following requirements must be met:

1. The resistors must be properly adjusted and must be sufficiently stable.

2. The impedance of the a-c resistors, R_m and R_s, must be equal to their d-c resistance to the desired accuracy.

3. The a-c–d-c difference of the thermal converter must be reasonably small over the desired frequency range.

4. The drift in the thermal converter and the internal d-c bucking circuit must be small enough that significant changes do not occur during a measurement.

5. The switches, wiring, and other components must be of the highest quality and with adequate insulation resistance. Switches and other contacting parts should show low and repeatable values of contact resistance and should not introduce objectionable thermal electromotive forces.

6. A null potentiometer of suitable range and accuracy must be used.

2.2. Compensating Circuits

The basic formulas show that the results are partially dependent on the heater resistance of the thermal converter, R_h. Because of its temperature coefficient, the value of the heater resistance is dependent upon the heater current. In addition, as explained later, the resistance may be permanently changed by moderate overloads, so that it cannot be relied upon with the same certainty as the other resistors in the circuit. Fortunately, for the usual current and voltage ranges, $R_s \ll R_h \ll R_m$, so that the heater resistance need not be highly stable and need not be known with great accuracy. However, it was found possible to modify the basic circuits so that this resistance need not enter into the formulas.

As shown in figure 2,a, the modification for voltage measurements consists in adding to the internal d-c circuit a resistor, R_m, equal to the resistor (multiplier) connected in series with the thermal converter in the a-c position of the selector. For current measurements, as shown in figure 2,b, a resistor, R_s, equal to the shunt resistance, is added to the d-c circuit.

From figure 2,a, we have, with the switch thrown to the left, $V_a = I_a(R_m + R_h)$. With the switch thrown to the right, we have $V_p = I_d R_p$ and $I_h R_h = (I_d R_h R_m)/(R_h + R_m)$, where I_h is the current through the heater. Thus $V_p = (I_h R_p)(R_m + R_h)/R_m$ and, since $I_h = I_a$, we find that $V_a = (V_p R_m)/R_p$.

From figure 2,b, we have, with the switch thrown to the left $(I_a R_h R_s)/(R_h + R_s) = (I_h R_h)$, where I_h is the current through the heater. With the switch thrown to the right, we have $V_p = I_d(R_h + R_s)$. Thus, as $I_h = I_d$, we find that $I_a = V_p/R_s$.

Thus, rather remarkably, when these compensating circuits are used, the measured quantity is not dependent upon the heater resistance, R_h. The circuits are practical, and the added resistors (one for each voltage and current range) need be of only moderate accuracy.

2.3. Description of Volt-Ampere Converter

A wiring diagram and a photograph of the instrument constructed in accordance with the principles and requirements just outlined are shown in figures 3 and 4. The instrument combines both current- and voltage-measuring circuits, with switch-selected ranges of 15, 30, 75, 150, and 300 v, and 0.1, 0.25, 0.5, 1, 2.5, and 5 amp. It is completely self-contained and is intended for use with the usual general-purpose 1.5-v null potentiometer of 0.01- or 0.02-percent accuracy. For these voltage ranges, the series resistances, R_m, are so high that there is

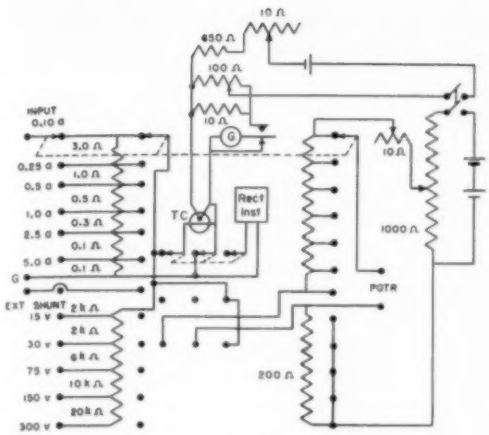

FIGURE 3. *Wiring diagram of volt-ampere converter.*

FIGURE 4. *Volt-ampere converter.*

little need to compensate for heater resistance. The compensation for the current ranges was incorporated, however, and made it unnecessary to adjust each shunt to odd resistance values. The nominal output voltage, V_p, at rated input voltage is 1.5 v, and is 0.5 v at rated input current. The latter value was chosen so that a series of 0.5-v a-c shunts normally used at the Bureau for current-transformer testing could be connected to this instrument for measurements of currents above 5 amp [2].

A 7.5-ma, 10-mv thermal converter of the insulating-bead type (one thermocouple junction attached to the heater by an electrically insulating bead) is used in this instrument. Its a-c–d-c difference is not more than 0.01 percent at audiofrequencies. The a-c resistors for the voltage ranges and the two lowest current ranges are high-grade 0.05-percent audiofrequency resistance cards. The four-terminal bifilar (parallel-strip) a-c shunts for the 5- and 2.5-amp ranges were constructed at NBS of 8-mil manganin strip 0.5 cm wide, with 4-mil woven-glass tape as insulation. Bifilar shunts of No. 20 manganin wire were constructed for the 1- and 0.5-amp ranges. Considerable care was taken in connecting all of the a-c shunts to minimize inductive coupling between the current and potential circuits of the shunts. These arrangements were adequate to keep the a-c impedance within 0.05 percent of the d-c resistance, even at 20 kc/s. The wire and strip were initially annealed at 500° C, and the completed shunts were aged at 150° C for 24 hr before final adjustment.

The 200-ohm resistor, across which the d-c potentiometer is connected for voltage measurements, was made of manganin. The compensating resistors in the d-c circuit need not be carefully adjusted. Actually, 1-percent wire-wound resistors were used. The built-in light-beam galvanometer has a sensitivity of 0.3 μa/mm, a resistance of 10 ohms, and an external critical-damping resistance of 30 ohms.

Newly developed commercially available rotary switches with enclosed solid-silver contacts and a unique internal circuit are important components in the instrument. Mercury cells of 3-amp-hr capacity are used as the internal d-c sources because of their flat discharge-voltage characteristic and very long shelf life. The combined drifts in the balancing circuit and the thermal converter are less than 0.001%/min.

A useful feature of this volt-ampere converter is a 7.5-ma, 0.5-v rectifier instrument, which is switched in place of the heater when the thermal converter is connected to the internal d-c source. This instrument tells at a glance what effect circuit changes have on the measured current or voltage. It also indicates within 5 percent what voltage to set on the potentiometer. In addition, it can serve as a valuable overload protector, if the thermal converter is switched to the a-c circuit only when the rectifier instrument is on scale.

A spare 7.5-ma thermal converter having a bifilar manganin resistor in series with the heater, to adjust the total resistance to 66⅔ ohms ±0.6 percent, is mounted in the instrument. As the calibration of the instrument does not depend on the conversion characteristic of the thermal converter used, the converter, if burned out, may be replaced by this spare quickly and easily and without any effect on the accuracy of the instrument.

In use, the volt-ampere converter is switched to the desired range, and, with the selector on "Rect Inst," is connected to the circuit to be measured and to a suitable null potentiometer. If the rectifier instrument is on scale, the selector is switched to the No. 1 position to connect the thermal converter to

the a-c circuit, and the controls of the bucking circuit (marked No. 1) are adjusted to bring the deflection of the built-in galvanometer to zero.[4] The selector is then switched to the No. 2 position, and the controls of the internal d-c source (marked No. 2) are adjusted to give zero galvanometer deflection. The potentiometer is then balanced and read in the usual way, and the observed voltage is multiplied by the factor marked on the range switch of the volt-ampere converter to obtain the measured a-c voltage or current. Separate coarse and fine three-turn helically wound adjustable resistors permit both the No. 1 and No. 2 adjustments to be made reasonably quickly and easily and with the required precision.

2.4. Tests of Converter

Table 1 shows the results of a-c–d-c difference tests[5] and of successive reversed d-c calibrations of the volt-ampere converter. They are an indication of the accuracy that is possible with this instrument. In the table the percentage d-c correction, d, is the value to be added to the reading of the potentiometer (connected to the "Potr" posts of the converter) to obtain the true direct voltage or current. The percentage a-c–d-c difference, a, is the percentage difference in voltage or current required for the same indication of the converter, a plus sign signifying that more alternating than direct voltage or current is required. For measurements that justify the application of these corrections, the alternating quantity, Q, being measured can be computed by the formula $Q=NV_p(1+a+d)$, where N is the factor marked on the range switch, and V_p is the potentiometer voltage.

The d-c tests showed an early change in the 200-ohm resistor across which the potentiometer is connector for voltage ranges but have not shown any other significant drifts. The heater of the thermal converter used in this instrument is of nickel-chromium alloy with a +0.02%/deg C temperature coefficient. The resulting change in resistance with current (about 3% at rated current) causes the correction of the lowest voltage range to depend slightly upon applied voltage. Because of the compensation circuit, the change in heater resistance does not affect the accuracy of even the lowest current range.

The a-c–d-c tests show that the voltage ranges are useful to 200 kc/s and the current ranges to somewhat more than 20 kc/s. It is believed that if thinner manganin strip and thinner insulation were used in place of the 4-mil strip and the No. 20 manganin wire for the shunts of the four higher current ranges, this frequency limit could be raised to 100 kc/s.

3. Thermocouple Volt-Ammeter

3.1. Principle

The second instrument is a thermocouple volt-ammeter having a suitable millivoltmeter connected to the output of the thermal converter. The sustained accuracy in service of the usual instrument of this type is limited by the relatively high temperature coefficient of the combination (0.1 to 0.3%/deg C), and by changes in the converter, probably due to stress relaxation of the heater, to moderate overloads, or to leakage of air into the evacuated bulb. It is often desirable, but seldom convenient, to test such

[4] Actually, any deflection is permissible, provided that the *same* deflection is repeated with the selector in the No. 2 position.

[5] These tests were made with the equipment described in reference [1]. The thermal converters and newly developed voltmeter elements have now been intercompared and tested at frequencies up to 1 Mc/s.

TABLE 1. *Tests of NBS volt-ampere converter*

Range	Applied quantity	Reversed d-c corrections				a-c–d-c differences					
		1952		1953		20 c/s	10 kc/s	20 kc/s	50 kc/s	100 kc/s	200 kc/s
		April	July	Jan.	July						
p	p	%	%	%	%	%	%	%	%	%	%
300	300	+0.01	−0.04	−0.04	−0.04	−0.01	.....	−0.01	.....	0.00	.....
	200	+.01	.....	.....	.....	.....	.....	.....	.....	.....	+0.08
150	150	+.01	−.03	−.04	−.06	.....	0.00	−.01	.....	−.02	−.03
	90	+.02	.....	.....	.....	.....	.....	.....	.....	.....	.....
75	75	+.02	−.02	−.02	−.04	.....	−.01	−.01	.....	−.01	−.02
	60	+.01	.....	.....	.....	.....	.....	.....	.....	.....	.....
30	30	+.05	.00	+.01	−.02	.....	.....	−.01	.....	.00	.00
	20	+.02	.....	.....	.....	.....	.....	.....	.....	.....	.....
15	15	+.12	+.06	+.08	+.06	−.01	.....	−.01	.....	.00	−.02
	10	+.06	.....	.....	.....	.....	.....	.....	.....	.....	.....
amp	amp										
5	5	.00	−.01	.00	−.01	.00	.00	−.01	−0.11	.....	.....
	3	.00	.....	.....	.....	.....	.....	.00	.....	.....	.....
2.5	2.5	+.04	+.02	.00	+.02	.....	.00	−.03	−.18	.....	.....
1	1	+.01	+.01	.00	.00	.....	−.01	−.04	−.27	.....	.....
0.5	0.5	+.01	−.01	−.03	−.05	.....	−.01	−.05	−.32	.....	.....
.25	.25	+.01	−.04	−.04	−.04	.....	−.01	−.03	.....	.....	.....
.1	.1	+.05	+.04	+.04	+.05	−.01	−.02	−.02	−.08	.....	.....
	.05	+.05	.....	.....	.....	.....	.....	.....	.....	.....	.....

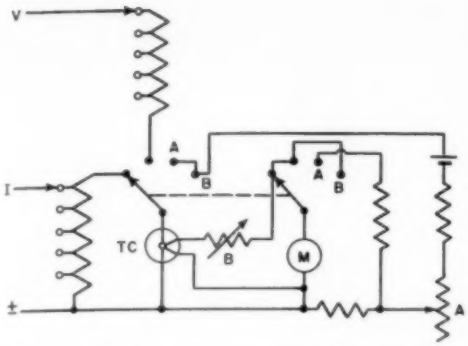

FIGURE 5. *Elementary diagram of volt-ammeter.*

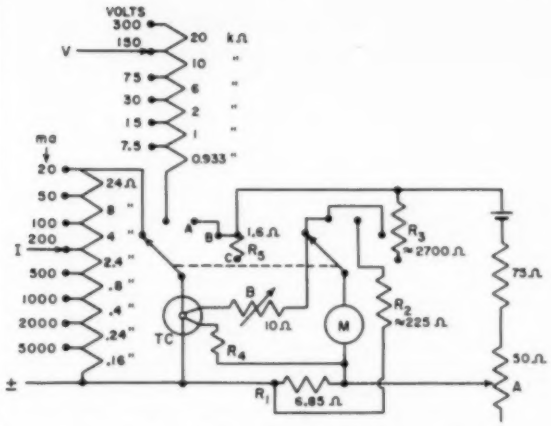

FIGURE 6. *Wiring diagram of volt-ammeter.*

an instrument by comparison with a d-c instrument at one scale point before important measurements are made with it.[6] In this new instrument, the d-c millivoltmeter itself, together with appropriate resistors, is arranged as a milliammeter to provide for the important single-point check of the thermal converter, and adjustable resistors are incorporated to compensate for any changes.

Figure 5 is an elementary diagram of the circuit. With the selector switch in check position A, the heater of the 7.5-ma converter is connected to an internal d-c circuit , and the millivoltmeter, M, in series with a manganin resistor is connected across a 50-mv manganin shunt. The resulting milliammeter (7.5-ma full scale) has negligible temperature influence. Resistor A is then manually adjusted for full-scale deflection of the instrument, which corresponds to rated heater current. In check position B the millivoltmeter is connected to the thermocouple circuit, and resistor B is adjusted to give the same full-scale deflection, which is the correct deflection for this current.[7] The checks can be made quickly and conveniently without disconnecting the leads from the terminals of the instrument.

3.2. Changes in Heater Resistance

Experience with thermal converters has shown, however, that additional precautions are necessary to insure complete accuracy in the measurement of current. The heater resistance of a converter may be permanently changed by as much as 0.5 to 1 percent by moderate overloads that do not burn out the converter. If the heater is shunted for current measurements, such changes can cause an almost equal error. Furthermore, some alloys used for heaters have such a large temperature coefficient of resistance that the corresponding resistance change must be taken into account.

Table 2 shows the results of measurements of the permanent change in resistance caused by overloads of typical low-range thermal converters. In these tests the current was held for a few seconds at the overload indicated, and the change in resistance was then measured at normal current. The altered value of resistance was not affected by subsequent operation at rated current.

TABLE 2. *Effect of overloads on resistance of thermal converters*

Converter range	Rated current	Change in resistance at rated current
ma	*%*	*%*
5	200	+0.5
7.5	200	.0
	300	+ .4
	350	+ .9
10	200	+ .1
	250	+ .6

To guard against errors due to changes in heater resistance, a circuit was provided in this instrument, as shown in figure 6, for checking the heater resistance with the same millivoltmeter. In check position C the millivoltmeter, in series with manganin resistor R_3, is connected across the heater and shunt R_1. Resistor R_5 keeps the effective resistance of the battery circuit the same in this position as in check position A, so that the battery current does not change. If the resistance of the heater of the converter has the proper value, the millivoltmeter will deflect to the full-scale mark.

[6] As an example, embarrassing errors were caused in a recent instance by a 10-percent change in reading of a thermocouple voltmeter between regularly scheduled tests of the instrument, probably because of air leakage into the glass bulb of the thermal converter.

[7] An a-c "self-checking" instrument, which accomplishes the same end purpose as this instrument, but in a different way, has recently been developed commercially [3]. It uses a standard cell and galvanometer connected across a resistor as the direct-current standard.

3.3 Description of Volt-Ammeter

The instrument (fig. 7) was constructed in accordance with the diagram in figure 6. With this instrument, voltage and current can be measured successively in the same circuit without changing leads to the instrument. Ranges of 7.5, 15, 30, 75, 150, and 300 v, and 20, 50, 100, 200, 500, 1,000, 2,000, and 5,000 ma are provided. The thermal converter is of the same type and range used in the first instrument, as are the a-c resistance cards for the voltage ranges. As in the other instrument, a bifilar manganin resistor is connected in series with the heater of the converter to adjust it to the proper value. An Ayrton-Mather ring shunt [8] was constructed for the current ranges, with commercial a-c resistance cards for the four lower ranges and bifilar manganin wire and strip for the higher ranges. Resistors R_1, R_2, and R_3 were wound of manganin, and after artificial aging, were adjusted to fit the 5-mv, 25-ohm millivoltmeter. R_4 is in part a negative-temperature-coefficient resistor, which greatly reduces the temperature coefficient of the overall thermocouple instrument. The long-time stability of this resistor is not important because of the compensating circuit.

As shown in figure 7, the range switches and input binding posts are on the left side of the millivoltmeter, and the selector switch and the helically wound adjusting resistors, A and B, on the right. A submerged screwdriver-operated control prevents accidental rotation of resistor B. The temperature-sensitive resistor and the converter are mounted in the wooden box that houses the millivoltmeter.

As in the first instrument, the feasibility of these circuits depends upon the quality of the components. The leakage resistance, contact resistance, and thermal electromotive force introduced by the switches and adjustable resistors must not exceed certain easily computable limits. This is especially important in the low-voltage thermocouple circuit. Here, too, the enclosed silver-contact switches, originally developed for d-c potentiometers, are important components. Tests by the manufacturer indicate that in ordinary use the contact resistance of the switches are less than 0.001 ohm, the thermal electromotive forces generated are less than 1 μv, and the insulation resistance is greater than 10^{12} ohms.

No overload protection has been built into this instrument, but matched thermal converters have been selected for replacement. It has been found possible to select converters in this current range from larger lots, which match within 0.3 percent of full scale when adjusted for equality of millivoltmeter deflection at rated current, as in this instrument. Thus the expense of recalibration should not be necessary in case of burnout.

The instrument is used like any conventional thermocouple instrument. Readings are made directly in divisions and tenths of a division on a 100-division scale for the current ranges and a 150-division scale for the voltage ranges, and are multiplied by a simple factor given on the range switch to convert to volts or milliamperes. Besides simplifying the marking of the scale, this greatly reduces errors of estimating and reading. The checks can be made at any time, without disconnecting the leads from the circuit to the instrument, by simply rotating the selector switch to check positions A, B, and C in succession, and adjusting the A resistor for full-scale deflection of the millivoltmeter. Adjustment of the B resistor is rarely necessary, and only an overload or a very large temperature change could be expected to cause the reading in the C position to be in error.[9]

3.4. Tests of Volt-Ammeter

Table 3 shows the results of a-c–d-c difference tests and d-c tests of the thermocouple instrument. In

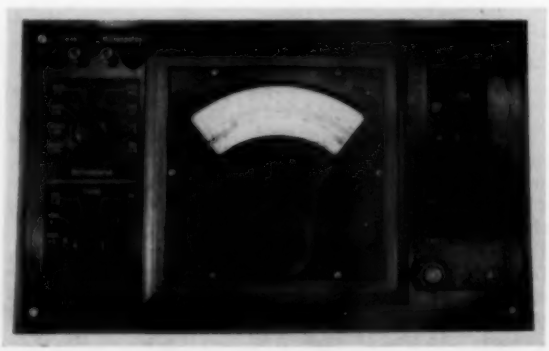

FIGURE 7. *NBS volt-ammeter.*

TABLE 3. *Tests at full scale of NBS 0.5-percent thermocouple volt-ammeter*

Range	Applied quantity	Reversed d-c corrections			a-c–d-c differences				
		Oct. 1952	Jan. 1953	July 1953	100 c/s	20 kc/s	50 kc/s	100 kc/s	200 kc/s
v	*v*	%	%	%	%	%	%	%	%
300	300	.....	.....	−0.1	0.0	−0.1	.....	−0.3	.....
150	150	0.0	0.0	−.1	.....	−.1	.....	−.1	−0.3
75	75	.0	+.1	.0	.0	.0	.....	.0	−.1
30	30	−.1	.0	−.1	.....	.....	.....	.....	−.1
15	15	−.1	.0	.0	.....	.....	.....	.....	.0
7.5	7.5	−.1	+.1	.0	.0	.0	.....	.....	.0
amp	*amp*								
5	5	−.1	.0	−.1	.....	−.1	−0.6	.....	.....
2	2	−.1	+.1	.0	.0	.0	−.3	.....	.....
1	1	+.1	+.2	+.1	.0	−.1	−.4	.....	.....
ma	*ma*								
500	500	.0	+.2	+.1	.0	.0	−.2	−.7	.....
200	200	+.1	+.2	+.1	.0	.0	−.1	−.3	.....
100	100	.0	+.2	+.1	.0	.0	.....	−.2	.....
50	50	.0	+.2	+.1	.0	.0	.....	−.1	.....
20	20	−.1	+.2	.0	.0	.0	.....	.0	.....

[8] With a constant heater current, the ratio of the input currents on any two ranges for this type of shunt is independent of the heater resistance. Thus the same scale can be used for all current ranges in spite of the dependence of heater resistance upon temperature and therefore upon current.

[9] If the heater resistance has changed, a correction to be applied to each current range can readily be determined from the resulting change in deflection of the instrument in check position C. Because an Ayrton-Mather shunt is used, the correction is the same on each current range. Calculations and tests show that the percentage of the indication to be added to the reading on any current range due to a change in heater resistance is approximately equal to the percentage increase in deflection in check position C.

this table the percentage correction is the value to be added to the indication of the instrument to obtain the true direct current or voltage, and the a-c–d-c difference is the percentage difference in alternating and direct current or voltage to produce the same indication. Only the tests at full scale are included in the table. Reversed d-c measurements were made at the time of the first test at every cardinal scale point on the 150-v and 2-amp ranges. The observed correction in divisions at each of these cardinal points was adjusted by subtracting a proportional part of the observed full-scale correction (that is, by subtracting $C_f D/D_f$, where C_f is the full-scale correction, and D_f and D are the number of full-scale divisions and the number of divisions at that cardinal point, respectively). The plotted results, figure 8, show the scale corrections for both scales and were verified by tests at two cardinal points on other ranges. Such a plot and a table of full-scale corrections for each range greatly simplify the application of corrections to the reading of a multirange instrument such as this. The d-c correction at any point is simply the scale correction plus a proportional part of the full-scale correction for that range, and is easily calculated mentally. The a-c value is simply the corrected d-c value plus the a-c–d-c difference of the instrument (which is usually negligible). The a-c–d-c difference and the scale corrections need be determined only once, and subsequent tests need be made only at full scale on each range with reversed direct current.

The results of the a-c–d-c tests of this instrument show negligibly small frequency influence on all ranges even at 20 kc/s. Measurements at two cardinal points on several ranges showed no significant dependence of a-c–d-c difference upon scale position. The voltage ranges are actually useful to 200 kc/s or more, and the current ranges to 50 kc/s.[10]

Tests of the temperature influence of the instrument were made on the 150-v and 1-amp ranges at temperatures between 25° and 40° C. The temperature coefficients calculated from these results were less than +0.02%/deg C before the checking procedure was carried out and were less than +0.01%/deg C afterward. Preliminary tests had shown that the temperature coefficient of the instrument before the temperature-sensitive resistor and checking circuits were connected was about +0.12%/deg C, and that a large part of this arose in the thermal converter itself. It does not appear to be generally realized that thermal converters may have temperature coefficients ranging up to +0.3%/deg C.

These tests indicate that this instrument may properly be considered to be in the 1/2-percent-accuracy class and will remain within this accuracy over an extended range of temperatures. The construction of a ¼-percent instrument of this type might prove feasible, but would depend largely on the inherent stability and readability of the millivoltmeter.[11]

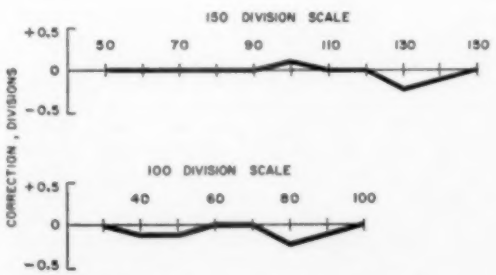

FIGURE 8. *Scale corrections for volt-ammeter.*

[10] The instrument was originally constructed with a helically wound adjustable resistor in series with the heater of the thermal converter to compensate in check position C for any change in heater resistance. However, its inductance limited the frequency range of the instrument to 20 kc/s, so that it was later removed, and the checking circuits were rewired in their present form.

4. Summary

4.1. Volt-Ampere Converter

The volt-ampere converter can serve as an accessory to the d-c potentiometer to make possible the measurement of alternating current and voltage over a wide range of frequencies, just as a volt box or shunt box is used to extend the range of the potentiometer for d-c measurements. The formulas are the same in appearance as those used with a volt box or shunt box, and, indeed, the multiplying factor to convert the potentiometer readings to a-c volts or amperes are exactly the same as those that would appear on the d-c range-extending devices. Thus the volt-ampere converter, by an adaptation of the transfer principle, may be considered to extend potentiometric techniques to a-c volt-ampere measurements, with the following advantages:

1. High accuracy is possible—better than that obtainable with any portable deflecting instrument.
2. This accuracy is realized over a greatly extended frequency range; 20 to 20,000 c/s.
3. Without any attendant loss in accuracy, it is entirely feasible to construct a multirange instrument—one instrument can be designed to cover a wide range of measurement of both voltage and current.
4. The volt-ampere converter is portable, self-contained, requires no external d-c source or controls, and is reasonably convenient and easy to use.
5. The accuracy of the volt-ampere converter is not dependent, as are other thermocouple instruments, on the long-time stability of the thermal converter used. As a consequence, a thermal converter can easily be replaced by another of the same range and heater resistance without affecting the accuracy of the volt-ampere converter and without requiring its recalibration.

[11] It is recognized that a sensitive millivoltmeter suitable for indicating thermocouple electromotive forces is not as rugged, and therefore may not be as stable as the more usual d-c milliammeters, of ranges greater than about 2 ma, that utilize higher operating torques.

6. To insure continued high accuracy, the instrument can easily be periodically tested on direct current by means of the potentiometer and its d-c accessories. The a-c–d-c differences are permanent and need ordinarily be determined only once.

7. The small rectifier instrument insures some of the advantages provided by a deflecting instrument, and, in the normal sequence of operations, can serve to prevent converter burnout.

The volt-ampere converter has the disadvantage of requiring two extra balancing operations for each measurement, but experience shows that these can be made quickly and easily. It has the weakness that inadvertent adjustment of the thermocouple balancing voltage instead of the heater current when the converter is on direct current can give erroneous results. This could be prevented, however, in a number of ways, such as by incorporating a mechanical device to disconnect the adjusting resistors of the bucking circuit when the converter is switched to the internal battery, or by providing a sliding cover plate, rotated by the selector switch so as to cover up the controls that should not be used.

4.2. Thermocouple Volt-Ammeter

The ½-percent thermocouple volt-ammeter is a conventional multirange instrument, except that it is provided with additional circuits and components to permit using its indicating instrument to check the thermal converter, and with manual adjustments in the thermocouple circuit for compensating for converter changes. In addition to detecting and compensating for changes in the thermal converter, this makes possible a thermocouple instrument of very small temperature coefficient. The added circuits are simple, the components are inexpensive, and the instrument is easy to use. Although more limited in accuracy, this instrument retains many of the advantages of the volt-ampere converter, and is, in addition, direct-reading.

5. Conclusions

Two electrothermic instruments have been developed to meet specific needs at the National Bureau of Standards. The first serves as a standard for the a-c testing of ammeters and voltmeters in the ¾-percent-accuracy class or better that are sent in to NBS for certification. The second is used for general measurements at audiofrequencies and for tests of electronic and panel instruments, and, in conjunction with a suitable attenuator, has proved very convenient for the testing of electronic voltmeters. These instruments have been described because of their novelty and usefulness, and because it is believed that similar instruments may well meet like needs in other laboratories.

The development of these instruments, based on the transfer principle, has served to demonstrate the high order of accuracy attainable by this method for the measurement of both current and voltage over wide frequency ranges. The demonstrated gains overcome the limitations of conventional thermocouple instruments arising from temperature influence or the likelihood of changes in the thermal converter, and, it is hoped, will lead to wider laboratory use of electrothermic instruments.

6. References

[1] F. L. Hermach, Thermal converters as a-c–d-c transfer standards for current and voltage measurements at audio frequencies, J. Research **48,** 121 (1952) RP2296.

[2] F. B. Silsbee, Notes on the design of four terminal resistance standards for alternating current, BS J. Research **4,** 73 (1930) RP133.

[3] Electrical Measurements **19,** No. 4 (Sensitive Research Instrument Co., Mt. Vernon, N. Y., 1952).

Washington, December 3, 1953.

Journal of Research of the National Bureau of Standards Vol. 52, No. 5, May 1954 Research Paper 2495

Fatigue Notch Sensitivity of Some Aluminum Alloys

J. A. Bennett and J. G. Weinberg

The notch sensitivity in fatigue was determined for 24S-T4, 61S-T6, and 75S-T6 aluminum alloys. Specimens having theoretical stress-concentration factors of 1.0, 1.4, and 1.8 were used, and the fatigue-strength reduction factor was based on the number of cycles required to initiate the fatigue crack. The values of notch sensitivity for 61S-T6 in the small radius specimens and for 24S–T4 were close to unity, whereas that for 75S–T6 was much lower. The data also provide information on the dispersion of fatigue results for the different alloys and the portion of the total life required for a fatigue crack to grow to fracture.

1. Introduction

The widespread use of aluminum alloys in aircraft has been due in large measure to the favorable strength-weight ratios of the high-strength alloys. However, as design stresses have increased, the problem of failure by fatigue has assumed continually greater importance. The problem has been studied extensively, and the literature dealing with the fatigue properties of aluminum alloys is voluminous [1].[1]

Because fatigue failures in high-strength metals usually occur at stresses lower than those necessary for appreciable macroscopic plastic deformation, such failures will normally originate at points where the stress is concentrated by notches such as holes, grooves, scratches, or inhomogeneities in the metal. Consequently, the effect of notches on the fatigue strength of metals has been extensively studied, and several attempts have been made to predict the behavior of notched specimens from theoretical considerations [2, 3, 4, 5].

In studying the results of previous work on fatigue notch sensitivity, it was felt that two factors connected with the experimental work may have affected the results in such a way as to obscure the true effect of notches on fatigue properties. These factors were: (1) In many cases no attempt was made to make sure that the condition of the surface of the unnotched specimen was the same as that of the notched specimen at the point where the fatigue crack would be initiated. This was particularly true in tests with very sharply notched specimens. As the presence of a cold-worked layer is known to have a great effect on fatigue properties, any appreciable difference in the degree of cold-work between the two types of specimen would be expected to affect the apparent notch sensitivity. (2) The life of a fatigue-test specimen is made up of two periods; that in which no visible change occurs but which culminates in the formation of a small crack, and that in which the crack grows until fracture takes place. In smooth specimens the second stage is usually only a small part of the total life, so that no serious error is involved in ignoring it. However, as shown in previous work [10], the second stage may constitute 50 percent of the life of mildly notched specimens, and cannot be neglected. The factors that control the rate of growth of fatigue cracks are quite different from those governing the first stage. Therefore, if both stages are taken together, as in a test run to fracture, there is little hope of obtaining agreement with theoretical considerations.

With these considerations in mind, experimental work was undertaken to evaluate the fatigue notch sensitivity of three aluminum alloys. The following report gives the results and a discussion of these experiments.

The symbols used in this report are largely the same as those listed in reference [7], namely, S_a, stress amplitude; N, fatigue life (N_e denotes the number of cycles to the initiation of the first crack, N_f the number of cycles to fracture); K_t, stress concentration factor; K_f, fatigue strength reduction factor; and q, notch sensitivity, equals $(K_f-1)/(K_t-1)$.

2. Materials and Test Methods

The three materials, 24S-T4, 61S T6, and 75S-T6, were obtained in the form of ½-in. diam rod treated commercially. No further heat treatment was given any of the alloys. The composition of each of the alloys, determined by spectrochemical analysis (table 1), was within the specification limits. The static mechanical properties listed in table 2 are also within the ranges typically found in these alloys.

Metallographic examinations showed the three materials to be normal in regard to grain size and microstructure, except that the 75S contained a large number of oversized particles of insoluble constituent believed to be the chromium-bearing constituent referred to in reference [8]. Particles as large as that shown in figure 1 were not unusual, and this is considerably larger than the example referred to as oversize in reference [8].

Fatigue tests were made on R. R. Moore rotating-beam machines usually operated at 5,000 to 7,000 rpm. The three types of specimens used are shown in figure 2. Fillets were used rather than grooves for stress raisers in order to permit better illumination of the surface where the fatigue crack would start. The theoretical stress-concentration factors, as determined from the curves in reference [5], were 1.40 and 1.79 for the 1/16-in. and 0.025-in. radius fillets, respectively.

[1] Figures in brackets indicate the literature references at the end of this paper.

FIGURE 1. *Large particle of segregated phase in 75S-T6.*

Particles of this size were not unusual in the material tested. Unetched, × 200.

TABLE 1. *Spectrochemical analyses of alloys tested*

Alloy	Cu	Si	Fe	Mn	Mg	Zn	Cr
	percent	percent	percent	percent	percent	percent	percent
24S	3.99	0.11	0.36	0.56	1.20	0.03	0.02
61S	0.33	.60	.44	.10	0.85	.03	.25
75S	1.50	.14	.29	.10	2.20	5.80	.25

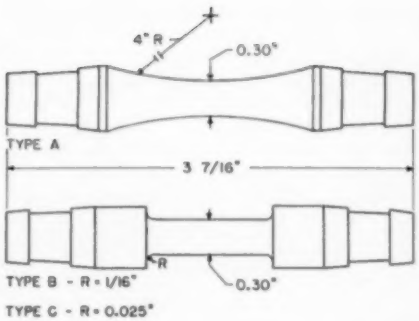

FIGURE 2. *The three types of specimens used in the investigation.*

TABLE 2. *Mechanical properties of specimens*

Alloy	Tensile strength	Yield * strength	Elongation 2 in.	Brinell hardness number (500 kg; 10-mm ball)
	lb/in.²	lb/in.²	percent	
24S-T4	73,500	56,500	17.8	126
61S-T6	48,000	40,000	21.0	94
75S-T6	84,500	73,500	10.4	151

* 0.2-percent offset.

Because of previous difficulty with hand polishing of unnotched fatigue specimens, a machine was developed to do this operation automatically. As shown in figure 3, it consists of three parts: a wheel carrying an abrasive belt, a means for supporting and rotating the specimen during the polishing operation, and a means for moving the specimen across the belt during polishing. The wheel consists of a number of thin spring leaves, radiating from a hub, which press against the belt. This causes the belt to conform to the contour of the specimen and assures a small uniform pressure between the specimen and the abrasive. The specimen rotates 1 revolution for 40 revolutions of the wheel, and is simultaneously moved across the belt by means of a drive nut and cord arrangement. This assures that fresh abrasive is being used at all times and reduces the possibility of a burnishing action. With the wheel rotating at 180 rpm, the specimen moves across the belt in about 1 min, and this was usually sufficient to eliminate previous machining marks, using 600 Aloxite paper as the abrasive. No attempt was made to obtain a highly polished surface, but the above procedure appeared to give very uniform results from specimen to specimen.

The filleted specimens were polished in the conventional manner with a rotating wire, over which was carried 302 emery suspended in a mixture of glycerine and water. The polishing wire was supported in a pivoted jig to assure uniform pressure. Figure 4 shows a comparison of the surfaces of the unnotched and 1/16-in.-radius fillet specimens. All specimens were carefully examined to make sure that all circumferential tool marks and scratches had been removed before testing.

The minimum diameter of each specimen was measured at four positions around the circumference on a toolmaker's microscope at 30 magnification. Specimens having a variation of more than 0.0002 in. in diameter were discarded. The fillet radii of the stress-concentration specimens were checked at the same time that the diameter was measured.

The determination of the number of cycles at which a fatigue crack starts is a difficult and somewhat uncertain procedure; it is obvious that accuracy of the determination will depend primarily on the minimum size of crack it is possible to detect. In previous investigations at the Bureau small cracks have been detected by (1) measurement of the increased deflection under the test load [9], (2) observation of the specimen under stroboscopic light [6], and (3) the use of fracture wires [10].

Three methods of crack detection were used in the present investigation. The first was a deflection method similar to (1) above, except that the contact was mounted on a lever attached to one bearing box. When the machine had run long enough to reach temperature equilibrium the contact was advanced to a position just short of touching a fixed plate. Any increase of deflection then caused contact with

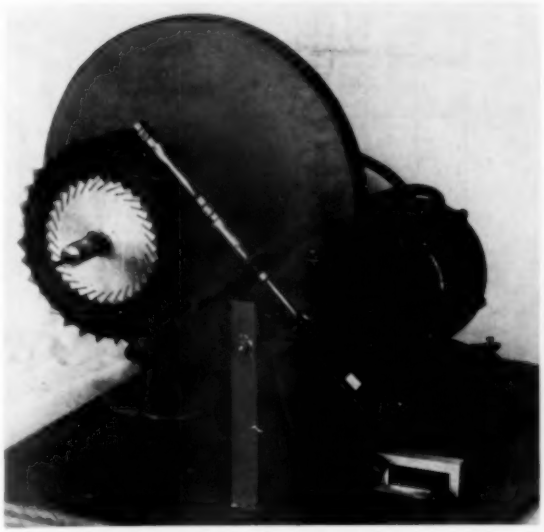

FIGURE 3. *Apparatus used for polishing unnotched fatigue test specimens.*

The polishing wheel, consisting of a number of metal spring leaves, presses an abrasive belt against the specimen with uniform pressure. The specimen rotates at a constant rate and advances slowly over the abrasive surface.

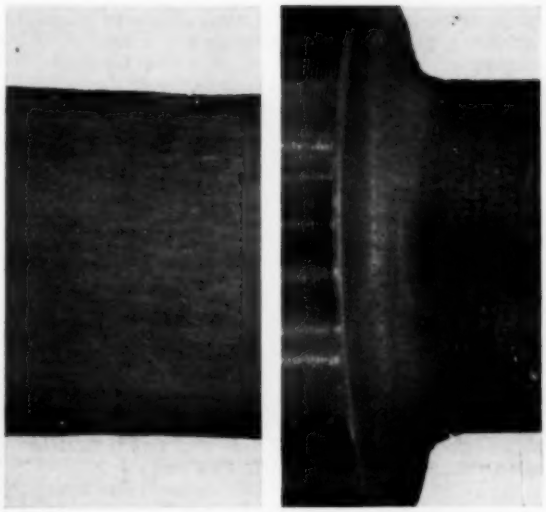

FIGURE 4. *Comparison of the surface finish on an unnotched specimen with that on a 1/10-inch-radius filleted specimen.* ×7.

the plate, which operated an electronic relay to shut off the machine.

The second was a vibration-responsive method, which depended for its operation on the fact that a cracked specimen will deflect more when the crack is on the tension side than when it is on the compression side. This condition results in increased vibration of the specimen bearing-box assembly. Two vibration-sensitive devices were used to stop the machine; the first consists of a three-pronged pedestal on which a steel ball is balanced. The second, shown in figure 5, is similar, except that the pedestal is horizontal and the ball is held on the pedestal by the magnetic field of a small permanent magnet. In both devices the increased vibration caused by a crack shakes the ball from the pedestal; the ball drops between metal plates, completing a circuit that shuts off the machine. The second device was somewhat more useful than the first because the force holding the ball onto the pedestal could be varied by an adjustable soft-iron shunt across the poles of the permanent magnet.

The effectiveness of either the deflection method or the vibration method was closely associated with the degree of vibration present at the beginning of the test. When this was sufficient to be felt by touching the bearing box, there was little chance of detecting a small crack.

The third method of crack detection was merely that of inspecting the specimen at intervals during the part of the test when there was a chance of the crack developing. Often this method was combined with one of the other two by setting the automatic

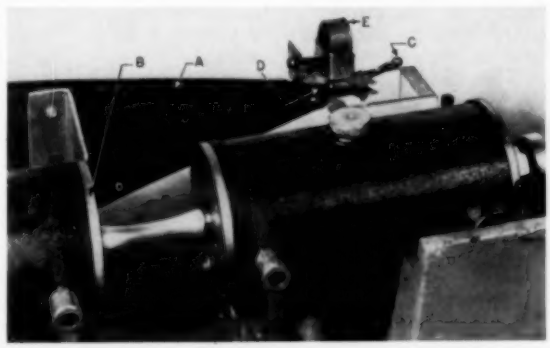

FIGURE 5. *Vibration-responsive stopping device.*

At the end of a 12-inch lever (A) fastened to bearing box (B) a small steel ball (C) is delicately balanced on three prongs by means of a magnetic field created by a small permanent magnet (D). An adjustable "keeper" (E) controls the strength of the magnetic field that holds the steel ball in place. Vibration caused by the formation of a crack in specimen (F) causes the steel ball to drop which closes an electrical circuit stopping the machine.

device so closely that numerous "false alarms" occurred. By inspecting the specimen each time the device tripped, the probability of finding a small crack was increased, but there was still a large element of chance involved.

For inspection, the specimen and bearing boxes were removed from the machine and supported in an inverted position on the loading-point knife-edge seats. Small weights were applied to the ends of the bearing boxes to put the upper surface of the specimen in tension, and the examination was made with a binocular microscope. A small fluorescent

amp was found to give the most satisfactory illumination for the detection of small cracks. The central angle subtended by a crack was measured by means of a divided drum fitted on one of the bearing-box spindles, the ends of the crack being located by means of cross hairs in one eyepiece.

When a crack was found, its growth was followed by measurements after appropriate periods of stressing, and an attempt was made to determine by extrapolation the number of cycles at which the crack started. Although the variation in the rate of crack growth at a given stress was considerably less than that in the first stage of the test, it appeared that reasonable accuracy of extrapolation could be obtained only if the crack had been first observed when its length was less than 10 percent of the circumference. This requirement was considerably more difficult to fulfill with the notched specimens than with the smooth ones, because the cracks were much shallower in proportion to their length and were therefore more difficult to observe.

In order to make sure that the periodic stopping of the tests did not affect the results, many of the tests were run without interruption, but in these tests the crack usually extended over more than 10 percent of the circumference when detected. At each stress level an attempt was made to obtain two or more reliable curves of crack growth; the N_c values for the uninterrupted tests were obtained by extrapolation based on the most reliable crack-growth curves for that stress level.

The uncertainty inherent in the determination of N_c was minimized in two ways. First, in tests that were interrupted periodically there were numerous instances when the origin of the crack was bracketed rather closely by two consecutive inspections, the first of which did not disclose any crack, and the second of which did. Second, the ratio of N_c to N_f was a fairly reproducible function of the stress amplitude for a given specimen type and material. These relationships, shown in figure 6 for the 24S-T4 specimens, provided a means of comparing the data obtained at different stress levels and assisted in determining when crack-growth data of sufficient accuracy had been obtained. The accuracy of the measurement of small cracks was verified on a few specimens by removing them from the fatigue machine after the first observation of the crack. The specimens were then extended under axial tension, which made the extent of the crack clearly discernible.

3. Results and Discussion

It was originally planned to determine the notch sensitivity over a range from about 5×10^4 to 5×10^7 cycles. On the basis of some preliminary tests, five stress levels were chosen for the tests on each alloy. However, as the experimental work progressed it was found that the dispersion of the data for the 75S-T6 unnotched specimens was so large at the lowest stress level that it was not possible to obtain significant results with a reasonable number of specimens. Accordingly, the data for this alloy do not go beyond about 10^6 cycles.

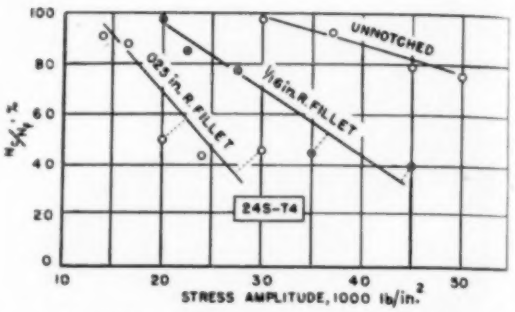

FIGURE 6. *Effect of stress amplitude on the proportion of the total life required to initiate a crack in 24S-T4 specimens.*

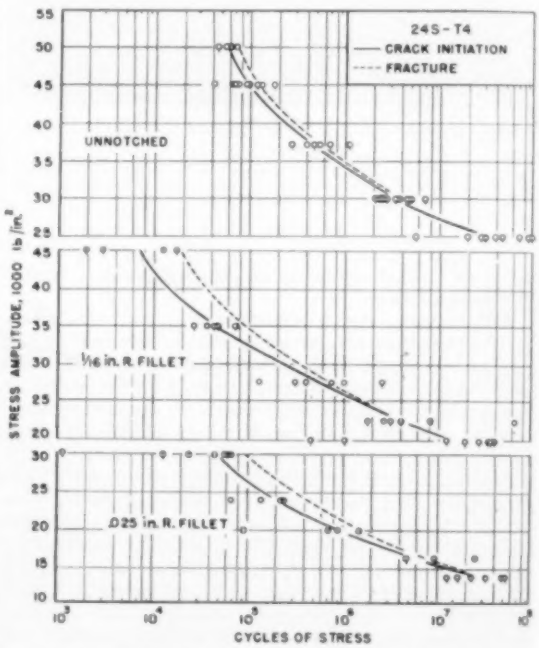

FIGURE 7. *S-N curves for 24S-T4 specimens.*

The data points and the solid curves represent the number of cycles for crack initiation. A short vertical line below a point indicates that the value of N_c was obtained from N_f by using crack-growth data from other specimens.

Figures 7, 8, and 9 show the N_c data for the three alloys. The trend of the data for the number of cycles to fracture is shown by the dashed lines. The short vertical lines below some of the data points indicate that the cracks in these specimens were relatively large when first observed, or that the specimen was run to fracture without stopping, so that the N_c values plotted were obtained by extra-

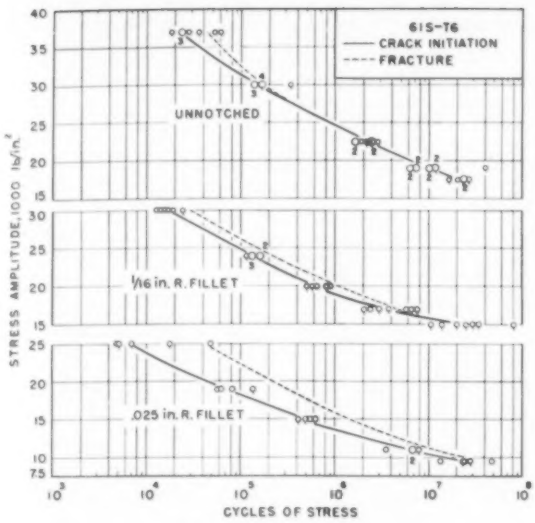

FIGURE 8. *S-N curves for 61S-T6 specimens.*

See figure 7 for explanation of symbols.

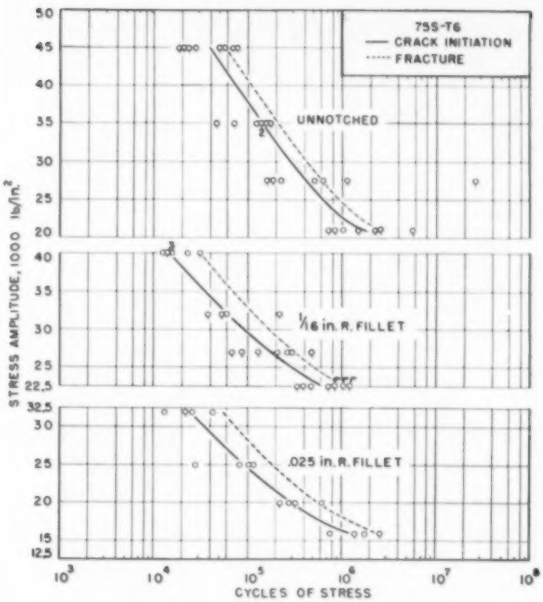

FIGURE 9. *S-N curves for 75S-T6 specimens.*

See figure 7 for explanation of symbols.

polation, using other crack-growth data. The number of cycles for fracture of each specimen is listed in table 3. The number of specimens listed in this table at each stress level does not correspond in all cases to the points on the graphs of figures 7 to 9 because of the specimens mentioned above, which were removed from the fatigue machine after the first observation of the crack and extended under static load. These specimens are represented by a point on the graph, but no fracture value is available.

In tests of the type B (1/16-in.-radius fillet) specimens of 75S-T6, some difficulty was experienced with specimens breaking in the straight section rather than at the fillet. This was not eliminated by careful smoothing of the straight section. If a crack was found in the fillet after this type of fracture, the extrapolated value of N_c was obtained in the usual way. If no crack was found in either fillet, it was obvious that N_c for that specimen had not been attained. Data from these specimens could be used in determining the median if the number of cycles actually run was larger than the median, otherwise they had to be disregarded. Data of this type that were used are indicated in figure 9 by the conventional symbol for a specimen that did not break. All fractures occurred in the fillets in both of the other alloys.

The median N_c values are plotted in figures 10, 11, and 12 in the manner suggested in reference [10]. In some cases the data plotted in this way lie more nearly on a straight line than in the conventional plot, thus facilitating interpolation. In other cases there is no advantage, but for the sake of consistency, all determinations of notch sensitivity were based on the curves of figures 10 to 12.

The fatigue-strength reduction factors for the two types of specimens of each of the three alloys are shown in figure 13. The notch sensitivity, q, was computed by using these data and values of theoretical stress-concentration factor obtained from the graphs of reference [5]. These data are listed in table 4 and shown in figure 14.

Because of the widespread current interest in the statistical characteristics of fatigue data [11], consideration was given to the significance of the dispersion of results presented here. It should be pointed out that the measurement of N_c, unlike that of N_f, is not precise for a given specimen. As there was no way to separate the error of measurement from the inherent variability from specimen to specimen, it was not thought worthwhile to make any extensive quantitative analysis of the dispersion of N_c.

However, it was thought that a reasonable comparison between the three materials could be obtained by considering the data for unnotched specimens at all stress levels. This was done by comparing each value of N_c with the median for that stress level. The results were as follows:

24S-T4: 50% of the data were within 34% of the median N_c values.
61S-T6: 50% of the data were within 12% of the median N_c values.
75S-T6: 50% of the data were within 76% of the median N_c values.

TABLE 3. *Results of fatigue tests*

Unnotched		⅛-in.-radius specimen		0.025-in.-radius specimen	
Stress amplitude	Cycles to fracture	Stress amplitude	Cycles to fracture	Stress amplitude	Cycles to fracture
24S-T4 SPECIMENS					
lb/in.²		*lb/in.²*		*lb/in.²*	
50,000	90×10³	45,000	14×10³	30,000	73×10³
	75		31		105
	75		15		91
	65		25		125
45,000	61	35,000	133	24,000	490
	121		115		308
	144		82		485
	150		98		419
	103		98	20,000	1,659
	103		90		1,677
	91	27,500	2,812		782
	162		1,194		2,571
	215		513	16,500	6,607
37,000	1,209		906		11,860
	516		532		31,957
	730		490		19,618
	521	22,500	2,563	14,000	16,306
	551		3,445		58,059
	446		5,047		39,774
	3,052		70,964		59,049
	7,405		9,381		20,812
	4,900		3,919		
	3,714	20,000	29,865		
30,000	4,105		39,624		
	2,677		38,223		
	2,301		43,721		
	5,296		1,763		
	2,621		13,774		
	101,622		988		
	6,000		21,566		
	76,395				
	39,832				
25,000	49,328				
	42,978				
	29,139				
	98,382				
	22,024				
61S-T6 SPECIMENS					
	69×10³		37×10³		74×10³
	76		29	25,000	53
	51	30,000	30		33
37,000	43		32		31
	37		27		393
	36		39	19,000	372
	47		223		316
	34		231		194
	163	24,000	190		1,452
	187		197	15,000	1,419
	352		230		946
30,000	156		183		1,543
	186		1,349		14,176
	174		1,017	11,000	11,844
	176	20,000	1,031		16,617
	163		1,212		9,986
	2,979		1,351		42,806
	2,482		8,342	9,500	27,743
	2,205		4,712		37,783
22,500	2,762		2,462		54,412
	2,838	17,000	2,996		
	2,803		3,882		
	2,038		6,548		
	2,050		7,291		
	11,669		35,806		
	12,181		27,333		
	51,145	15,000	82,428		
	11,955		31,269		
19,000	7,492		21,852		
	11,053		12,337		
	7,322		16,096		
	7,820				
	7,714				
	27,635				
	24,127				
17,500	27,042				
	20,101				
	24,597				

TABLE 3. *Results of fatigue tests*—Continued

Unnotched		⅛-in.-radius specimen		0.025-in.-radius specimen	
Stress amplitude	Cycles to fracture	Stress amplitude	Cycles to fracture	Stress amplitude	Cycles to fracture
75S-T6 SPECIMENS					
lb/in.²		*lb/in.²*		*lb/in.²*	
45,000	34×10³	40,000	49×10³	32,000	54×10³
	90		30		60
	87		26		43
	64		39	25,000	164
	32		40		184
	74		34		179
	36		73	20,000	231
	41	32,000	421		626
35,000	136		107		517
	233		104		1,254
	195		96	16,000	420
	221		726		2,147
	111		132		2,109
	199		104		4,479
	210	27,000	316		2,850
	1,356		196		
27,500	26,392		434		
	389		408		
	260		469		
	354		994		
	798		662		
	838	22,500	540		
	1,377		1,093		
	2,626		811		
21,000	2,857		1,212		
	6,240				
	1,179				
	1,836				

TABLE 4. *Strength-reduction factors and values of notch sensitivity*

Cycles	K_f		$q=(K_f-1)/(K_t-1)$	
	$K_t=1.40$	$K_t=1.79$	$K_t=1.40$	$K_t=1.79$
24S-T4				
50×10³	1.43	1.73	1.07	0.92
100	1.41	1.72	1.02	.92
500	1.37	1.74	0.93	.91
1,000	1.34	1.74	.87	.94
5,000	1.32	1.74	.82	.94
10,000	1.31	1.74	.79	.94
20,000	1.30	1.74	.75	.94
61S-T6				
50×10³	1.27	1.72	0.68	0.91
100	1.28	1.71	.70	.90
500	1.27	1.72	.68	.91
1,000	1.27	1.75	.68	.95
5,000	1.22	1.79	.58	1.00
10,000	1.19	1.79	.48	1.00
20,000	1.15	1.80	.38	1.01
75S-T6				
50×10³	1.29	1.53	0.73	0.67
100	1.26	1.51	.65	.65
500	1.18	1.47	.45	.60
1,000	1.12	1.41	.30	.52

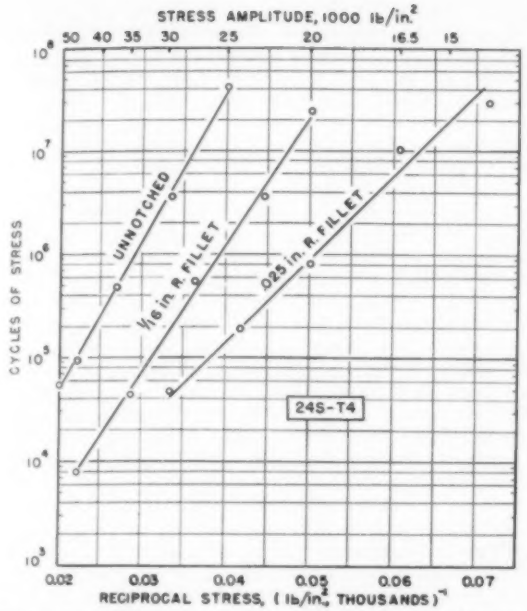

FIGURE 10. *Median N_c values for 24S-T4 plotted as a function of reciprocal stress.*

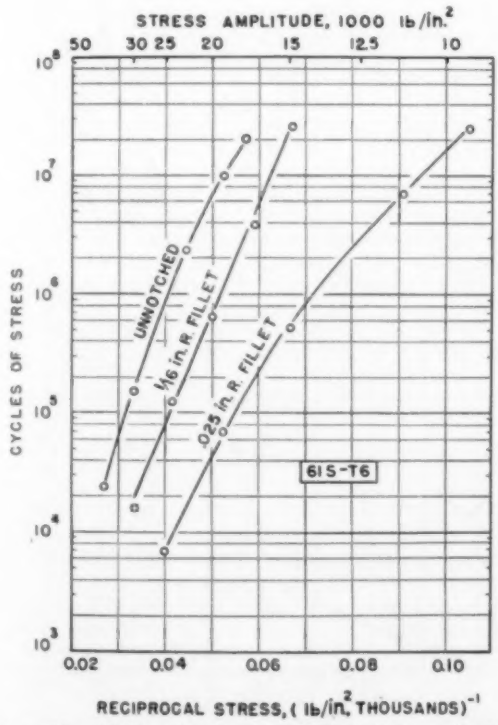

FIGURE 11. *Median N_c values of 61S-T6 plotted as a function of reciprocal stress.*

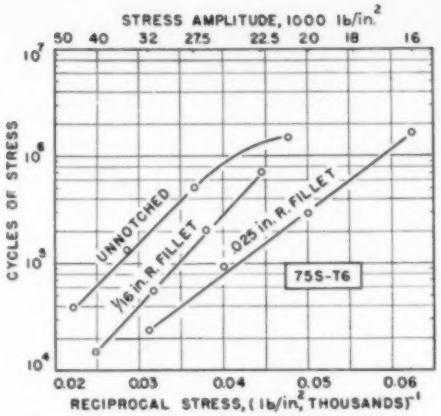

FIGURE 12. *Median N_c values for 75S-T6 plotted as a function of reciprocal stress.*

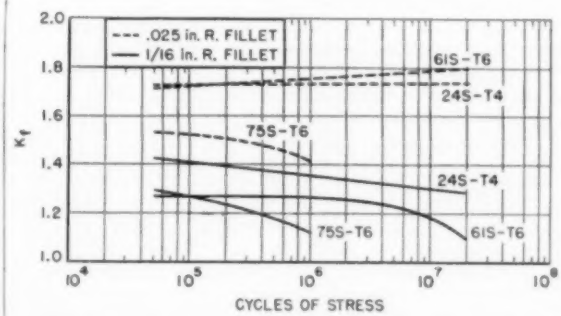

FIGURE 13. *Variation of fatigue strength reduction factor K_f with N_c.*

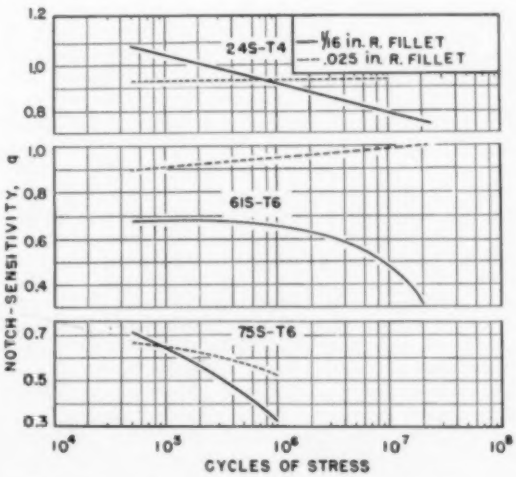

FIGURE 14. *Variation of notch sensitivity, q, with N_c.*

The Statistical Engineering Section of the NBS made a more rigorous statistical analysis of these same data and found that after eliminating one extreme value for each of the three materials, they all passed the homogeneity of variance test. That is, the variances at the different stress levels for each metal do not exhibit any more scatter than would be expected by chance in a sequence of estimates of a single variance. This analysis gave the following results regarding the dispersion of all the data for a given material.

Alloy	Standard deviation of log N_c
24S-T4	0.194
61S-T6	.123
75S-T6	.283

As these data were obtained under essentially identical conditions, the figures above should give a fair representation of the relative variability of the fatigue properties of the three alloys.

It has been suggested [12] that fatigue data are more nearly normally distributed with regard to log N than with regard to N, and that consequently the mean of log N is the most desirable representation of a group of data. Several groups of the results obtained in the present investigation were analyzed in this way, but it did not appear to give significantly different results from the median. As this method of analysis did not permit the use of the results from specimens that broke away from the fillets, it was abandoned.

An attempt was also made to analyze the data from the filleted specimens by considering each fillet as a separate specimen and treating the data on a "weakest of two" basis. Again, no significant change in the overall results was noted.

It has been pointed out [13] that there should be a correlation between the dispersion of the number of cycles to failure in fatigue tests and the dispersion of the location of the fatigue-crack nucleus relative to the point of maximum stress. It was felt that some information on the latter dispersion would be of value in studying the effect of microstructure on fatigue behavior. Accordingly, the positions of the origins of the cracks, relative to the point of maximum stress, were determined for about two-thirds of the fractured smooth specimens, selected at random. The three materials were compared on the basis of the proportion of cracks starting at points where the stress was less than 98 percent of the maximum, as follows:

Alloy	Percentage of crack origins at less than 98% of S_{max}
24S-T4	8
61S-T6	6
75S-T6	22

It was also noted that no cracks started in 24S or 61S specimens at points where the stress was less than 96 percent of the maximum, whereas about 10 percent of the 75S specimens had cracks starting where the stress was 90 percent or less. Thus the data on location of fracture verify the conclusion that the 75S-T6 is more inhomogeneous than the other alloys as regards resistance to fatigue.

The locations of the fatigue-crack nuclei were also determined on about a quarter of the filleted specimens by measuring, on a toolmakers microscope, the angle between the axis of the specimen and the surface of the fillet at the origin of the crack. The accuracy of this measurement was probably only fair, particularly on the small radius specimens, but the results are thought to be of some value. No significant difference could be noted between the distribution of locations for different materials or for different stress levels. Accordingly, the data for all specimens of a given fillet radius were grouped together, and the resulting distribution curves are shown in figure 15. There appears to be a definite tendency for the cracks to occur at larger angles in the small-radius specimens.

These distribution curves provide a basis for comparing the areas in which the stress is sufficiently high to initiate fracture in the different specimens. The data discussed above showed that for the 24S-T4 and 61S-T6 smooth specimens, about 93 percent of the cracks were initiated at points where the stress was 98 percent of the maximum or greater. These points were in an area extending 0.09 in. each side of the center. Using the curves of figure 15 to determine the arc length in the fillets in which 93 percent of the cracks would be expected to occur, it is possible to compare the "critically stressed area"

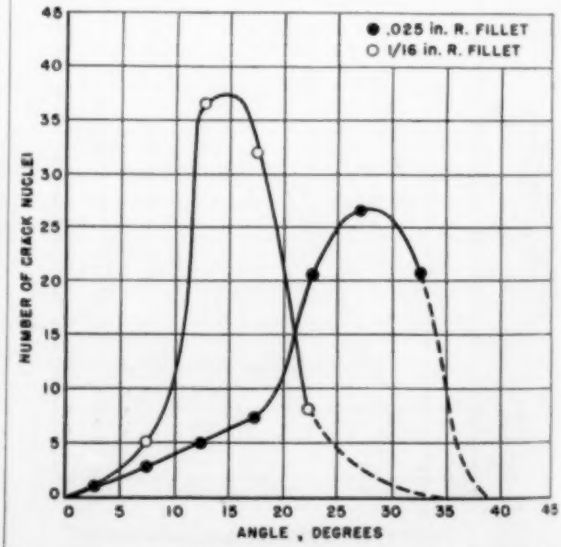

FIGURE 15. *Variation in number of crack nuclei with angle between specimen axis and tangent to the surface.*

in the three types of specimens. The ratios obtained are as follows:

Specimen type	Relative critically stressed area
Smooth	100
1/16-in. radius	22
0.025-in. radius	14

On the same relative basis, the area of the straight section of the filleted specimens is 550.

Two decided differences will be noted between the trends of the notch-sensitivity data obtained in this work and most of those previously reported in the literature. First, the value of q for some of the test conditions is close to unity, while many of the previously available data show lower values. Second, more than half of the curves in figure 14 show that q decreases with increasing number of cycles to failure, which is opposite to that often found.

The explanation for the first discrepancy probably lies in differences in the methods of specimen preparation mentioned in the introduction. If the methods used were such that the surface of notched specimens was more severely cold-worked than that of the unnotched specimen, the resultant value of q would be lower than the value obtained from specimens having comparable surface preparation. The second discrepancy, that in the variation of q with stress level, can be explained in part on the basis of the divergence between the number of cycles to fracture and the number of cycles to initiate a crack. The curves of figures 7 to 9 show that in general the proportion of the life required for the crack to grow to fracture increases with the stress amplitude and with the sharpness of the notch. Therefore, in tests run to fracture there will be less difference in fatigue strength between smooth and notched specimens than in tests based on N_c, particularly at high stress levels. In order to get an idea of the magnitude of this effect, the notch sensitivity was computed on the basis of N_f, and it was found that for the sharper notch, q did increase with increasing number of cycles to failure in the tests of 24S-T4 and 61S-T6. However, for the mild notch the reverse was true. The values for 75S-T6 specimens for both notches were approximately constant at a notch sensitivity of about 0.5.

In attempting to explain the behavior shown on figure 14, one naturally starts with the observation that 3 of the 6 curves lie close to a q value of unity over most of their length. It is convenient, therefore to assume that this is the normal expectancy, and that it is the deviations from this behavior that require explanation. It should be noted that the values of K_t used in the computation of q were based on the maximum principal stress in the fillet, so the above assumption is equivalent to saying that the normal criterion for failure in fatigue is the maximum principal stress.

The notch sensitivity of the 75S-T6 alloy was well below that of the other materials in both types of specimens. In considering the possible reasons for this, certain other differences between the behavior of this alloy and the lower strength ones appeared significant. These were:

1. The ratio of the fatigue to static strengths was lower in 75S-T6, as shown below. (The fatigue strengths used are those of the unnotched specimens at 10^6 cycles.)

Alloy	Fatigue strength / Yield strength	Fatigue strength / Tensile strength
24S-T4	0.60	0.46
61S-T6	.60	.50
75S-T6	.32	.27

2. As mentioned above, some of the 75S specimens with the 1/16-in.-radius fillets broke in the straight section rather than at the fillet.

3. The dispersion of N_c values for the smooth specimens was greater in this alloy.

4. Difficulty was experienced in polishing the 4-in.-radius specimens, in that small pits were sometimes found after the standard polishing procedure. Also some specimens that appeared satisfactory after polishing were found to have pits at the origin of the fatigue crack.

Because it appeared that the above differences could be explained by the presence of a relatively few weak or brittle particles randomly distributed in the 75S alloy, an attempt was made to observe the microstructures at the origins of the fatigue cracks in this alloy. Several specimens were sectioned transversely and repeatedly ground and polished to permit examination through these regions of origin. One specimen, which was polished with diamond abrasive, contained a particle of the chromium segregate very near the origin of the fatigue crack, as shown in figure 16. This indicates that the segregate particles, if they occur at the surface, may break out, leaving pits that would serve as stress raisers.

On the basis of these observations, a qualitative explanation of the behavior of 75S-T6 may be proposed; assume that the specimen is composed of a large number of unit volumes that are identical except in the orientation of the direction of greatest strength in the volume relative to the applied stress. The stress required to start a fatigue crack in a given volume then would depend only on this orientation, and in a homogeneous material the distribution of the fatigue strengths of the individual volumes for a given stress direction would have a sharp cutoff, something like that shown in figure 17, and there would be no volumes whose strength was less than some minimum value, S_0. In a smooth specimen a

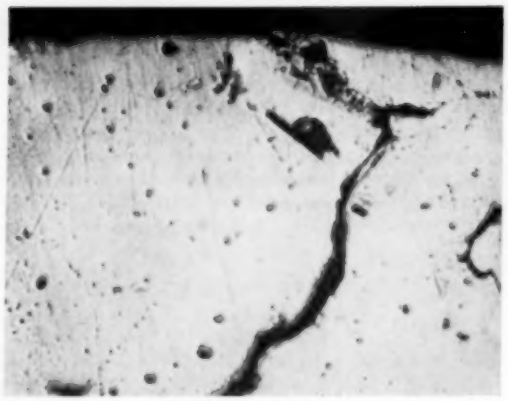

FIGURE 16. *Segregate particle associated with a fatigue crack very near its origin in a specimen of 75S-T6.*

Unetched, × 250.

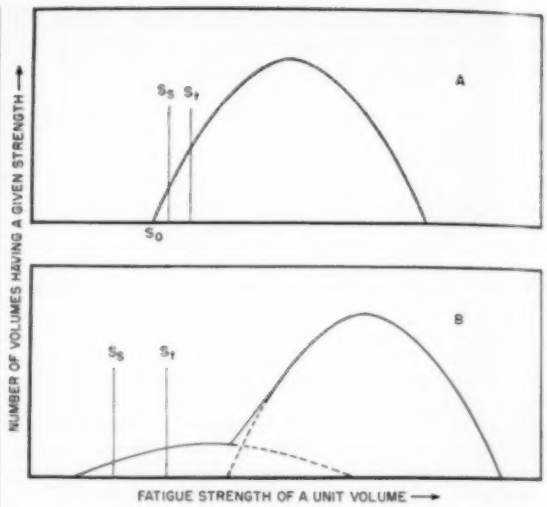

FIGURE 17. *Hypothetical distribution of the strengths of unit volumes of a homogeneous material (A) and one having internal defects (B).*

large number of unit volumes are subjected to a high stress. If this number is M_s, then the strength of the weakest volume in the specimen would be expected to be that represented by a stress value (S_s in fig. 17, A) which would cut off $1/M_s$ of the area under the curve. In a notched specimen the number of unit volumes to which high stress is applied is smaller, M_t, and the expected fatigue strength would cut off $1/M_t$ of the area (S_t in fig. 17,A). The nominal fatigue strength of the notched specimen is equal to S_t divided by the theoretical stress-concentration factor, K_t. The fatigue strength reduction factor would be given by $K_f=(S_sK_t)/S_t$, and as S_s and S_t are close together, it would be expected that K_f would be nearly as large as K_t.

In a material having internal stress raisers, one would no longer expect a simple distribution of strengths. Each volume adjacent to one of these stress raisers would have its effective strength decreased, so these volumes would represent a second population, whose strength distribution is shown schematically by the lower curve in figure 17,B. The resultant total distribution would have a much longer tail than that of a homogeneous material. If we determine S_s and S_t for this distribution as we did for the first case, the difference between them is much greater than before, so that the strength-reduction factor would be smaller than that of the homogeneous material.

This qualitative discussion is, of course, oversimplified, but similar considerations can be used to explain the fact that only 75S-T6 filleted specimens broke in the straight section, where the stress is only 71 percent of the maximum in the fillet. The tail of the inhomogeneous distribution apparently extends far enough down to intercept a stress value 71 percent of S_t, but that of the homogeneous distribution does not.

The suggested explanation of the observed fatigue characteristics of 75S-T6 is obviously not the only possible one.[2] It appears to be the simplest hypothesis on which to base further experiments, and is offered with that in mind.

The other curve in figure 14 which was not close to unity was that for 61S-T6 in the 1/16-in.-radius specimen. No cause for this anomaly was apparent, but the effect of grain size has not been considered, and this is reported to have an effect on notch sensitivity [14].

An interesting characteristic of the data from all materials is noted if the K_f values for the two filleted specimens are compared; the values in the table below are the ratios of the strength-reduction factors for the 1/16-in.-radius specimens to those for the 0.025-in.-radius specimens.

Alloy	K_{f1}/K_{f2} at the indicated number of cycles, N_c		
	10^5	10^6	10^7
24S-T4	0.82	0.77	0.75
61S-T6	.75	.73	.66
75S-T6	.83	.79	----

Again, no adequate explanation for the decrease of the ratio with increase in N_c can be offered, but the trend is surprisingly consistent.

[2] Information has been received that the 75S-T6 cold-finished drawn rod used in this investigation was from a lot produced by an ingot practice that differed from that of the other alloys. This special practice was used for only a short period at the plant that produced this rod.

4. Summary

The notch sensitivities of three aluminum alloys, 24S-T4, 61S-T6, and 75S-T6, for two different notches were evaluated on the basis of the number of cycles to initiate a fatigue crack in a rotating-beam test. The values for 61S-T6 in the sharp notch and for 24S-T4 were close to unity, indicating that in these cases the maximum stress was the criterion for failure. 75S-T6 showed low values of notch sensitivity, and it is suggested that this may be due to inhomogeneity of the alloy, which would be expected to lower the fatigue strength of smooth specimens more than that of notched specimens.

The dispersion of the data for unnotched specimens was the smallest for 61S-T6 and greatest for 75S-T6.

The proportion of the total life required for a fatigue crack to grow to fracture increased with increasing stress and with increasing notch severity.

The experimental work during the early part of this investigation was conducted by James L. Baker.

5. References

[1] R. L. Templin, F. M. Howell, and E. C. Hartmann, Effect of grain direction on fatigue properties of aluminum alloys, Product Eng. (July 1950).

[2] Paul Kuhn and Herbert F. Hardrath, An engineering method for estimating notch-size effect in fatigue tests on steel, NACA Tech. Note 2805 (October 1952).

[3] H. Neuber, Theory of notch stress—principles for exact stress calculation (J. W. Edwards Brothers, Inc., Ann Arbor, Mich., 1946).

[4] C. S. Yen and T. J. Dolan, A critical review of criteria for notch sensitivity in fatigue of metal, ONR Progress Report 13, Project NR–031–005 (Engineering Experiment Station, Univ. of Illinois, 1949).

[5] R. E. Peterson, Design factors for strength calculations for stress concentration cases, Scientific Paper 1540, p. 27 (Westinghouse Research Laboratories, East Pittsburgh, Pa., Oct. 1950).

[6] J. A. Bennett, A study of the damaging effect of fatigue stressing on SAE X4130 steel, J. Research NBS **37**, 133 (1946) RP1733.

[7] Manual on fatigue testing, Am. Soc. Testing Materials, STP No. 91 (1949).

[8] F. Keller, Metallography of Alcoa 75S alloy, Iron Age (Oct. 4, 1945).

[9] J. A. Bennett, Early detection of cracks resulting from fatigue stressing, NACA Bul. **41**, 15 (Sept. 1944).

[10] J. A. Bennett and James L. Baker, Effect of prior static and dynamic stresses on the fatigue strength of aluminum alloys, J. Research NBS **45**, 455 (1950) RP2157.

[11] Symposium on fatigue with emphasis on statistical approach, Am. II, Soc. Testing Materials, STP 137 (1953).

[12] G. M. Sinclair and T. J. Dolan, Effect of stress amplitude on statistical variability in fatigue life of 75S–T6 aluminum alloy, Trans. ASME (July 1953).

[13] F. A. McClintock (unpublished report).

[14] R. W. Karry and T. J. Dolan, Influence of grain size on fatigue notch sensitivity, (Office of Naval Research, U. S. Navy, June 1952), ASTM Preprint 72 (1953).

Washington, November 5, 1953.

Journal of Research of the National Bureau of Standards Vol. 52, No. 5, May 1954 Research Paper 2496

Compressibilities of Crystalline and Glassy Modifications of Selenium and Glucose[1]

Charles E. Weir

Data are reported for the compression of selenium and α-glucose in both glassy and crystalline modifications at 21° C between 1,000 and 10,000 atmospheres. The compressibilities of the glassy form were found to be considerably larger than those of the crystals. A transition of unknown origin was observed to occur in glassy glucose between 7,000 and 8,000 atmospheres.

1. Introduction

It has been observed that the expansivity, α, of the glassy form of a given material is nearly equal to that of the crystalline form [1].[2] This agreement in expansivities appears to be the basis from which recent ideas concerning the nature of the glass transition and the changes that occur at the transition temperature, T_g [1, 2] are derived. As many second-order thermodynamic quantities appear to change discontinuously at T_g, this frequently has been denoted a second-order transition temperature. The expansivity is one of the quantities that changes markedly at T_g, being smaller for the glassy material than for the rubbery or liquid modification that exists at temperatures above T_g [1, 3].

It is believed that the isothermal compressibility, β, in analogy with expansivity, also changes discontinuously at T_g [1], but a recent report [4] indicates that most evidence for such a discontinuity in β is inconclusive. As expansivities of crystalline and glassy forms are about equal, the question arises whether the same is true of β. Compressibility data on glasses [3] show that the compressibility is high and varies rapidly but "irresponsibly" with temperature. Data covering any appreciable pressure range in which values for glassy and crystalline modifications can be compared, however, do not appear to be available. This report describes compression measurements at 21° C on two materials, selenium and glucose, in glassy and crystalline modifications. A considerable difference in compressibility of the two forms was observed over the whole pressure range (maximum 10,000 atm). A reversible first-order transition of unknown origin was observed in glassy glucose at about 7,000 atm.

2. Experimental Method

The experimental procedure used has been described in detail [5] and will not be discussed here. The only departure from previous techniques was in the use of a steel cylinder that was open at one end, to contain the glassy glucose, and containers made of thin polyethylene film for the other materials. Both types of containers were open to the confining liquid to permit application of hydrostatic pressure to the specimens. In each case the data were corrected for the compression of the corresponding container.

Specimens were prepared as follows:

Selenium.—Commercially available selenium was placed in a thick-walled glass tube, which was then evacuated and sealed off under vacuum. The evacuated tube and its contents were heated at 400° C for several hours cooled in air to approximately 200° C, and water-quenched. For glassy selenium specimens the tube was broken and the specimen removed. Such specimens exhibited the typical conchoidal fractures characteristic of glasses and were soluble in carbon disulfide [6]. For crystallization to the metallic form, the tube was not broken after quenching but reheated to 100° C for 2 weeks [7]. Such specimens on removal from the tube were not extractible with carbon disulfide and showed no conchoidal fractures.

Glucose.—Pure α-dextrose was melted carefully in a glass tube. When the material was cooled, no crystallization took place, and such specimens were used for glassy-state measurements. Crystalline specimens were obtained by seeding the glassy melt and permitting crystallization to take place. Crystallization was very slow, requiring several weeks to go to completion. Cylindrical crystalline specimens were obtained by breaking the glass container.

3. Results and Discussion

Compression data on the glucose and selenium specimens are shown in table 1 and figures 1 and 2. Each value given in the tables represents the average of two measurements made on different specimens. Agreement between duplicates was in general reasonably close in the last significant figure, but on occasion differences larger than the estimated reproducibility of ± 0.0004 in $\Delta V/V_o$ were obtained. Negative values shown at the two lower pressures arise from the use of 2,000 atm as the fiducial pressure. The values between 1 and 1,000 atm were obtained by successive approximations and are not measured values [5]; small changes in these values will have a negligible effect on the other data. The tabular data show that the glassy material is considerably more compressible than the crystalline form. This is also shown by the graphs, in which it is observed that this higher compressibility (the slope of

[1] This work was sponsored by the Office of Naval Research, Department of the Navy.

[2] Figures in brackets indicate the literature references at the end of this paper.

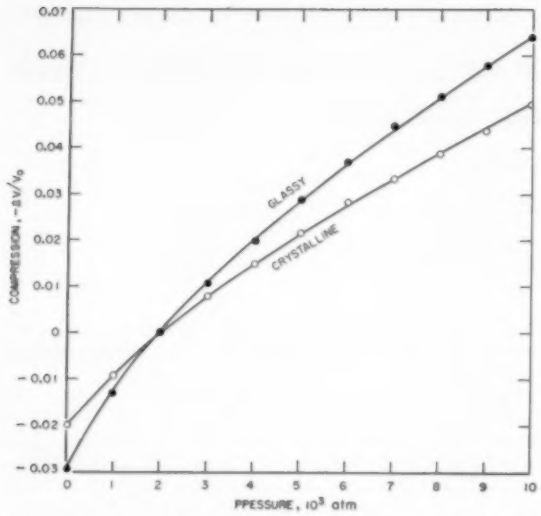

FIGURE 1. *Compression of glassy and crystalline selenium at 21° C.*

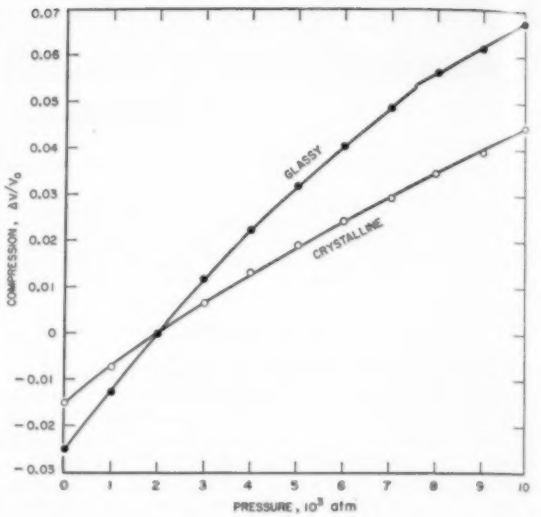

FIGURE 2. *Compression of glassy and crystalline α-glucose at 21° C.*

TABLE 1. *Compression of selenium and α-glucose at 21° C*

[Compression, $-\Delta V/V_0$]

Pressure	Selenium		α-Glucose	
	Crystalline	Glassy	Crystalline	Glassy
atm				
10,000	0.0494	0.0643	0.0448	0.0674
9,000	.0438	.0580	.0392	.0620
8,000	.0389	.0513	.0345	.0562
7,000	.0334	.0448	.0296	.0487
6,000	.0284	.0370	.0240	.0404
5,000	.0219	.0288	.0188	.0318
4,000	.0151	.0201	.0130	.0222
3,000	.0079	.0106	.0064	.0115
2,000	.0000	.0000	.0000	.0000
1,000	−.0093	−.0130	−.0074	−.0128
1	−.0200	−.0290	−.0150	−.0250

the curve) is not confined to the lower pressures but extends over the whole pressure range.

On the basis of present concepts [1, 2, 3], the glassy state contains essentially a frozen-in, liquid-like structure of such high viscosity that thermal readjustments are not possible in experimentally realizable time intervals. Therefore, the higher compressibility of the glass is to be anticipated. The compressibility of liquids is in general considerably greater than that of crystalline solids [8]. The difference is probably to be attributed to both the greater "free" volume of the liquid and a less orderly structure, with correspondingly less well-organized intermolecular forces. A glassy solid will then contain at least a greater free volume than the corresponding crystalline form, and its compressibility, therefore, will be the larger. In all probability, similar considerations apply to the intermolecular forces, which Bridgman [8] believes are intimately involved in this pressure range. In confirmation of this, a sample calculation shows that at 10,000 atm the specific volume of the glucose glass is considerably less than that of the crystalline material at 1 atm, yet its compressibility appears to be comparable to that of the crystals at 1 atm.

In figure 2 a discontinuity is shown between 7,000 and 8,000 atm. This is a reversible transition apparently involving a small discontinuity in volume and an associated latent heat. Several experiments were performed to establish the existence and reversibility of this transition, and a brief description of the phenomena involved may be of interest.

In these experiments, measurements are made on decompression [5], with the pressure being reduced in 1,050-atm steps. With attainment of thermal equilibrium after decompression, the pressure is raised again as closely as possible to the desired value. This process is followed to obtain reproducible motion of packing washers, etc. On decompression, the contents of the vessel are cooled, and a time interval ensues before thermal equilibrium is reattained. During this interval, heat is absorbed by the vessel and its contents and, as a result, the pressure rises. This "pressure regain" depends on factors such as pressure, compressibility of specimens, rate of decompression, etc., but for closely controlled conditions does not vary to a large degree. In these experiments a regain of approximately 15 to 20 atm is the rule. Any process that occurs on decompression involving appreciable thermal effects will cause an anomalous pressure regain and is readily noted because the pressure measurement is

quite sensitive. In these experiments the pressure regain in the interval noted was 2 to 3 times as great as those observed at higher and lower pressures, indicating a latent-heat phenomenon in the interval. This is shown in figure 2 by the discontinuity in volume, although no effort was made either to fix its pressure accurately or to measure the amount of discontinuity.

The phenomenon described cannot represent a crystallization of the glassy form for three reasons: no crystals are visible after a compression measurement; the process is reversible; and densities of specimens agreed to better than 1 part in 10,000 before and after compression. No explanation for the processes involved will be offered. It may be noted that the product formed at higher pressures is shown by figure 2 to be considerably less compressible than its low-pressure modification. A statistical study of the experimental data indicates that this effect may be real, but a definite conclusion cannot be made with certainty.

Previous data have been reported for the compression of these materials. Bridgman [9] has reported data on selenium (Se) to 50,000 kg/cm^2, which were apparently made on glassy Se. However, Bridgman [9] reports that in calculations the density of Se used was probably too high. Data for glassy Se reported here are in only fair agreement with Bridgman's data. Tammann and Jellinghaus [10] reported data for glassy Se to a maximum pressure of approximately 2,000 atm. Their measured value of $-\Delta V/V_0$ is approximately 0.039 at this pressure as compared with the 0.029 arrived at here and a graphical value of approximately 0.027 obtained from Bridgman's data [9]. Bridgman has also reported values for "dextrose" (d-glucose) [11] that are somewhat smaller than those obtained here. This difference may only be apparent however, as Bridgman [11] notes that his values are probably slightly too low, and it is also possible that his measurements were made on anhydrous material. In the measurements made here, the volume of the specimen was measured after compression, and it alone determined V_0. Densities calculated from this volume were lower than accepted values, probably as a result of occluded voids. This in no way affects the validity of the value of V_0.

4. References

[1] W. Kauzmann, Chem. Rev. **43**, 219 (1948).
[2] R. O. Davies and G. O. Jones, Proc. Roy. Soc. **217,** 26 (1953).
[3] G. W. Morey, The properties of glass (Reinhold Publishing Corp., New York, N. Y., 1938).
[4] C. E. Weir, J. Research NBS **50,** 311 (1953) RP2420.
[5] C. E. Weir, J. Research NBS **45,** 468 (1950) RP2160.
[6] J. W. Mellor, Comprehensive treatise on inorganic and theoretical chemistry, vol. X (Longmans, Green, and Co., New York, N. Y., 1930).
[7] S. R. Das and K. Das Gupta, Nature **143,** 165 (1939).
[8] P. W. Bridgman, The physics of high pressure (G. Bell & Sons, Ltd., London, 1949).
[9] P. W. Bridgman, Proc. Am. Acad. Arts Sci. **74,** 21 (1940).
[10] G. Tammann and W. Jellinghaus, Ann. Physik **394,** 269 (1929).
[11] P. W. Bridgman, Proc. Am. Acad. Arts Sci. **76,** 9 (1945).

Washington, December 8, 1953.

Journal of Research of the National Bureau of Standards Vol. 52, No. 5, May 1954 Research Paper 2497

Atypical pH Response of Some Nonsilicate Glasses

Herman F. Shermer, Gerald F. Rynders, Given W. Cleek, and Donald Hubbard

It is generally believed that a glass, in order to yield electrodes whose voltage characteristics serve as a satisfactory indicator of the hydrogen-ion activity of aqueous solutions in accord with the dictates of the Nernst equation, must possess at least a minimum hygroscopicity and an adequate chemical durability, uniform over an extended pH range. Three series of nonsilicate glasses, Na_2O-MgO-P_2O_5, Na_2O-GeO, and BaO-B_2O_3, were investigated for these three properties. In accord with the fact that all of the members of these series exhibited very poor chemical durability and many of them possessed very low hygroscopicity, none of them produced electrodes that had a satisfactory pH response. All of the series confirmed the generally accepted fact that hygroscopicity cannot be directly correlated with chemical durability of glasses. For example, some members of the BaO-B_2O_3 series possessed hygroscopic properties that compared favorably with Pyrex 7740, yet had unusually poor chemical durability.

1. Introduction

The question is often asked, "Is the presence of a silicate framework necessary in order that a glass may yield electrodes that possess satisfactory voltage response to hydrogen-ion activity of aqueous solutions?" Certainly, not all silicate glasses possess this interesting and useful characteristic. In fact, considerable evidence indicates that only those silicate glasses that have adequate hygroscopicity and uniform chemical durability over an extended pH range produce electrodes that approximate the dictates of the Nernst equation [1, 2, 3].[1] These past experiments indicate in a general way that these features of adequate hygroscopicity and satisfactory chemical durability may be of more significance than the particular chemical constituents of the electrode glass in determining the suitability for use in pH measurements. With these features in mind, the following limited series of glasses containing no SiO_2 were examined for their pH response: Soda-magnesia-phosphate (Na_2O-MgO-P_2O_5); soda-germania (Na_2O-GeO_2); and baria-boric oxide (BaO-B_2O_3).

2. Experimental Procedures

The experimental procedures followed in this investigation for chemical durability (surface alteration by an interferometer method [2, 4]), hygroscopicity (water sorbed, mg/cm^2 [3, 4]), and pH response (mv/pH [4]) were generally similar to those reported in earlier publications on silicate glasses. Such special alteration of procedures as were dictated by the nonsilicate glasses are mentioned in the text for those experiments in which changes were required.

As it was impossible to fuse phosphate mixtures in platinum without destruction of the crucible, the Na_2O-MgO-P_2O_5 glasses were prepared in a special zirconia (ZrO_2)-lined fire-clay crucible adopted for the purpose by Douglas H. Blackburn and Louis G. Cossette. The zirconia liner minimized objectionable contamination of the melts, which in turn greatly improved the spectral transmittance of the resulting glasses to ultraviolet light.

The Na_2O-GeO_2 glasses were melted and fined in a platinum crucible. No glasses were obtainable for 60 percent and 70 percent of GeO_2. Furthermore, the glasses near 85 percent and 90 percent of GeO_2 exhibited a strong tendency to devitrify, even on rapid chilling of the melts, whereas those above and below this region showed less tendency to do so.

The BaO-B_2O_3 series of glasses was also prepared in platinum. The compositions produced included the entire glass-making range for this binary system.

3. Results and Discussion

3.1. Na_2O-MgO-P_2O_5 Glasses—Chemical Durability, Hygroscopicity, and pH Response

Table 1 and figures 1, 2, 3, and 4 illustrate the chemical durability, hygroscopicity, and pH response of a series of Na_2O-MgO-P_2O_5 glasses compared with Corning 015 electrode glass, Pyrex 7740 (a glass of low hygroscopicity), and a P_2O_5 glass.[2] The chemical durabilities of these phosphate glasses (fig. 1) are markedly different in magnitude and in kind from the various series of silicate glasses previously studied. Each of the present glasses was attacked vigorously at all pH values, and none of them exhibited swelling in acid buffers, as was so characteristic of many of the silicate glasses [2, 4]. This indicates there was no preferential leaching at any pH of certain constituents of the glass, hence no leaving behind of a chemically durable, negatively charged framework [5], which in turn suggests that no satisfactory electrical equilibrium, either real, pseudo, or transient, could be set up suitably for indicating hydrogen-ion activity of aqueous solutions. Further, the hygroscopicity of these glasses (water sorbed in 1 hour), table 1 and figures 2 and 3,

[1] Figures in brackets indicate the literature references at the end of this paper.

[2] The P_2O_5 glass was prepared from ammonium dihydrogen phosphate, $NH_4H_2PO_4$, in the special fire-clay crucible with a ZrO_2 liner. The entire batch was placed in the crucible at room temperature and then heated to 1,000° C in approximately 2 hours. This procedure was necessary, because if the batch was added to a hot crucible, the chilling effect resulting from the rapid evolution of gases invariably cracked the crucible. The resulting glass at room temperature showed such features as flexibility upon the steady application of bending forces, but shattered readily under a sharp blow. It apparently can be maintained indefinitely with adequate desiccation.

TABLE 1. *Chemical durability, hygroscopicity, and* pH *response of some* Na_2O-MgO-P_2O_5 *glasses*

Composition (batch ratio)		Surface alterations for exposures of 6 hr at 80° C and pH—						Water sorbed in—		pH response between pH 4.1 and pH 8.2
$NaH_2PO_4H_2O$	$Mg(H_4(PO_4)_2$	2.0	4.1	6.0	8.2	10.2	11.8	1 hr	2 hr	
		Fringes	*Fringes*	*Fringes*	*Fringes*	*Fringes*	*Fringes*	*mg/cm²*	*mg/cm²*	*mv/pH*
0	10	18 attack	24 attack	24 attack	40 attack	156 attack	900 attack	17	34	1.
1	9	4½ attack	3 SC[b] attack	7½ attack	21 attack	27 attack	365 attack	19	37	
2	8		3 attack	9 attack	12 attack	20 attack	100 attack	19	32	17.
3	7	3 attack	2½ attack	6 attack	7½ attack	11 attack	90 attack	21	37	23.
4	6	6 attack		3 attack		15 attack	85 attack	22	48	Devit.[d]
5	5	6 attack	6 attack	6 attack	12 attack	18 attack	270 attack	23	60	Devit.
6	4	12 attack	9 attack	10 attack	12 attack	27 attack	540 attack	29	84	10.
P_2O_5 [12, 14]		WS[e]	WS	WS	WS	WS	WS	277	655	
Corning 015		2 /10—swell	2/10—swell	2/10—swell	SC	1/4+attack	2 attack	104	168	59.
Pyrex 7740		ND[a]	ND	ND	D[c]	1/4—attack	1¾ attack	17	24	12.

[a] ND, not detectable; [b] SC, surface cut; [c] D, detectable; [d] Devit., devitrification; [e] WS, water soluble.

was considerably less than for most pH responsive silicate glasses [4, 6].[3] Thus the second requirement for satisfactory electrical response to hydrogen-ion activity is also lacking in these glasses. In accordance with the poor durability and low hygroscopicity of the available members of this series, no electrodes were obtained possessing satisfactory pH response (table 1 and fig. 4).

The chemical durabilities of these phosphate glasses are so poor that they obviously cannot be used as containers for aqueous solutions. However, their hygroscopicity is such that they might tenta-

[3] The lower limit of hygroscopicity for a satisfactory pH responsive glass has not yet been established. For the Na_2O-CaO-SiO_2 and Na_2O-PbO-SiO_2 glasses a "sorption" value of about 30 mg/cm² seemed to be indicated for 1 hour exposure to 98-percent relative humidity, whereas the Li_2O-SiO_2 glasses showed a somewhat lower limit. See, Donald Hubbard, Given W. Cleek, and Gerald F. Rynders, Electrode function (pH response), hygroscopicity, and chemical durability of Na_2O-CaO-SiO_2 glasses, J. Research NBS **44,** 247 (1950) RP2076; Donald Hubbard, Mason H. Black, and Gerald F. Rynders, Electrode function (pH response), hygroscopicity, and chemical durability of soda-lead oxide-silica glasses, J. Research NBS **45,** 430 (1950) RP2154; Donald Hubbard and Given W. Cleek, Deuterium and hydrogen electrode characteristics of lithia-silica glasses, J. Research NBS **49,** 267 (1952) RP2363.

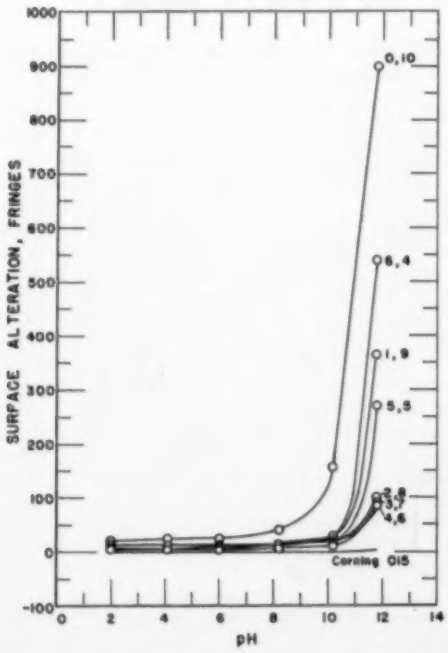

FIGURE 1. *Chemical durability of* Na_2O-MgO-P_2O_5 *glasses.*

Exposure 6 hr, 80° C. Curve designations refer to composition ratios of table 1.

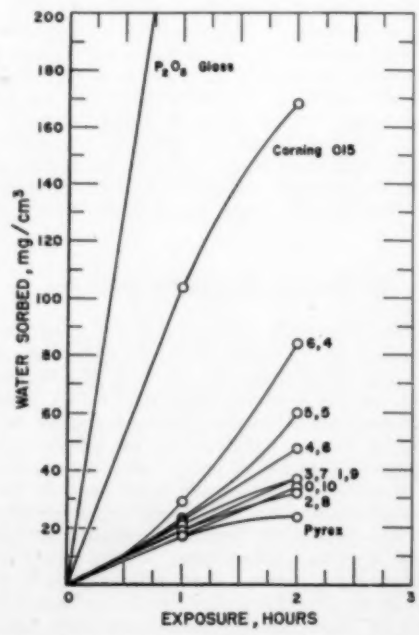

FIGURE 2. *Comparison of the hygroscopicity of a series of* Na_2O-MgO-P_2O_5 *glasses with Pyrex 7740 and Corning 015.*

Exposure to approximately 98-percent relative humidity. Experimental values for water sorbed by P_2O_5 glasses are given in table 1.

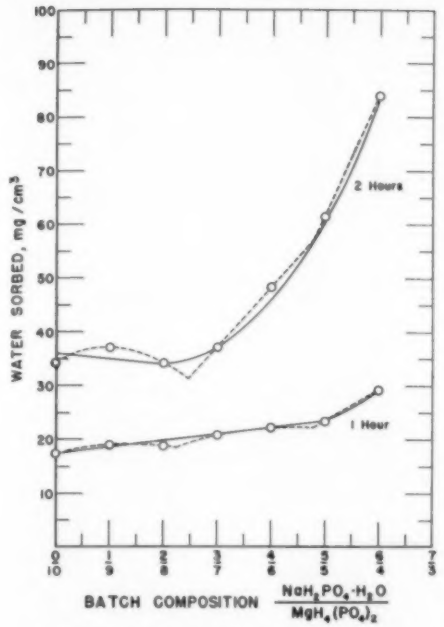

FIGURE 3. *Hygroscopicity-composition curves for a series of* Na_2O-MgO-P_2O_5 *glasses.*

tively be expected to maintain clear surfaces upon exposure to air.

Figure 3 shows the results of plotting the hygroscopicity against the batch composition ratios. In the absence of phase-equilibria data, and because of the uncertain composition and limited range, it is questionable if one is justified in plotting the broken lines other than to point out that the same features seem to be reflected in the chemical-durability curves and to a less and uncertain extent in the pH-response data (fig. 4). The pH response data was particularly uncertain because of pronounced devitrification while attempting to blow electrode bulbs. The procedure finally adopted was to merely seal the end of thin-walled tubes and fill them with mercury [7]. Even this simplified technique was inadequate for glasses 4:6 and 5:5.

3.2 Na_2O-GeO_2 Glasses—Chemical Durability-Hygroscopicity, and pH Response

Figure 5 shows the chemical durability-pH curve over the range pH 2 to pH 11.8 for a soda-germania glass containing 5 percent of Na_2O and 95 percent of GeO_2. This glass is more vigorously attacked in the acid range below pH 4 and in the alkaline range above pH 8 than at intermediate pH values; nevertheless, it is attacked vigorously by all the buffer solutions. No comparison is readily possible with the customary pH-responsive silicate glasses, as the

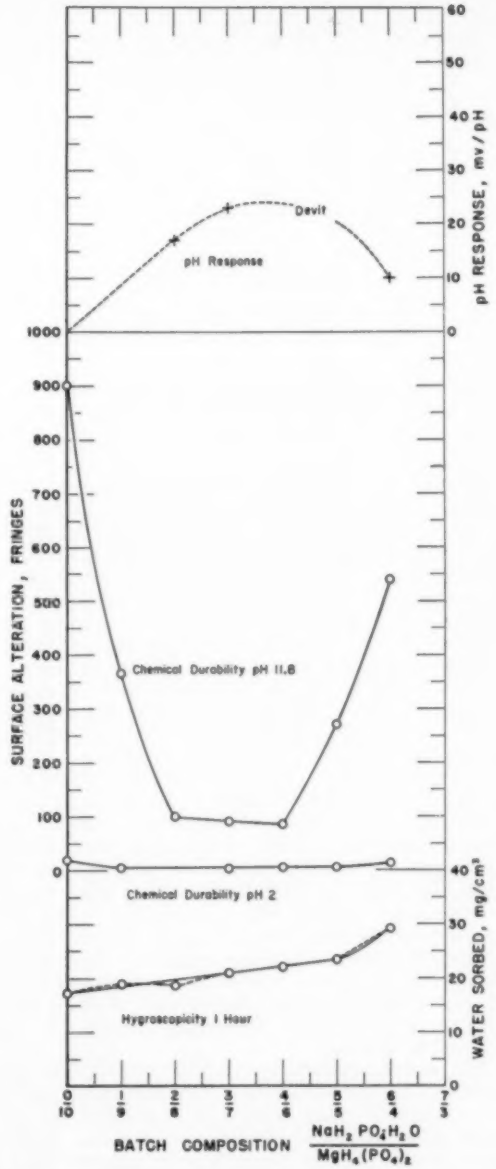

FIGURE 4. *Comparison of the* pH *response of electrodes prepared from some* Na_2O-MgO-P_2O_5 *glasses with the chemical durability and hygroscopicity of the glasses.*

surface alteration of this soda-germania glass exposed for 1 minute at 25° C is much larger than the attack or swelling exhibited by an acceptable silicate glass after 6 hours of exposure at 80° C. As the available samples of most of the germania glasses were of inadequate size for use as specimens for chemical

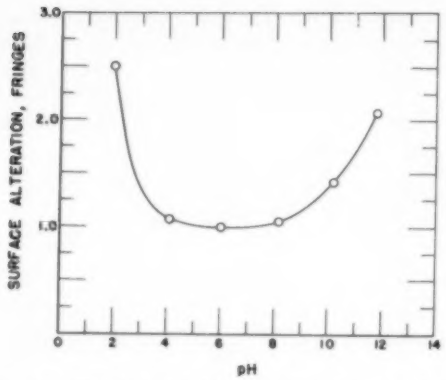

FIGURE 5. *Chemical durability of a soda-germania glass,* Na_2O, *5 percent;* GeO_2, *95 percent.*

Exposure 1 min at 25° C.

durability by the interferometer procedure, in addition to the fact that some of the members, such as the 85 percent GeO_2, devitrified so rapidly that clear specimens for interferometer flats could not be made even upon rapid chilling, another procedure for intercomparison of the chemical durability of the members of this series was tried. The total solids dissolved (milligrams per gram of glass) in 50 ml of distilled water in 1 hour with intermittent agitation at 25° C was determined on powders that passed a 150-mesh sieve. This procedure for determining the relative chemical durabilities of these Na_2O-GeO_2 glasses proved to be generally unsatisfactory, but at the same time gave interesting results (table 2 and fig. 6). The series revealed a minimum weight of total solids extracted near 85 percent GeO_2. Further, the samples for 85 percent and 100 percent of GeO_2 gave persistent colloidal suspensions that passed through the filters. This suspended material was recorded among the total solids. The other members of the series filtered clear. Pyrex 7740 and Corning 015 were similarly treated for comparison. The Pyrex powder gave a slightly opalescent filtrate. Obviously, the chemical durabilities of these Na_2O-GeO_2 glasses compare very unfavorably with pH-responsive glasses.

The hydroscopicity curves for 1 and 2 hours of exposure to 98 percent relative humidity and the water retained upon heating to 110° C after the 2 hours of exposure are given in figure 6. Each of these curves passes through a minimum near 90 percent of GeO_2.

As it was impossible to blow electrode bulbs of the usual Cremer-Haber type, an effort was made to produce glass electrodes by coating platinum wire with a thin unbroken layer of glass by dipping the wire in the molten glass, or by means of the burner to run a bead of the glass along the wire, leaving a thin glass coating [7]. If a successful continuous film of glass was established, electrodes of high resistance, as indicated by the megohm bridge, were obtained. This very high initial resistance fell

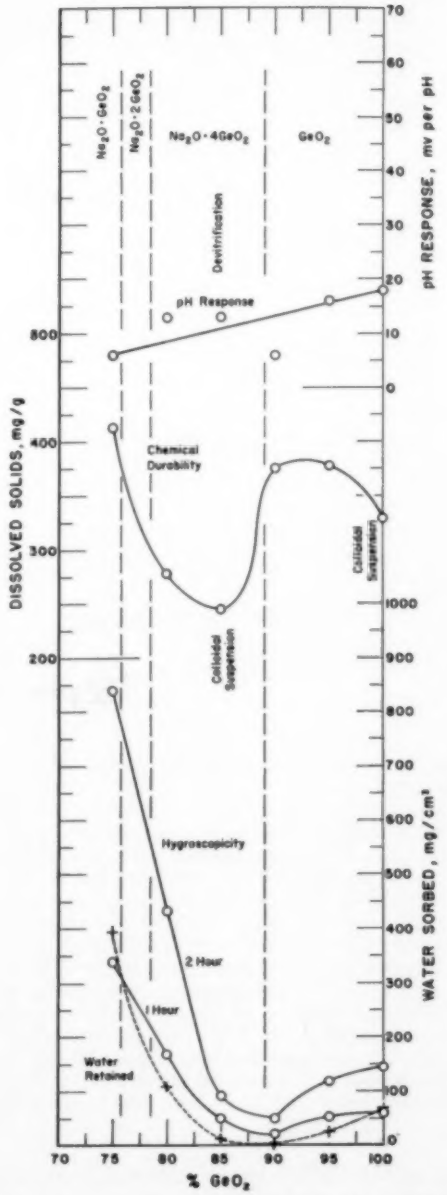

FIGURE 6. *Comparison of the* pH *response of electrodes prepared from some* Na_2O-GeO_2 *glasses with the chemical durability and hygroscopicity of the glasses.*

rapidly toward the lower limit of the instrument as the glass took on water and was dissolved in the buffers. The voltage responses obtained were transient and must be classified as superficial or even spurious. Certainly the pH-response characteristics of these electrodes were no better than the values

TABLE 2. *Chemical durability, hygroscopicity, and* pH *response of a series of* Na_2O–GeO_2 *glasses*

Glasses		Chemical durability in H_2O		Water sorbed in—		Water retained at 110° C	pH response
Na_2O	GeO_2	Solids dissolved	Remarks	1 hr	2 hr		
Percent	*Percent*	*mg/g*		*mg/cm²*	*mg/cm²*	*mg/cm²*	*mv/pH*
25	75	412	Filtered clear	338	841	392	6
20	80	278	do	168	432	109	13
15	85	246	Colloidal suspension	50	91	11	13
10	90	375	Filtered clear	21	49	4	6
5	95	377	do	52	116	28	16
0	100	329	Colloidal suspension	60	144	67	18
Corning 015		81	Filtered clear	104	168	.....	59
Pyrex 7740		22	Filtrate, opalescent	17	24	Trace.	12

recorded. Although the hygroscopicity values for these soda-germania glasses were adequate for pH-responsive electrodes, the chemical-durability characteristics were hopelessly unsatisfactory. Under these circumstances, no physicochemical equilibria is possible, and hence no satisfactory pH response can be expected.

The same difficulties in blowing electrodes were encountered with a soda-lime-germania glass prepared by John K. Taylor [4] for comparison with Corning 015 electrode glass of the soda-lime-silica series. Although his glass exhibited acceptable hygroscopic characteristics, no successful electrodes were obtained.

An overall picture of the interrelation of hydroscopicity, chemical durability, and pH response with the composition is given in figure 6. Also included in this figure are the approximate compositions at which new phases appear in the equilibrium diagrams (table 3) [8]. Although the data are too meager for definite conclusions, they do suggest some correspondence between the chemical and physical properties of the glasses and the critical points of the phase equilibrium diagram for this system of oxides.

TABLE 3. *Known compounds and eutectics of the* Na_2O-GeO_2 *phase-equilibrium system [8]* [a]

Compounds	Melting point	GeO_2
	°C	*Percent*
Metagermanate ($Na_2O \cdot GeO_2$)	1,083	
Eutectic I	778	73.8
Digermanate ($Na_2O \cdot 2GeO_2$)	799	
Eutectic II	789	78.5
Tetragermanate ($Na_2O \cdot 4GeO_2$)	1,052	
Eutectic III	1,042	89.2

[a] George M. Ugrinic reviewed the literature of the phase-equilibria work on germanium-oxide systems.

[4] Personal communication.

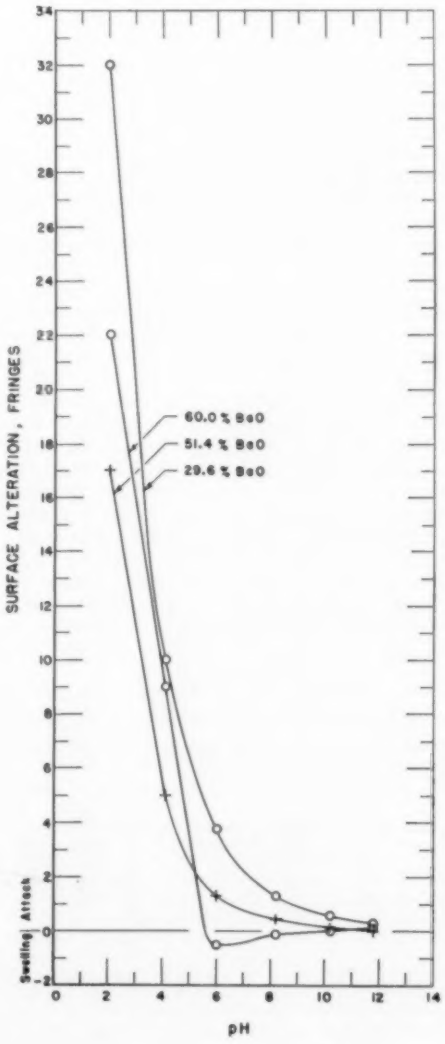

FIGURE 7. *Surface alteration (exposure 5 min, 25° C) of three* BaO-B_2O_3 *glasses over the range* pH *2 to* pH *11.8.*

These glasses represent the extremes of behavior for the series. The chemical durabilities of all other members of the series fall between these limits.

290819—54——3

3.3. BaO-B_2O_3 Glasses

a. Chemical Durability

Table 4 gives the data obtained on a series of BaO-B_2O_3 glasses for chemical durability, hygroscopicity, and pH response. This series of glasses extends over the composition range 29.6 percent of BaO, where two immiscible layers appear [9], to near 60 percent of BaO, above which devitrification limits the glass-making range. Figure 7 illustrates the extremes of chemical durability over the range pH 2 to pH 11.8 exhibited by these glasses. The chemical durability of this BaO-B_2O_3 series was so poor that the exposure time was reduced to 5 minutes and less at 25° C instead of the conventional 6 hours of exposure at 80° C previously adopted for silicate glasses. These abbreviated exposures were necessary in order to keep the surface alterations within the limitations of the interferometer method. The nature of the attack-pH curves for these glasses was markedly different from the numerous silicate glasses previously studied [2, 4], with all the members of the series being more vigorously attacked in the acid buffers than at the higher pH values. The glass of 60 percent of BaO exhibited swelling at pH 6 and pH 8.2, resulting in a conspicuous nonreflecting film on the surface of the specimens involved. This feature was so unexpected that the experiments were repeated, with the same results. A more easily understood picture of the chemical-durability characteristics of this series of glasses is given in figure 8, in which the chemical durability in the buffers at various pH values is plotted against the chemical composition (percentage of BaO). For pH 2 and pH 4.1 the surface alteration (attack) declines with increasing percentages of BaO and then increases again with further increase above 51.4 percent of BaO. The curve at pH 6 shows the same features over the composition range, except for the glass containing 60 percent of BaO. For this glass the surface alteration is one of swelling, plotted as negative attack in the figures, giving the curve a unique hook at the end. The curve for pH 8.2 exhibits this same feature, although not so conspicuously.

The question always arises as to what is the significance of the changes in chemical and physical properties with composition. In presenting the data for chemical durability and hygroscopicity of the BaO-B_2O_3 series of glasses, lines are drawn (fig. 8) at the eutectic and compound compositions indicated by the phase-equilibrium diagram for this binary system [9]. There is little to decide as to whether the eutectic or compound compositions herald the change in direction that appears in the plotted data. The maximum and minimum composition ranges that might enter the argument are represented by vertical solid and dashed lines, respectively. Obviously, all that these data indicate is that the chemical and physical properties of glasses are influenced by the materials from which the glasses are made, and that the phase-equilibrium diagram is probably the best indicator available at present as to what compounds are melted, dissolved, or dissociated in the glassy state. The departure from randomness upon cooling the glasses from above the liquidus to room temperature, including the annealing schedule, probably contributes to emphasize the position and sharpness of the breaks as surely as does the sensitiveness or reliability of the physical and chemical indicators used. Certainly the rates of departure from randomness are very different for glasses of different composition in the same series [10].

b. Hygroscopicity

The hygroscopicity data for 1 and 2 hours of exposure to the high humidity maintained by a saturated solution of $CaSO_4 \cdot 2H_2O$ at room temperature are given in table 4 and show these glasses to be very nonhygroscopic (approximately equivalent to Pyrex 7740 [11]) at 46.9 percent BaO and greater. Below this percentage of BaO the hygroscopicity rises with increase in the percentage of B_2O_3. These glasses furnish an interesting example illustrating the distinction between a chemical-durability test (ability to withstand attacks by liquids) and one for serviceability of optical glass (the ability to maintain a polished surface upon exposure to air). These glasses obviously would be worthless as containers for most aqueous solutions over the range pH 2 to pH 12, but acceptable for optical elements, at least in their first line of defense against atmospheric moisture.

TABLE 4. *Chemical durability, hygroscopicity, and* pH *response of a series of* BaO-B_2O_3 *glasses [15]*

Composition		Surface alterations for exposures of 5 min at 25° C and pH—						Water sorbed in—		pH response	
BaO[a]	B_2O_3	2.0	4.1	6.0	8.2	10.2	11.8	1 hr	2 hr		
Percent	*Percent*	*Fringes*	*Fringes*	*Fringes*	*Fringes*	*Fringes*	*Fringes*	*mg/cm²*	*mg/cm²*	*mr/pH*	
29.6	70.4	32	10	3¾	1¼+	½	¼	43	109	8	Very short-lived.
36.6	63.4	22	5½	2½	1¼	½+	¼−	31	65	No electrode	High resistance.
41.9	58.1	20	5	1¾	½+	½	1/10+	25	40	(54, 57)?	Very short-lived.
46.9	53.1	17	5	1¼+	¼	¼+	1/10+	17.3	27	No pH response	High resistance.
51.4	48.6	17	5	1¼+	¼	D	D	16.7	25	do	Do.
53.6	46.4	19−	6−	2¼	½−	1/10	D	16.9	25	do	Do.
56.1	43.9	19	6¾	2½	½	D	1/10	17	24	do	Do.
60.0	40.0	22	9	½ swell[b]	1/10 swell[b]	D	1/10+	16.5	22.6	do	Do.
Corning 015		See table 1; 6 hr of exposure at 80° C.						104	168	39	
Pyrex 7740		See table 1; 6 hr of exposure at 80° C.						17	24	12	

[a] Analyses made by Nancy J. Tucker and Jean Rahauser Rogers. [b] Specimens showed nonreflecting films [13].

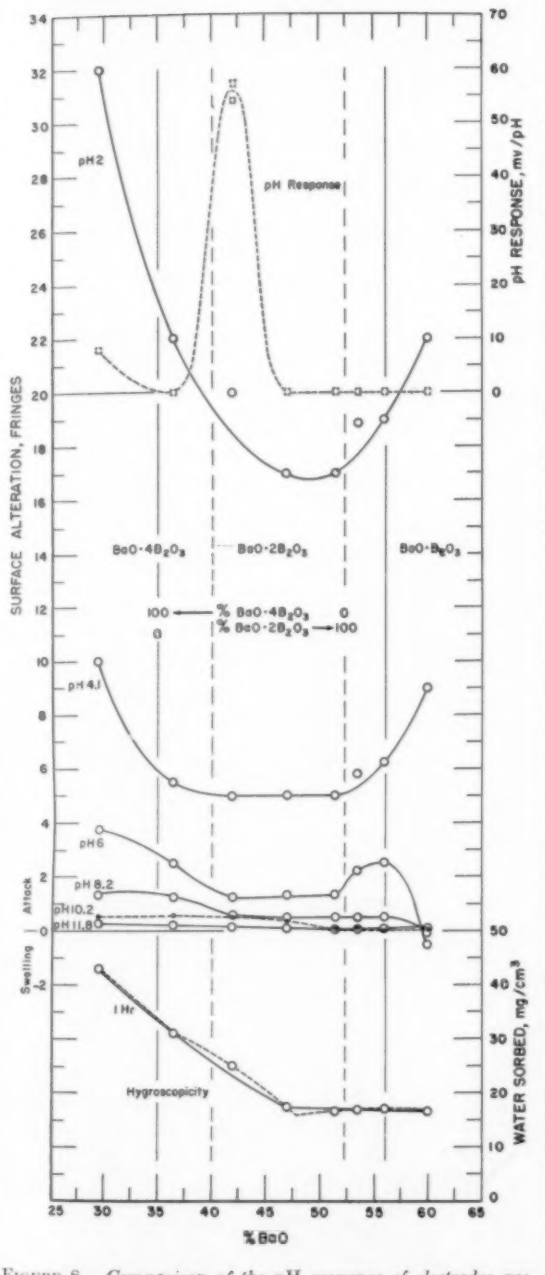

FIGURE 8. *Comparison of the* pH *response of electrodes prepared from some* BaO-B_2O_3 *glasses with the chemical durability and hygroscopicity of the glasses.*

(See text concerning the pH-response characteristics of these glasses.)

c. pH Response

For this BaO-B_2O_3 series only those glasses containing less than 47 percent of BaO exhibited hygroscopicity values sufficiently high to be classified as possible pH-responsive glasses. Of these, the glass of 29.6 percent of BaO showed evidence of inhomogeneity, probably separation into two immiscible phases [9]. An electrode prepared from this glass was very short-lived and gave very indifferent pH-response values. Glasses containing 46.9 percent of BaO and greater had hygroscopicity values that correspond favorably with Pyrex 7740, and in accordance with their low hygroscopicity, electrodes prepared from them showed no evidence of voltage response to hydrogen-ion activity of the buffer solutions. The glass of 41.9 percent of BaO gave one electrode that started off with no pH response, then gave two quick values of 54 and 57 mv/pH between pH 4.1 and pH 8.2. This performance was followed in a relatively few seconds by failure of the bulb. Whether those two readings should be classified as transient or spurious is uncertain. In light of past experience of the effect of poor chemical durability on pH response of glass electrodes, it seems reasonable to classify these readings as both transient and spurious. Certainly this electrode performance could not be repeated, even after many attempts involving the consumption of several yards of tubing. The overall picture of relation of pH response (drawn as a dashed line), chemical durability, and hygroscopicity as a function of the composition is given in figure 8.

4. Conclusions

None of the Na_2O-MgO-P_2O_5, the Na_2O-GeO_2, and BaO-B_2O_3 glasses examined had sufficiently good chemical durability to produce electrodes that even approximated the theoretical voltage response dictated by the Nernst equation. In addition, many of the glasses had very low hygroscopic properties, thus ruling them out as possible sources of electrodes acting as hydrogen-ion indicators. Hence, for all practical purposes, the electrical response of all these glasses to hydrogen-ion activity of aqueous solutions must be classified as superficial or negligible.

5. References

[1] Malcolm Dole, The glass electrode (John Wiley & Son, Inc., New York, N. Y., 1941)

[2] Donald Hubbard, Edgar H. Hamilton, and Alfred N. Finn, Effect of the solubility of glass on the behavior of the glass electrode, J. Research NBS **22,** 339 (1939) RP1187.

[3] Donald Hubbard, Hygroscopicity and electrode function (pH response) of glasses as a measure of serviceability, J. Research NBS **36,** 511 (1946) RP1719.

[4] Donald Hubbard, Mason H. Black, Sylvanus F. Holley, and Gerald F. Rynders, Electrode function (pH response), hygroscopicity, and chemical durability of soda-potash-silica glasses, J. Research NBS **46,** 168 (1951) RP2189.

[5] Donald Hubbard and Richard G. Goldman, Heterogeneous equilibria at the glass electrode-solution interface, J. Research NBS **48,** 428 (1952) RP2333.

[6] Richard G. Goldman and Donald Hubbard, pH response of nonhygroscopic glasses, J. Research NBS **48,** 370 (1952) RP2324.
[7] M. R. Thompson, A metal-connected glass electrode, BS J. Research **9,** 833 (1932) RP511.
[8] R. Schwarz and F. Heinrich, Germanate der Alkali und Erdalkalimetalle, Z. anorg. allgem. Chem. **205,** 43 (1932).
[9] Ernest M. Levin and Howard F. McMurdie, The system BaO-B_2O_3 J. Research NBS **42,** 131 (1949) RP1956.
[10] Oscar H. Grauer and Edgar H. Hamilton, An improved apparatus for the determination of liquidus temperatures and rates of crystal growth in glasses, J. Research NBS **44,** 495 (1950) RP2096.
[11] Donald Hubbard, Lillie B. Jenkins, and Elizabeth M. Krumrine, Amelung glasses (early U. S. industrial 1785–1795) compared with some modern commercial glasses (1951); Sci. Monthly **LXXV,** 327 (1952).
[12] Ernest Kordes, Physicochemical researches on the fine structure of glasses, IV. Changes in the fine structure in the system P_2O_5-ZnO, Z. physik. Chem. **B50,** 194 (1941).
[13] I. V. Grebenshchikov and O. S. Molchanova, Formation of macrofilm on soda-borosilicate glasses and its properties, J. Gen. Chem. (U. S. S. R.) **12,** 588 (1942).
[14] J. M. Stevels, Monograph No. 20 on the Progress of Research in Holland. Progress on the Theory of the Physical Properties of Glass, Section 6, Phosphate Glasses. (Elsevier Publishing Co., Inc., New York, N. Y., 1948).
[15] Edgar H. Hamilton, Given W. Cleek, and Oscar H. Grauer, Some properties of glasses in the BaO-B_2O_3-SiO_2 system and a theory of glass structure, (personal communication).

WASHINGTON, November 16, 1953.

Journal of Research of the National Bureau of Standards Vol. 52, No. 5, May 1954 Research Paper 2498

A Numerical Solution of Schrödinger's Equation in the Continuum [1]

W. Futterman, E. Osborne, and David S. Saxon [2]

Continuum solutions of Schrödinger's equation for two particles that interact according to a central Yukawa potential are obtained by numerical integration. The resulting wave functions are tabulated, as are the phase shifts which determine the asymptotic behavior of the solutions.

1. Introduction

The solution of the Schrödinger equation for two particles that interact according to the Yukawa potential,

$$V(r)=C\frac{e^{-r/r_0}}{r/r_0}, \tag{1}$$

is unknown in closed form. Numerical solutions of this problem are of some interest from a purely formal as well as physical viewpoint, since the literature of recent years shows increased activity in the use of a variational principle [3,4] to obtain certain parameters of physical consequence. As yet, however, with respect at least to solutions in the continuum there exist no intrinsic criteria for the deviation of such approximate results from the correct values. An exact solution of the problem, of course, permits an exact calculation of these parameters, thus providing a comparison by which the validity and usefulness of the variational principle can be gaged.[5] Further, although the Yukawa interaction (1) is an idealized one, it nonetheless forms a reasonable basis for the description of physical phenomena such as the photoelectric disintegration of the deuteron and the so-called deuteron-stripping process.[6]

2. Schrödinger Equation

For the Yukawa interaction (1) the Schrödinger equation, expressed in the relative coordinates of the two particles, is

$$\left\{\nabla^2+\frac{2m}{\hbar^2}\left[E-V(r)\right]\right\}\Psi(\boldsymbol{r})=0\,, \tag{2}$$

where E is the energy of the system, and m is the reduced mass. In virtue of the spherical symmetry of $V(r)$, the solution of (2) can be decomposed into spherical harmonics; that is, $\Psi(\boldsymbol{r})$ can be written in the form

$$\Psi(\boldsymbol{r})=\sum_{l,\,m} a_{l,\,m}\Psi_l(r)Y_l^m(\theta,\phi), \tag{3}$$

where the $a_{l,\,m}$ are arbitrary constants, and the Y_l^m are the usual normalized spherical harmonics. The radial functions $\Psi_l(r)$ then satisfy the equation

$$\frac{1}{r^2}\frac{d}{dr}\left(r^2\frac{d\Psi_l}{dr}\right)+\left\{\frac{2m}{\hbar^2}\left(E-V(r)\right)-\frac{l(l+1)}{r^2}\right\}\Psi_l=0. \tag{4}$$

Introducing the function

$$u_l(r)=r\Psi_l(r) \tag{5}$$

and using (1), it is convenient to rewrite (4) in the dimensionless form

$$\frac{d^2u_l}{dx^2}+\left\{K^2+\beta\frac{e^{-x}}{x}-\frac{l(l+1)}{x^2}\right\}u_l=0, \tag{6}$$

where

$$K^2=2mr_0^2E/\hbar^2 \tag{7}$$

$$\beta=2mr_0^2C/\hbar^2 \tag{8}$$

$$x=r/r_0. \tag{9}$$

and where the parameters r_0 and C (or β) will be chosen to fit the low energy triplet neutron-proton data.

As a consequence of (5), $u_l(r)$ satisfies the boundary condition $u_l(0)=0$, and thus we seek the solution of (6) regular at $x=0$. It is easily established that in the neighborhood of the origin, this solution behaves as

$$u_l(x)\sim x^{l+1}, \qquad x\to 0. \tag{10}$$

It should be noted that the complete solution of the Schrödinger equation consists of a sum over all spherical harmonics. However, for sufficiently large l the effect of the interaction term can be shown to be very small, and the solutions may be obtained by perturbation methods, such as the Born approximation. Consequently, the numerical integration of (6) need be carried out only for the first few l values.

One should also remark that for sufficiently large values of x, no matter what value l has, the interaction term becomes negligible, and hence the asymptotic form of u_l must be

$$u_l(x)\simeq xB_l\cos\delta_l\left[j_l(Kx)-\tan\delta_l y_l(Kx)\right], \tag{11}$$

[1] The preparation of this paper was sponsored (in part) by the Office of Naval Research, USN.

[2] National Bureau of Standards, Los Angeles, Calif.

[3] Lippman and Schwinger, Phys. Rev. **79**, 469 (1950).

[4] Blatt and Jackson, Phys. Rev. **76**, 18 (1949).

[5] In particular, reference is made to a calculation of differential cross sections, using variational methods, which is in preparation.

[6] Schiff, Phys. Rev. **78**, 733 (1950); Serber, Phys. Rev. **72**, 1008 (1947). (Applications of our results to these problems are in preparation.)

where $j_l(z)$ is the regular and $y_l(z)$ the irregular spherical Bessel function,[7] of order l, and where the factor $\cos \delta_l$ is introduced for reasons of convenience. Thus the numerical integration need extend only to such values of x that (11) is valid, as discussed in section 3.

The physical significance of the phase shifts δ_l defined by (11) may be seen from the fact that in the absence of interaction, (11) holds exactly everywhere. In this special case, the requirement of regularity at the origin is satisfied only if each δ_l is zero. Thus the phase shifts measure the influence of the interaction on the asymptotic form of the field and so directly determine the scattering.[8]

3. Procedure

Integration of (6) is based upon the Gauss-Jackson or Σ^2 difference method for reasons of accuracy and convenience.[9] Let us rewrite (6) in the form

$$\frac{d^2u}{dx^2}=g_l(x)u, \tag{12}$$

where

$$g_l(x)=-\left(K^2+\beta\,\frac{e^{-x}}{x}-\frac{l(l+1)}{x^2}\right). \tag{13}$$

In central difference notation

$$u^{(r)}=\frac{1}{4S}\left[\delta^{-2}F_r+\frac{1}{12}\,F_r-\frac{1}{240}\,\delta^2F_r+\ldots\right], \tag{14}$$

where we tabulate

$$F_r=4Sh^2g(x)u^{(r)}, \tag{15}$$

and where h is the interval, S is an arbitrary rounding-off factor, and $u_l^{(0)}=u_l(0)$.

Because (12) has a regular singular point at $x=0$ care must be taken to determine the F_0 for the various l values. However, they are readily obtained from (10), which gives

$$\begin{aligned} &l=0 \qquad g_0\,(0)u_0^{(0)}=\text{constant}\\ &l=1 \qquad g_1\,(0)u_1^{(0)}=\text{constant}\\ &l\geq 2 \qquad g_l\,(0)u_l^{(0)}=0, \end{aligned} \tag{16}$$

where the constants determine the otherwise arbitrary normalization.

The series (14) is approximated to the order of the second difference term, using the third difference as a predictor. As a consequence, F_1 and F_2 are needed as starting values in addition to F_0. These are obtained from (10), which is a suitable first approximation, as indicated by the rapid convergence of F_2 to a constant value. Three iterations were made at each point to assure the constancy of the tabulated value.

Keeping the interval small, $h=.05$, in this region of rapidly changing ordinate, we march out to $x=1$ where the interval is shifted to $h=.1$. The integration is then carried out to a large value of $x(\sim 5)$. Rather than joining this solution to (11), which is obtained by neglecting the interaction term entirely, a more refined procedure was used in which the interaction was treated as a small perturbation. By a modified WKB technique,[10] the asymptotic solution can be obtained in the form

$$u_l(x)=A_l\cos\delta_l\,\frac{z(x)}{\sqrt{z'(x)}}\,[j_l(z(x))-\tan\delta_l y_l(z(x))], \tag{17}$$

where the prime denotes differentiation with respect to x, and where z is given by the semiconvergent series

$$z(x)=Kx+\frac{1}{(1+1/4K^2)}\,\beta\,\frac{e^{-x}}{x}\left[-1+\frac{1}{x}\left(\frac{1+3/4K^2}{1+1/4K^2}\right)-\cdots\right]+O\left(\frac{e^{-2x}}{x^2}\right). \tag{18}$$

It is observed that as x approaches infinity, $z(x)$ properly approaches Kx. A few terms of this alternating series were always sufficient to give z with satisfactory accuracy. The logarithmic derivative of (17) was equated to the numerically obtained logarithmic derivative of the numerical solution at its end point, thus determining the phase shift. The amplitude factor was then found by equating (17) to the numerical solutions.

In carrying out the actual computation, the original data was programmed to six significant figures on the IBM card-programmed calculator, so that at least four figures could be assured for the phase shifts. With a few exceptions, integrations were carried out to $x=5$ at all energies. An internal check on the error was maintained through the third differences, which were kept uniform and small.

To check the machine error a comparison of two integrations for $K^2=1$, $\beta=0$ was made with the known solutions $j_l(Kx)$. For the cases $l=2$ with the end point $x=4$, and $l=3$ with $x=5$ there was, at most, a 0.0002 percent error in the numerical solution.

4. Numerical Results

As mentioned earlier, the constants in the Yukawa interaction were chosen to fit the low-energy triplet neutron-proton interaction. Using the tables of Blatt and Jackson,[11] we choose

$$\beta=2.36500, \qquad r_0=1.35000\times 10^{-13}\ \text{cm}. \tag{19}$$

[7] These functions are defined in P. M. Morse, Vibrations and sound, p. 316-317, and they are tabulated in "Tables of spherical Bessel function" (Columbia University Press, 1947).

[8] Mott and Massey, The theory of atomic collisons (Oxford, 1949).

[9] Samuel Herrick, Mathematical tables and other aids to computation **5**, 61-67 (1951). (*See also*, page 131 of reference given in footnote 8.) Recently, P. O. Lowdin and A. S. Jölander, Arkiv für Fysik, Band 3, No. 11, (1951), claim an improvement over Σ^2 procedure on the basis that no initial Taylor expansion is needed. However, in our case no special difficulties were encountered in this respect.

[10] The details are given in the appendix.

[11] See footnote 4.

The parameter K^2 is easily expressed in terms of the incident neutron energy,[12]

$$K^2 = 2.19700 \times 10^{-2}\ E_{lab.}\ (\text{Mev}). \qquad (20)$$

Computations were carried out for the values of the energy, with the corresponding values of K^2 listed in table 1.

TABLE 1

$E_{lab.}$ (Mev)	20	50	90	120	150
K^2	0. 439588	1. 09897	1. 97815	2. 63753	3. 29691

The radial wave functions $u_l(x)$ corresponding to these parameters are tabulated in table 2 for $l=0(1)5$ and for $x=0(0.1)5$ (in a few cases for $x=0(0.1)4.0$ or 4.2). For values of x that lie beyond the tabulated values, u_l is given by (17) where the parameters δ_l are listed in table 3. For convenience in physical applications, these functions have been normalized according to the rule

$$\int_0^\infty u_l^K(x) u_l^{K'}(x) dx = \frac{\pi}{2K} \delta(K-K'),$$

where $u_l^K(x)$ is the solution when the energy corresponds to K and where $\delta(K-K')$ is the Dirac δ-function. With this normalization the factors A_l, which appear in (17), are then simply unity.

Finally, for values of l that lie beyond the tabulated values, the wave functions can be obtained by perturbation methods, such as the Born approximation, since, as already mentioned, the effects of the interaction are then very small.

5. Appendix

We seek asymptotic solutions of eq (6) valid when x is so large that the term $\beta e^{-x}/x$ can be treated as a small pertubation. For this purpose we consider the *general* spherical Bessel function $c_l(z)$, which is defined as the general solution of the equation

$$\frac{d^2 c_l}{dz^2} + \frac{2}{z}\frac{dc_l}{dz} + \left[1 - \frac{l(l+1)}{z^2}\right] c_l(z) = 0, \qquad (A\text{-}1)$$

and which is thus expressible in the form

$$c_l(z) = \alpha j_l(z) + \beta y_l(z). \qquad (A\text{-}2)$$

Now as x increases, $u_l(x)$ is ultimately given by

$$u_l(x) \sim Kx c_l(Kx),$$

as indicated in eq (11). Hence, we try to find an asymptotic solution of (6) of the form

$$u_l(x) = A(x) z(x) c_l[z(x)]. \qquad (A\text{-}3)$$

Substitution into (6) and use of (A-1) then yields

$$[2A'zz' + Azz''] \frac{dc_l}{dz} - Azz'^2 \left[1 - \frac{l(l+1)}{z^2}\right] c_l(z)$$

$$+ \left\{ Az \left[K^2 + \frac{\beta e^{-x}}{x} - \frac{l(l+1)}{x^2} \right] + 2A'z' + Az'' + A''z \right\} c_l(z) = 0, \qquad (A\text{-}4)$$

where the prime denotes differentiation with respect to x. The unknown functions $A(x)$ and $z(x)$ are now determined by setting the coefficients of $c_l(z)$ and dc_l/dz separately equal to zero. The latter gives at once

$$A^2 z' = \text{constant}, \qquad (A\text{-}5)$$

whence, eliminating A, the former gives

$$-z'^2 \left[1 - \frac{l(l+1)}{z^2}\right] + K^2 \left[1 - \frac{l(l+1)}{K^2 x^2}\right] + \frac{\beta e^{-x}}{x} + \sqrt{z'}\,\frac{d^2}{dx^2}\left(\frac{1}{\sqrt{z'}}\right) = 0, \qquad (A\text{-}6)$$

which is an exact equation for $z(x)$. Note that for $\beta=0$, $z=Kx$ is properly a solution of this equation. Adopting β as a convenient parameter of smallness (since it occurs multiplied by the small factor e^{-x}/x), we now find approximate solutions by expanding $z(x)$ in a power series in β as follows:

$$z(x) = Kx + \sum_1^\infty \beta^n v_n(x), \qquad (A\text{-}7)$$

whence, by substitution into (A-6) we obtain upon setting the coefficients of like powers of β equal to zero

$$\frac{v_1'''}{4K^2} + \left[1 - \frac{l(l+1)}{K^2 x^2}\right] v_1' + \frac{l(l+1)}{K^2 x^3} v_1 = \frac{e^{-x}}{2Kx} \qquad (A\text{-}8)$$

and similarly for v_2, etc. Since x is presumed large, we solve (A-8) approximately by writing

$$v_1 = \frac{e^{-x}}{2K} \sum_{n=0} \frac{a_n}{x^{n+1}}, \qquad (A\text{-}9)$$

which finally yields

$$a_0 = -\frac{1}{1+1/4K^2}$$

$$a_1 = -\frac{1+3/4K^2}{1+1/4K^2} a_0$$

$$a_2 = -\frac{1}{1+4K^2}\left\{[6-4l(l+1)]a_0 + 2(4K^2+3)a_1\right\}$$

. . .

Assembling these results, we then obtain eq (17) and (18).

[12] For convenience in physical applications, K^2 is expressed in terms of the energy in the laboratory system of coordinates in which the proton is initially at rest. In (2) the energy that appears is that in the coordinate system in which the center of mass is at rest.

TABLE 2

$E_{lab.}=20$ Mev							$E_{lab.}=50$ Mev						
x	$u_0(x)$	$u_1(x)$	$u_2(x)$	$u_3(x)$	$u_4(x)$	$u_5(x)$	x	$u_0(x)$	$u_1(x)$	$u_2(x)$	$u_3(x)$	$u_4(x)$	$u_5(x)$
0.1	0.2592	0.0042					0.1	0.24687	0.0076	0.0001			
.2	.4592	.0158	0.0003				.2	.43753	.0286	.0009			
.3	.6178	.0338	.0010	0.00002			.3	.58090	.0610	.0031	0.0001		
.4	.7297	.0572	.0022	.00007			.4	.68385	.1026	.0070	.0004	0.00002	
.5	.8134	.0852	.0042	.00018	0.00001		.5	.75211	.1519	.0132	.0009	.00005	
.6	.8701	.1172	.0071	.00036	.00002	0.000001	.6	.79046	.2073	.0221	.0018	.00012	0.00001
.7	.9041	.1526	.0110	.00065	.00003	.000001	.7	.80298	.2675	.0339	.0032	.00025	.00002
.8	.9189	.1911	.0160	.00109	.00006	.000003	.8	.79317	.3312	.0489	.0054	.00048	.00004
.9	.9174	.2322	.0222	.00172	.00011	.000006	.9	.76407	.3972	.0673	.0084	.00084	.00007
1.0	.9021	.2755	.0297	.00257	.00018	.000011	1.0	.71839	.4644	.0892	.0126	.00140	.00013
1.1	.8749	.3207	.0386	.00370	.00029	.000019	1.1	.65855	.5318	.1147	.0179	.00221	.00023
1.2	.8375	.3675	.0490	.00515	.00044	.000031	1.2	.58674	.5983	.1438	.0247	.00335	.00038
1.3	.7915	.4157	.0609	.00698	.00065	.000050	1.3	.50498	.6630	.1765	.0332	.00489	.00060
1.4	.7381	.4648	.0744	.00925	.00093	.000078	1.4	.41517	.7250	.2126	.0435	.00694	.00093
1.5	.6784	.5147	.0895	.01199	.00130	.000116	1.5	.31905	.7833	.2520	.0558	.00959	.00138
1.6	.6133	.5651	.1063	.01529	.00177	.000169	1.6	.21830	.8373	.2944	.0702	.01295	.00199
1.7	.5436	.6158	.1249	.01918	.00237	.000241	1.7	.11449	.8862	.3396	.0870	.01714	.00281
1.8	.4702	.6664	.1451	.02374	.00312	.000336	1.8	.00912	.9291	.3873	.1062	.02229	.00388
1.9	.3937	.7168	.1671	.02903	.00404	.000461	1.9	−.09637	.9656	.4371	.1279	.02852	.00527
2.0	.3147	.7667	.1908	.03509	.00516	.000620	2.0	−.20062	.9951	.4885	.1522	.03597	.00702
2.1	.2338	.8158	.2162	.04200	.00650	.000823	2.1	−.30236	1.0170	.5410	.1792	.04476	.00921
2.2	.1515	.8639	.2434	.04981	.00811	.001077	2.2	−.40037	1.0309	.5943	.2089	.05503	.01192
2.3	.0685	.9108	.2721	.05858	.01000	.001392	2.3	−.49350	1.0365	.6476	.2411	.06690	.01522
2.4	−.0150	.9561	.3025	.06835	.01222	.001778	2.4	−.58071	1.0336	.7005	.2760	.08049	.01920
2.5	−.0984	.9997	.3345	.07919	.01479	.002248	2.5	−.66103	1.0220	.7524	.3133	.09592	.02395
2.6	−.1813	1.0413	.3679	.09114	.01777	.002814	2.6	−.73357	1.0017	.8027	.3529	.11330	.02957
2.7	−.2632	1.0808	.4027	.10425	.02117	.003491	2.7	−.79757	0.9727	.8507	.3947	.13270	.03616
2.8	−.3439	1.1178	.4388	.11855	.02506	.004294	2.8	−.85234	.9350	.8959	.4384	.15420	.04382
2.9	−.4228	1.1522	.4761	.13408	.02946	.005240	2.9	−.89732	.8891	.9376	.4837	.11786	.05265
3.0	−.4997	1.1837	.5146	.15088	.03442	.006349	3.0	−.93204	.8350	.9753	.5305	.20772	.06275
3.1	−.5742	1.2122	.5539	.16896	.03998	.007638	3.1	−.95617	.7733	1.0084	.5782	.23178	.07424
3.2	−.6460	1.2375	.5941	.18835	.04618	.009130	3.2	−.96946	.7045	1.0363	.6266	.26204	.08720
3.3	−.7148	1.2593	.6750	.20907	.05306	.010846	3.3	−.97182	.6291	1.0587	.6753	.29445	.10173
3.4	−.7802	1.2777	.6765	.23111	.06068	.012811	3.4	−.96326	.5478	1.0749	.7239	.32895	.11791
3.5	−.8421	1.2923	.7183	.25449	.06906	.015049	2.5	−.94389	.4613	1.0847	.7718	.36546	.13583
3.6	−.9000	1.7031	.7603	.27918	.07825	.017587	3.6	−.91397	.3704	1.0877	.8186	.40383	.15556
3.7	−.9539	1.3099	.8024	.30518	.08829	.020451	3.7	−.87384	.2759	1.0835	.8629	.44392	.17715
3.8	−1.0034	1.3127	.8443	.33247	.09922	.023671	3.8	−.82399	.1787	1.0721	.9071	.48555	.20064
3.9	−1.0483	1.3114	.8860	.36101	.11107	.027275	3.9	−.76497	.0798	1.0531	.9478	.52850	.22607
4.0	−1.0885	1.3058	.9271	.39077	.12388	.031293	4.0	−.69746	−.0198	1.0266	.9854	.57262	.25345
4.1	−1.1238	1.2961	.9675	.42169	.13768	.035758	4.1	−.62222	−.1193	0.9926	1.0194	.....	.28276
4.2	−1.1541	1.2820	1.0070	.45374	.15251	.040700	4.2	−.54008	−.2176	.9511	1.0495	.....	.31398
4.3	−1.1792	1.2636	1.0454	.....	.16837	.046152	4.3	−.45197	−.3137	.9024	1.0750	.....	.34706
4.4	−1.1990	1.2410	1.0826	.....	.18531	.052147	4.4	−.35887	−.4067	.8466	1.0957	.....	.38194
4.5	−1.2135	1.2141	1.1182	.....	.20333	.058717	4.5	−.26180	−.4957	.7840	1.1110	.....	.41850
4.6	−1.2226	1.1830	1.1522	.....	.22245	.065895	4.6	−.16184	−.5796	.7151	1.1206	.....	.45664
4.7	−1.2262	1.1478	1.1844	.....	.24269	.073714	4.7	−.06009	−.6577	.6404	1.1243	.....	.49621
4.8	−1.2244	1.1085	1.2145	.....	.26405	.....	4.8	.04232	−.7291	.5603	1.1216	.....	.53704
4.9	−1.2172	1.0652	1.2424	.....	.28652	.....	4.9	.14426	−.7932	.4755	1.1124	.....	.57894
5.0	−1.2045	1.0182	1.2679	.....	.31011	.....	5.0	.24461	−.8491	.3867	1.0965	.....	.62169
							5.1	.34227	−.8964	.2946	1.0738	.....	.66504

TABLE 2.—Continued

$E_{lab.}=90$ Mev							$E_{lab.}=120$ Mev						
z	$u_0(z)$	$u_1(z)$	$u_2(z)$	$u_3(z)$	$u_4(z)$	$u_5(z)$	z	$u_0(z)$	$u_1(z)$	$u_2(z)$	$u_3(z)$	$u_4(z)$	$u_5(z)$
0.1	0.24151	0.01070	0.00025				0.1	0.24053	0.01259	0.00035			
.2	.42629	.04031	.00192	0.00007			.2	.42279	.04734	.00270	0.00011		
.3	.56129	.08540	.00622	.00034	0.00001		.3	.55251	.09995	.00873	.00056	0.00003	
.4	.65235	.14282	.01417	.00104	.00006		.4	.63614	.16631	.01980	.00170	.00012	0.00001
.5	.70460	.20961	.02658	.00246	.00018		.5	.67735	.24250	.03698	.00402	.00035	.00002
.6	.72296	.28303	.04406	.00494	.00044		.6	.68126	.32475	.06096	.00804	.00084	.00007
.7	.71078	.36046	.06704	.00887	.00093	0.0001	.7	.65246	.40946	.09215	.01486	.00175	.00018
.8	.67289	.43943	.09577	.01465	.00177	.0002	.8	.59550	.49324	.13002	.02358	.00332	.00038
.9	.61274	.51762	.13029	.02270	.00310	.0004	.9	.51493	.57288	.17613	.03628	.00579	.00076
1.0	.53391	.59283	.17048	.03341	.00511	.0006	1.0	.41527	.64547	.22814	.05300	.00948	.00139
1.1	.43986	.66303	.21603	.04717	.00800	.0011	1.1	.30104	.70835	.28581	.07421	.01473	.00239
1.2	.33396	.72634	.26646	.06434	.01200	.0018	1.2	.17670	.75922	.34805	.10029	.02193	.00390
1.3	.21946	.78108	.32112	.08522	.01735	.0029	1.3	.04665	.79614	.41352	.13147	.03146	.00611
1.4	.09952	.82575	.37923	.11002	.02434	.0044	1.4	−.08488	.81757	.48071	.16785	.04373	.00920
1.5	−.02281	.85910	.43986	.13892	.03322	.0064	1.5	−.21384	.82240	.54793	.20937	.05913	.01343
1.6	−.14462	.88008	.50196	.17199	.04428	.0092	1.6	−.33643	.81001	.61337	.25577	.07801	.01905
1.7	−.26316	.88793	.56439	.20919	.05779	.0129	1.7	−.44918	.78020	.67517	.30665	.10069	.02635
1.8	−.37584	.88212	.62594	.25040	.07401	.0176	1.8	−.54897	.73326	.73148	.36137	.12742	.03562
1.9	−.48028	.86242	.68533	.29538	.09316	.0235	1.9	−.63314	.66996	.78045	.41915	.15836	.04717
2.0	−.57436	.82885	.74128	.34378	.11546	.0309	2.0	−.69946	.59149	.82038	.47901	.19360	.06130
2.1	−.65617	.78173	.79250	.35913	.14106	.0399	2.1	−.74627	.49945	.84967	.53983	.23310	.07832
2.2	−.72413	.72163	.83774	.44886	.17007	.0508	2.2	−.77241	.39585	.86697	.60035	.27668	.09849
2.3	−.77693	.64940	.87581	.50430	.20253	.0638	2.3	−.77730	.28300	.87113	.65919	.32406	.12204
2.4	−.81358	.56512	.90559	.56067	.23843	.0791	2.4	−.76994	.16347	.86133	.71492	.37480	.14916
2.5	−.83344	.47313	.92609	.61713	.27767	.0969	2.5	−.72387	.04007	.83704	.76605	.42832	.17998
2.6	−.83620	.37194	.93645	.67274	.32008	.1173	3.6	−.66720	−.08429	.79809	.81109	.48391	.21455
2.7	−.82187	.26425	.93599	.72653	.36541	.1406	2.7	−.59251	−.20962	.74467	.84860	.54071	.25282
2.8	−.79084	.15191	.92417	.77748	.41331	.1667	2.8	−.50188	−.32395	.67732	.87720	.59776	.29468
2.9	−.74378	.03589	.90070	.82455	.46336	.1959	2.9	−.39778	−.43342	.59698	.89565	.65397	.33987
3.0	−.68169	−.07879	.86544	.86671	.51504	.2280	3.0	−.28304	−.53230	.50491	.90288	.70819	.38807
3.1	−.60588	−.19306	.81852	.90294	.56778	.2632	3.1	−.16073	−.61815	.40271	.89799	.75919	.43880
3.2	−.51789	−.30385	.76025	.93228	.62090	.3012	3.2	−.03414	−.68880	.29229	.88035	.80570	.49150
3.3	−.41952	−.40913	.69118	.95383	.67367	.3421	3.3	.09336	−.74245	.17581	.84957	.84646	.54547
3.4	−.31275	−.50598	.61208	.96678	.72531	.3855	3.4	.21838	−.77773	.05562	.80553	.88022	.59993
3.5	−.19973	−.59557	.52393	.97043	.77498	.4312	3.5	.33760	−.79369	−.06575	.74846	.90380	.65400
3.6	−.08273	−.67325	.42789	.96420	.82181	.4788	3.6	.44787	−.78990	−.18570	.67884	.92210	.70769
3.7	.03592	−.73854	.32530	.94766	.86491	.5279	3.7	.54627	−.76640	−.30157	.59751	.92815	.75997
3.8	.15386	−.79021	.21766	.92055	.90341	.5781	3.8	.63021	−.72371	−.41077	.50559	.92316	.80375
3.9	.26874	−.82725	.10660	.88277	.93643	.6288	3.9	.69748	−.66289	−.51081	.40449	.90849	.84591
4.0	.37828	−.84894	−.00516	.83440	.96312	.6793	4.0	.74631	−.58540	−.59934	.29588	.87774	.88235
4.1	.48031	−.85483	−.11881	.77570	.98271	.7291	4.1	.77541	−.49317	−.67427	.18167	.83673	.91197
4.2	.57280	−.84477	−.22953	.70714	.99446	.7774	4.2	.78404	−.38851	−.73379	.06396	.78356	.93373
4.3	.65394	−.81891	−.33647	.62936	.99773	.8235	4.3	.....	−.27402	−.77642	−.05500	.71856	.94667
4.4	.72211	−.77770	−.43783	.54318	.99200	.8665	4.4	.....	−.15260	−.80107	−.17286	.64235	.94995
4.5	.77597	−.72188	−.53186	.44960	.97684	.9058	4.5	.....	−.02731	−.80705	−.28722	.55581	.94284
4.6	.81447	−.65248	−.61693	.34977	.95196	.9406	4.6	.....	.09867	−.79413	−.39570	.46009	.92479
4.7	.83684	−.57077	−.69152	.24500	.....	.9700	4.7	.....	.22214	−.76251	−.49597	.35657	.89543
4.8	.84264	−.47827	−.75430	.13672	.....	.9934	4.8	.....	.33996	−.71286	−.58585	.24689	.85459
4.9	.83177	−.37673	−.80411	.02644	.....	1.0100	4.9	.....	.44911	−.64627	−.66332	.13283	.80233
5.0	.80444	−.26805	−.84001	−.08423	.....	1.0193	5.0	.....	.54679	−.56425	−.72661	.01639	.73891
							5.1	.....	.63050	−.46872	−.77423	−.10035	.66487

TABLE 2.—Continued

$E_{lab.}=150$ Mev							$E_{lab.}=150$ Mev						
x	$u_0(x)$	$u_1(x)$	$u_2(x)$	$u_3(x)$	$u_4(x)$	$u_5(x)$	x	$u_0(x)$	$u_1(x)$	$u_2(x)$	$u_3(x)$	$u_4(x)$	$u_5(x)$
0.1	0.27994	0.01427	0.00046				2.6	−0.40735	−0.41883	0.55142	0.84835	0.62495	0.32625
.2	.42044	.05357	.00350	0.00017	0.00001		2.7	−.28848	−.52147	.45161	.85348	.68178	.37771
.3	.54636	.11272	.01129	.00081	.00005		2.8	−.15996	−.60809	.34040	.84405	.73443	.43202
.4	.62237	.18662	.02555	.00249	.00019	0.00001	2.9	−.02609	−.67594	.22042	.81922	.78123	.48879
.5	.65321	.27031	.04749	.00585	.00057	.00005	3.0	.10865	−.72286	.09468	.77893	.82051	.54584
.6	.64379	.35898	.07786	.01166	.00136	.00013	3.1	.23977	−.74733	−.03359	.72298	.85065	.60327
.7	.59923	.44801	.11691	.02072	.00285	.00032	3.2	.35293	−.74853	−.16093	.65201	.87017	.65942
.8	.52488	.53306	.16443	.03382	.00537	.00070	3.3	.47405	−.72634	−.28387	.56703	.87776	.71295
.9	.42627	.61016	.21972	.05169	.00932	.00137	3.4	.59946	−.68141	−.39895	.46949	.87232	.76242
1.0	.30905	.67573	.28166	.07495	.01517	.00250	3.5	.64601	−.61509	−.50288	.36126	.85304	.80636
1.1	.17895	.72670	.34873	.10406	.02342	.00428	3.6	.70120	−.52942	−.59262	.24462	.81941	.84331
1.2	.04166	.76058	.41908	.13930	.03461	.00695	3.7	.73320	−.42707	−.66549	.12216	.77130	.87182
1.3	−.09728	.77548	.49057	.18071	.04925	.01080	3.8	.74098	−.31123	−.71928	−.00327	.70894	.89058
1.4	−.23255	.77021	.56086	.22807	.06785	.01616	3.9	.72430	−.18554	−.75230	−.12860	.63296	.89836
1.5	−.35923	.74425	.62749	.28090	.09085	.02340	4.0	.68372	−.05397	−.76344	−.25069	.54479	.89416
1.6	−.47285	.69782	.68796	.33844	.11860	.03290	4.1	.62058	.07930	−.75225	−.36638	.44465	.87717
1.7	−.56952	.63180	.73984	.39965	.15133	.04508	4.2	.53607	.21006	−.71892	−.47259	.33553	.84685
1.8	−.64604	.54777	.78082	.46325	.18915	.06033	4.3	.43567	.33413	−.66433	−.56641	.....	.80297
1.9	−.69991	.44792	.80884	.52771	.23199	.07905	4.4	.32001	.44755	−.59000	−.64522	.....	.74561
2.0	−.72948	.33499	.82217	.59172	.27958	.10158	4.5	.19381	.54668	−.49805	−.70675	.....	.67521
2.1	−.73390	.21218	.81945	.65222	.33147	.12821	4.6	.06122	.62834	−.39117	−.74917	.....	.59254
2.2	−.71318	.08307	.79977	.70846	.38698	.15915	4.7	−.07338	.69990	−.27251	−.77114	.....	.49873
2.3	−.66817	−.04859	.76273	.75807	.44526	.19450	4.8	−.20556	.72937	−.14562	−.77190	.....	.39525
2.4	−.60050	−.17866	.70846	.79911	.50521	.23426	4.9	−.33098	.74546	−.01431	−.75124	.....	.28390
2.5	−.51255	−.30337	.63762	.82975	.56558	.27828	5.0	−.44551	.73763	.11743	−.70960	.....	.16675

TABLE 3. δ_l (*radians*)

x	$E_{lab.}$ (Mev)				
	20	50	90	120	150
0	1.5886	1.2958	1.1255	1.0483	0.9907
1	0.1871_5	0.3078	0.3607	0.3767	.3844
2	.0314	.0878	.1331	$.1566_5$	.1723
3	.0040	.0284	.0555	.0712	.0839
4	.0007	.0049	$.0234_5$	.0339	.0424
5	$.0000_5$	.0027	$.0103_5$	.0168	.0223

LOS ANGELES, February 12, 1953.

Journal of Research of the National Bureau of Standards Vol. 52, No. 5, May 1954 Research Paper 2499

Electrical Measurements in the Selection of Bolt Materials for Service Underground

W. J. Schwerdtfeger

Electrical measurements made in the laboratory are useful in generally predicting the relative behavior of bolt materials underground as pertaining to the corrosive effect of the soil. Some arbitrarily chosen low-alloy ferrous materials are shown to be superior to plain cast iron or steel commonly used for the fabrication of bolts. The effect of exposure on the potentials of cast iron and galvanized iron as components of galvanic couples is described

1. Introduction

Although failures of plain ferrous bolts underground are confined chiefly to severely corrosive environments, the costs attributed to shutdowns and repairs are high. Figure 1 shows bolts removed from couples exposed to 14 underground environments, including cinders (site 67), and illustrates the effect of 13 years of exposure at the National Bureau of Standards test sites. The 13 soils range from moderate to severe corrosivity, except for sites 53 and 55, which are slightly corrosive.

In very corrosive soils, bolt failures may occur before severe corrosive effects take place on the structures to which the bolts are coupled. Primarily responsible for such failures, aside from normally accelerated corrosion due to stress and edge effects, are probably the effects due to galvanic action between the bolts and the structures.

The solution to the problem then seemingly lies in the use of bolts fabricated from materials that are cathodic to the structure. Although ferrous bolts containing certain alloying constituents to make them cathodic to iron are available, their use might be discouraged because of greatly increased cost. Also, because of the potential difference between the coupled elements, it would appear that excessive localized attack might be expected to occur on the adjacent anodic structure. However, based on experimental work of other investigators, such fears are not always justified [1, 2, 3].[1] The corrosion rates of materials, or their resistance to corrosion, can be measured by their polarizing characteristics, and it has been shown, for iron exposed to soil, that an increase in cathodic polarization is synonymous with a reduced rate of corrosion [4]. Direct current flowing to stainless-steel or nickel-copper alloy (70–30) causes marked polarization because these materials are relatively free of potent local action. Thus, the coupling of relatively small areas of such materials to plain cast-iron or steel structures need not result in excessive galvanic corrosion to the structure. Also, whatever the galvanic current, the weight loss on the adjacent anodic structure will not be increased by an amount equivalent to the magnitude of the current because the galvanic current will reduce local action on the affected anodic area [4, 5].

[1] Figures in brackets indicate the literature references at the end of this paper.

In order to determine what electrical measurements might be of value in predicting the probable behavior of bolts for use underground, potential measurements were made on the components of galvanic couples, followed by exposure of the couples to a very corrosive soil for 1 year in the laboratory. Potentials and currents were measured during the exposure period and weight losses obtained at the conclusion. Donoho and MacKenzie [6] found that the addition of 1 percent of copper to cast-iron bolts resulted in a marked reduction of corrosion on the bolts when coupled with plain cast iron. The work of these investigators also suggested the use of a small amount of nickel as a constituent of ferrous bolts, the nickel being more soluble in iron than copper. As an extensive use of low-alloy bolts would not result in prohibitive installation costs to industry, such bolts were arbitrarily chosen for the main laboratory study, along with high-alloy cast-iron and nickel-copper alloy (70–30) bolts known to be cathodic to plain cast iron but which are relatively high in cost.

2. Laboratory Procedure

2.1. Preliminary Potential Measurements

Selecting bolts that are to be cathodic to a particular structure implies the necessity for a reproducible method of measuring potentials. It has been shown that potentials can be measured, with a reasonable degree of accuracy, by placing metallic specimens in puddled soil contained in a relatively airtight enclosure [7]. Under normal conditions of aeration underground, the open-circuit electromotive force between a bolt and the adjacent structure is not necessarily the same as the potential difference that exists in a relatively air-free environment. However, a reproducible method of measuring potentials would be useful in determining the effect of varying amounts of alloying constituents. As will be shown later, an inherent initial potential difference of only 10 mv between the components of a couple has the effect of making the cathodic element considerably more cathodic with time.

The laboratory investigation to be described was made with a very corrosive soil from Atlantic City, N. J., which has a pH of 4.4 and a resistivity of 140 ohm-cm.

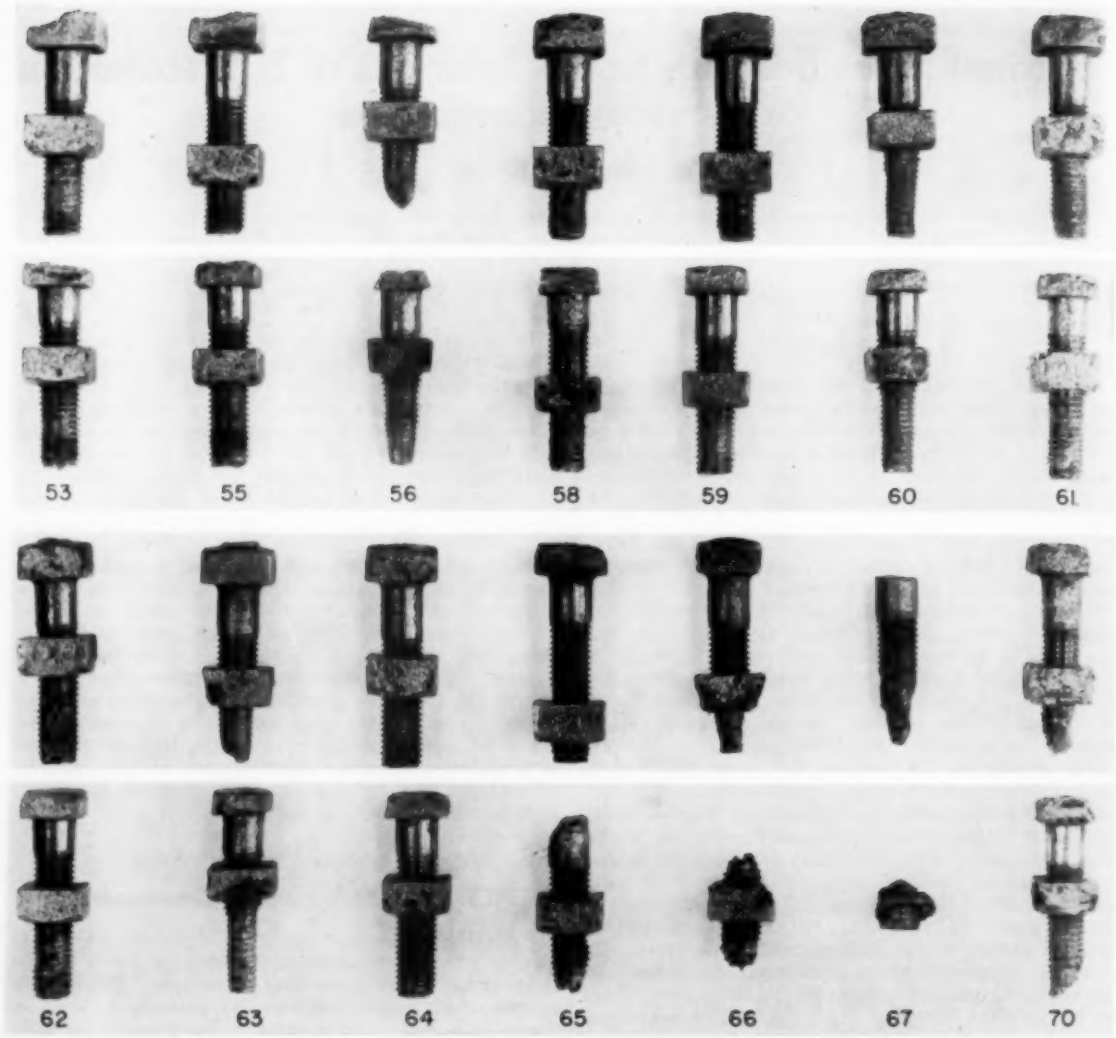

FIGURE 1. *Bolts removed from couples after an underground period of 13 years at 14 NBS test sites.*

A pair of bolts, cast iron (upper row) and steel (lower row), shown above the site numbers were components of a joint. Each pair of bolts (0.625 in. by 3 in.) joined two cast-iron plates (0.5 in. by 3.5 in. by 12 in.) that overlapped by 1.5 in.

Potential measurements on the bolts were made prior to exposure of the couples to the soil. The bolts were first cleaned with carbon tetrachloride and then wire brushed. The electrical connection for the potential measurement was made through a single conductor No. 8 rubber-covered copper wire screwed into the head of each bolt, with molten asphalt being applied around the point of contact. Dry soil was broken up, ground, and passed through a No. 20 sieve. A sufficient quantity for a complete series of potential measurements was thoroughly mixed, watered, and mechanically worked over, with water being added gradually until the soil was saturated. Two bolts of the same size and composition were each covered with the saturated soil and then horizontally and laterally placed in a crystallizing dish (190 mm diam by 70 mm high), with the wires from the bolts protruding vertically over the top of the dish. More puddled soil was placed into the dish and so distributed as to fill all space to a depth within about ½ in. from the top. Paraffin, barely molten, was then poured into the dish over the soil in sufficient quantity so as to flow around the wires and a No. 1 rubber stopper resting on top of the soil. An approximately ⅛-in. thickness of paraffin was found to form a fairly good air seal.

As soon as the paraffin congealed, the rubber stopper was twisted so as to break the seal of adhering wax and left to rest lightly in position. The hole formed by the rubber stopper, about midway between the bolts and about 1 in. from the side of the dish, served to relieve any pressure developed inside the dish and also as a point of access to the soil for the reference electrode.

The potential measurements are given in table 1, each value being the average for the two bolts. Except for high-alloy cast iron and the nickel-copper alloy, the average values might be considered as the steady-state potentials because of the slight deviations from the final values. The potentials of the high-alloy cast-iron and nickel-copper alloy bolts continued to get more anodic, presumably even after 45 days. The average variation of potential between similar bolts, except for high-alloy cast iron, was less than 2 mv. The potentials of the latter bolts differed on the average by 13 mv. Although the potentials of the high-alloy cast-iron and nickel-copper alloy bolts were still changing at the conclusion of the tests, there was no reason to doubt that the stable potentials would be cathodic to plain carbon steel and cast iron. Potentials of the cast-iron gland material, the other element of the couple, were found to be about the same as the values shown for plain carbon steel.

Earlier investigators have found that both nickel and copper additions will make iron more cathodic [6, 8]. Copper, however, is less soluble in iron than nickel, only about 0.5 percent being dissolved at room temperature. Nickel, on the other hand, is very soluble in iron and, in addition, appears to increase the propensity for copper to dissolve in iron. Thus, while iron containing dissolved copper should be more cathodic than unalloyed iron, alloys of iron containing both copper and nickel should be even more cathodic. This effect of nickel is substantiated by the results given in table 1, in which cast irons and steels containing copper and nickel are more cathodic than plain steel and cast iron containing 1 percent of copper.

TABLE 1. *Potentials of bolts in puddled soil*

Bolt material	Exposure time	Potential, referred to saturated calomel		
		Initial [a]	Final [a]	Average [b]
	Days	*v*	*v*	*v*
Cast iron (1 Cu)	13	−0.661	−0.678	−0.674
Cast iron (1 Ni, 1 Cu)	13	−.648	−.666	−.661
Cast iron (2 Ni, 1 Cu)	13	−.645	−.663	−.657
Plain carbon steel	13	−.673	−.670	−.670
Cr-Ni-Cu-Si steel (1 Cr, 0.5 Ni, 0.5 Cu, 0.5 Si)	13	−.653	−.663	−.661
Ni-Cu steel (1.5 Ni, 1 Cu)	13	−.646	−.656	−.654
High-alloy cast iron (15 Ni, 6.6 Cu, 2.6 Cr)	45	−.470	−.533	−.506
Nickel-copper alloy (70-30)	45	−.295	−.403	−.368

[a] Average of 2 bolts.
[b] Average for the exposure period (9 pairs of measurements in as many days for bolts exposed for 13 days and 19 pairs of measurements covering the 45-day exposure period).

2.2. Coupling and Soil-Moistening Procedure

Sections cut from 4-in. cast-iron pipe glands (components of mechanical joints) were bolted together to form test joints. Eight couples were assembled as shown in figure 2, using a different bolt material for each couple. In order to permit measurement of currents and potentials, the couple components were insulated by bushing the holes in the gland sections with Bakelite tubing and placing Bakelite washers under the heads and nuts of the bolts. For electrical connections, No. 8 single conductor rubber-covered copper wires were threaded and screwed into the gland sections and bolt heads, and molten asphalt was applied around the threads to reduce galvanic action. When electrical measurements were not being made, the bolts and gland sections were directly connected as shown in figure 2.

Prior to assembly, the bolts were degreased, wire-brushed, and weighed. The gland sections were also degreased, sand-blasted to remove paint, and weighed. Metal cans, 12 in. in diameter by 14 in. high, for holding the soil and couples were prepared by perforating the bottoms and covers with ¼-in. holes about 1 in. apart and painting the metal surface, inside and outside, with two coats of bituminous paint.

About 4 in. of dry soil was placed in the can, and the couple was centrally positioned on the top of the

FIGURE 2. *Couple of the type exposed to soil in the laboratory*
Gland sections were cut from 4-in. cast-iron pipe glands. Bolts are 0.75 in. by 3.5 in.

soil. The can was then filled with soil to within 4 in. from the top, allowing the insulated wires and connectors to protrude above the soil to within about ½ in. from the top of the can.

After being weighed, the cans containing the soil and couples were placed on ¾-in. high Bakelite supports in shallow galvanized pans (18 in. diam by 3 in. high). Water was poured into the shallow pan to a depth of about 1 in. and the soil moistening proceeded by capillarity. The water was maintained at this depth until the can and contents increased in weight by an amount equal to 30 percent of the weight of the dry soil contained therein. This final weight was maintained for the duration of the 1-year exposure period by the occasional addition of water. Except during the making of electrical measurements, the perforated covers were placed on the cans to reduce evaporation and drying of the soil.

2.3. Electrical Measurements During Exposure

Galvanic currents between the components of the couples and the open-circuit potentials of the components were measured biweekly during the initial 4 months of exposure, and monthly thereafter. The galvanic currents were measured with a zero resistance milliameter prior to placing the couples on open-circuit for the potential measurements. The potentials were measured with a potentiometer and a copper–copper-sulfate reference half-cell with the reference electrode being positioned on the surface of the soil directly over the couple. Two potentials were obtained on each bolt, the first being read as quickly as possible upon open-circuiting the couple, and the second after permitting the couples to stand on open-circuit for about 30 min. Polarization effects occurring on the bolts were indicated by the change in potential between the two readings, and, as will be shown later, such polarization was also indicated by the open-circuit electromotive force between a gland section and a bolt, because the gland section polarized relatively little.

Cathodic polarization curves were obtained on each bolt before disassembling the couples for cleaning and weight-loss measurements. These data were desirable because the breaks and slopes of such curves have been shown to be related to the instantaneous rates of corrosion [4]. Before obtaining the polarization curves, each couple was left standing on open-circuit for 24 hr to permit time for stabilization of the potentials and to observe the differences of potential between the various bolts and the glands. The polarization data were obtained with an electronic interruption measuring circuit [9]. Equal increments of current were applied at arbitrary time intervals of 3 min.

3. Results

3.1. Effect of the Galvanic Current on the Gland Sections

Although the study was directed chiefly to the behavior of the bolts, the possible corrosive effects on the anodic member of the couple could not be dismissed. The bolts of all the couples were cathodic to the gland sections throughout the test period, even though the potentials of the cast-iron bolt (1% Cu) and the plain carbon-steel bolt (table 1) were within 5 mv of the cast-iron gland material, which could result in a potential reversal. Such reversals have been observed at the Bureau with plain ferrous bolts and the cast-iron bolts containing only 1 percent of copper. The weight losses that occurred on the gland sections are tabulated in table 2. To compare the effect of normal corrosion on a gland section with the effect of galvanic corrosion superimposed on normal corrosion, a couple was assembled in which the components were left on open-circuit throughout the exposure period. It is noteworthy that the weight loss, 95.25 g, that occurred on the gland sections of this joint is greater than the weight losses of the gland sections removed from 50 percent of the galvanic couples, including the couple with the cast-iron bolts containing 2 percent of nickel in which the galvanic current was relatively high. These data show that local action currents on the gland sections were reduced as a result of galvanic current because, except for the couple with high-alloy cast-iron bolts, the weight losses of the gland sections were less than the sum of the weight loss attributed to galvanic current (table 2) and the weight loss (95.25 g) of the open-circuited gland sections. The reduction of the weight loss resulting from local action currents follows because of anodic polarization due to the galvanic current [4, 5]. Top and elevation views of the gland sections

TABLE 2. *Effect of the galvanic current on the corrosion of the gland sections*

Coupled bolts		Galvanic [a] current	Weight loss [b] of coupled gland sections—368 days	
Identification	Material		Loss resulting from galvanic current [c]	Total loss
		ma		
146	Cast iron (1 Cu)	1.15		
148	do	1.11	*g*	*g*
		2.26	20.80	97.14
336	Cast iron (1 Ni, 1 Cu)	0.70		
338	do	.76		
		1.46	13.43	90.04
321	Cast iron (2 Ni, 1 Cu)	1.76		
322	do	2.09		
		3.85	35.43	93.65
426	Plain carbon steel	1.09		
428	do	1.32		
		2.41	22.18	100.38
361	Cr–Ni–Cu–Si steel	0.78		
362	do	.47		
		1.25	11.50	76.66
516	Ni–Cu steel	1.04		
518	do	1.35		
		2.39	22.00	83.64
45	High-alloy cast iron	0.74		
47	do	.83		
		1.57	14.45	112.73
1Z	Nickel-copper alloy	2.06		
1ZZ	do	2.15		
		4.21	38.75	104.92

[a] Average value based on the area under the current versus time curve for 368 days.
[b] Weight loss of 2 gland sections, mechanically but not electrically coupled, was 95.25 g. The gland area exposed to the soil was 56.6 in.²
[c] Calculated by Faraday's law.

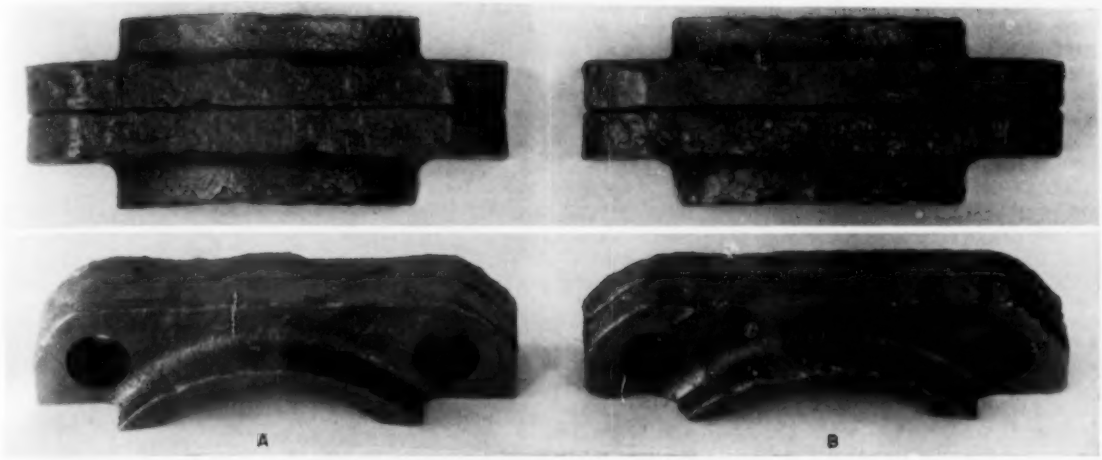

FIGURE 3. *Top and elevation views of two sets of gland sections after soil exposure for 1 year in the laboratory.*

Set A was bolted but not galvanically coupled; set B was bolted and galvanically coupled.

(A) left on open-circuit and gland sections (B) galvanically coupled by bolts 321 and 322 (table 2) are shown in figure 3. There is some slight evidence in the photograph B of concentrated attack, perhaps due to the galvanic current, which attack probably would be minimized on a normal underground structure, where the area relationship would be more favorable.

3.2. Effect of the Galvanic Current on the Bolts

Significant electrical measurements pertaining to the bolts are shown in table 3. The open-circuit electromotive force between the bolts and the gland sections after 100 days and 368 days of exposure are tabulated in columns 5 and 6, respectively. The values shown for the 100-day exposure period were obtained after the couple had been left on open-circuit for 30 min, and the potential differences given for the 368-day period were measured after the couple had been left on open-circuit for 24 hr. Even though the exposed gland-section to bolt-area ratio was approximately only 2 to 1, the change of the gland-section potentials, not shown, from closed-circuit to open-circuit was relatively small, in fact, a maximum of 25 mv in the case of the couple with the nickel-copper alloy bolts. The magnitude of the potential difference between a bolt and gland section, after open-circuiting, depended upon the amount of current that flowed when the circuit was closed. The reduction of the local action currents on the bolts, as a result of the galvanic current from

TABLE 3. *Relation between weight loss and polarization of bolts*

Coupled bolts		Galvanic current		Open-circuit emf between the gland section and bolt after—		Cathodic polarization curve of the bolt [b]		Weight loss of the bolt after exposure for 368 days [c]
Identification	Material	Average [a]	Final	100 days of exposure	368 days of exposure	I_p	Slope after I_p	
		ma	*ma*	*mv*	*mv*	*ma*	*v/ma*	*g*
146	Cast iron (1 Cu)	1.15	1.45	115	130	0.4	0.48	5.6
148	do	1.11	1.28	120	150	.4	.48	4.9
336	Cast iron (1 Ni, 1 Cu)	0.70	1.20	30	115	.5	.60	10.3
338	do	.76	1.10	50	115	.25	.65	7.9
321	Cast iron (2 Ni, 1 Cu)	1.76	1.85	160	200	<.10	.90	3.4
322	do	2.09	1.60	270	245	.10	.75	3.6
426	Plain carbon steel	1.09	1.03	55	95	1.20	.46	7.5
428	do	1.32	1.27	80	120	0.65	.44	7.7
361	Cr-Ni-Cu-Si steel	0.78	0.73	60	47	.45	.50	6.1
362	do	.47	.54	40	27	.70	.50	8.2
516	Ni-Cu steel	1.04	.86	140	70	.80	.48	4.8
518	do	1.35	1.20	140	130	.24	.52	2.8
45	High-alloy cast iron	0.74	1.00	250	180	.....	.....	0.66
47	do	.83	1.28	230	295	≪0.1	1.17	.57
1Z	Nickel-copper alloy	2.06	1.34	380	420	.....	.....	.23
1ZZ	do	2.15	1.60	400	445	≪0.1	3.75	.15

[a] Average value based on the area under the current-time curve for 368 days.
[b] Obtained at the end of the exposure period (see text).
[c] Includes weight loss of the nut. Hereafter, this is always so whenever the weight loss of the bolt is mentioned.

the gland sections, caused the bolts to assume cathodic potentials [7]. Thus, for bolts made of materials having similar rates of corrosion, such as the 3 varieties of cast iron or the 3 kinds of steel, table 3, the larger galvanic currents generally provided for better protection of the bolts, as shown by the larger open-circuit potentials and the correspondingly lower weight losses.

It has also been shown [7] that cathodic polarization curves can be of value in predicting the degree of protection achieved as a result of previously applied external current, provided not too much time is permitted to elapse after the current is removed. In the present study, after 368 days the couples were open-circuited, and then after the lapse of 24 hr were connected in series with an external source of direct current and cathodic polarization data obtained. Polarization curves were then drawn for each bolt. The currents, I_p, at which significant breaks in the curves were observed and also the slopes of the curves after the breaks are tabulated in table 3. Previous work [4] has shown that smaller values of I_p, or greater slopes after the break in the curve, signify lower instantaneous rates of corrosion. This relationship is generally shown by the data and reflected by the weight losses of the cast-iron bolts and also of the group of steel bolts.

The extent of reducing the corrosion on the bolts by making them cathodic to the gland sections that they coupled is shown by the data (cols. 3 and 4, table 4) and by figures 4 and 5. These data show the beneficial effects of relatively small amounts of alloying constituents, particularly 1.5 to 2 percent of nickel. The cathodic nature of high-alloy cast iron and nickel-copper alloy resulted in almost negligible corrosion of the bolts fabricated of these materials. Although the average galvanic current (table 3) on all but two specimens is much greater than the current, I_p, (current required for cathodic protection), complete cessation of corrosion is not

TABLE 4. *Comparison of weight losses of uncoupled and coupled bolts*

Bolt material	Weight loss of bolt [a] after 368 days of exposure		Reduction in weight loss of coupled bolts based on control (uncoupled)	
	Control uncoupled	Coupled cathodic	Based on the actual weight loss	Based on the [b] calculated corrosion rate at the end of the exposure period
	g	*g*	*Percent*	*Percent*
Cast iron (1 Cu)	28.5	5.3	81.4	89.5
Cast iron (1 Ni, 1 Cu)	25.6	9.1	64.4	88.7
Cast iron (2 Ni, 1 Cu)	33.8	3.5	89.7	97.9
Plain carbon steel	16.4	7.6	53.7	56.7
Cr-Ni-Cu-Si steel	19.7	7.1	64.0	77.7
Ni-Cu steel	14.2	3.8	73.2	71.9
High-alloy cast iron	8.8	0.61	93.1	>95
Nickel-copper alloy	0.95	.19	80.0	>95

[a] Average to 2 bolts.
[b] Weight loss (grams) $= KIt$, where $K = 2.8938 \times 10^{-4}$ g/coulomb; $t = 368$ days, expressed in seconds; and $I = 0.83\ I_p$ (table 3) in amperes (see text).

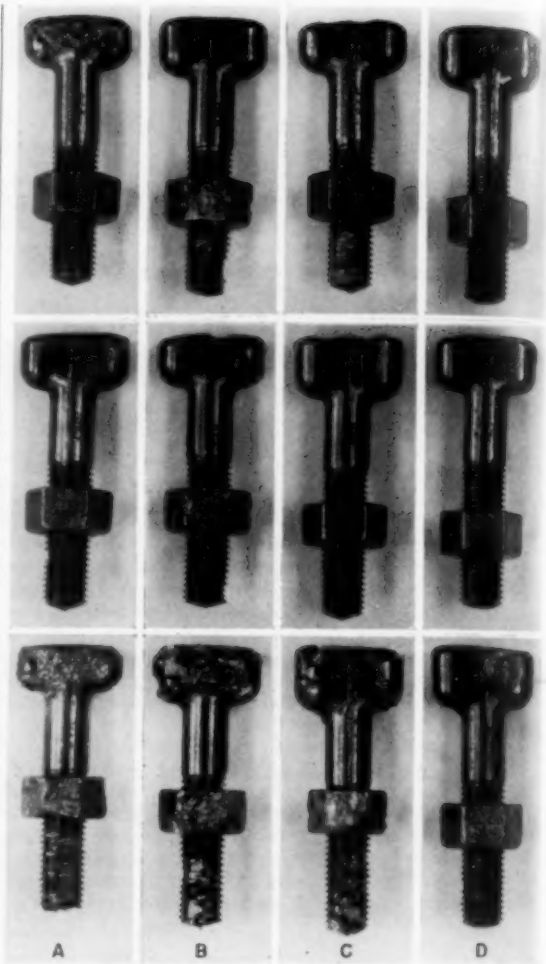

FIGURE 4. *Cast-iron bolts exposed to Atlantic City soil for 1 year in the laboratory.*

A, Cast iron (1 Cu); B, cast iron (1 Ni, 1 Cu); C, cast iron (2 Ni, 1 Cu); D, high-alloy cast-iron. Bolts in the upper two rows were coupled to gland sections. Bolts in the lower row are uncoupled controls. Parts of the controls not normally in direct contact with the soil were coated with bituminous paint.

to be expected because the gland sections furnishing the current limited the potentials assumed by the bolts, preventing a drift in potential to the protective value [7].

The effect of exposure time on the corrosion rates of the various bolts is shown by the calculated data (col. 5, table 4). The calculated weight losses on which the data in column 5 are based were figured from the breaks, I_p in the cathodic polarization curves (table 3). The value for I substituted in the Faraday equation, footnote b, table 4, has been previously shown to be quite reliable for plain ferrous

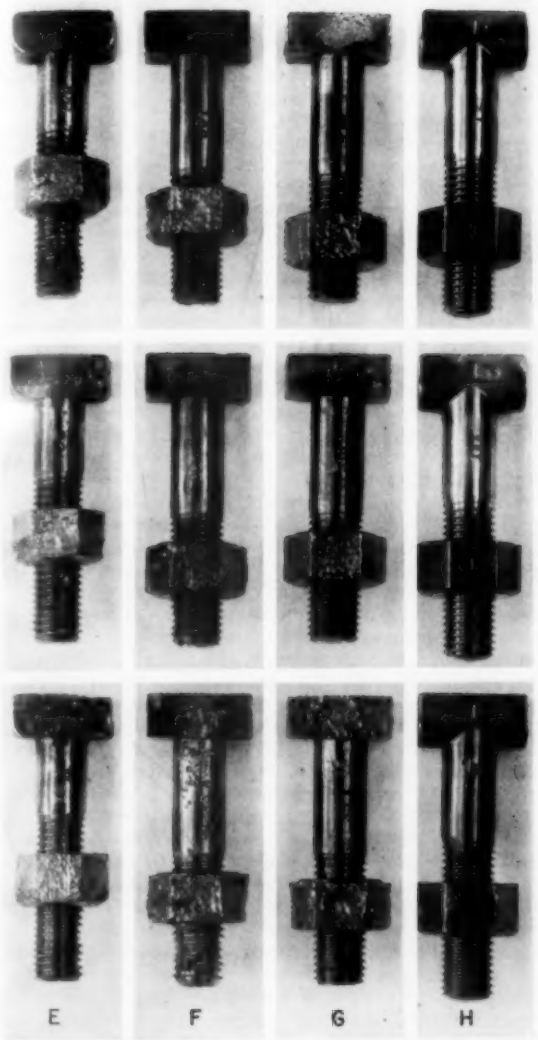

FIGURE 5. *Machined bolts exposed to Atlantic City soil for 1 year in the laboratory.*

E, Plain carbon steel; F, Cr-Ni-Cu-Si steel; G, Ni-Cu steel; H, copper alloy (70-30). Bolts in the upper two rows were coupled to gland sections. Bolts in the lower row are uncoupled controls. Parts of the controls not normally in direct contact with the soil were coated with bituminous paint.

materials corroding in soils [4]. A comparison of the data in columns 4 and 5 indicates, in general, that all of the bolts were corroding at a lesser rate at the conclusion of the laboratory-exposure period than previously and particularly so the cast iron (1 Ni, 1 Cu) and the Cr-Ni-Cu-Si steel bolts. Corrosion of the cast-iron bolt (2 Ni, 1 Cu) seems to have been halted.

4. Considerations in Bolt Replacement

4.1. Graphitization of Cast Iron

Wesley, Copson, and LaQue [10] have investigated experimentally the effect of graphitization on the normal corrosion of cast iron and also the galvanic action as a result of coupling graphitized and ungraphitized cast iron. These investigators found that the graphitized cast iron was cathodic, with the potential depending upon the thickness and porosity of the graphite coating. Such facts must be considered when planning the replacement of bolts, especially on underground cast-iron pipe lines.

In order to study potentials of graphitized and ungraphitized cast-iron specimens, with particular emphasis on the effect of time, measurements were made with Atlantic City soil by the method previously described. Approximately 6 in.^{2} each of duplicate specimens were exposed to puddled soil. The graphitized pieces were cut from the corners of a cast-iron plate that had been exposed to a corrosive soil for 13 years. The areas of iron that became exposed by cutting were covered with two coats of bituminous paint. The data obtained are shown in figure 6. As observed by Wesley, Copson, and LaQue, there is a decrease in potential difference with time between the graphitized and ungraphi-

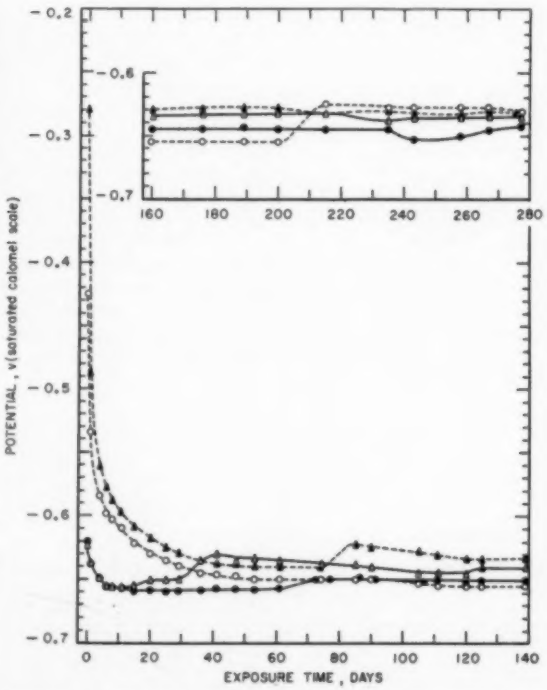

FIGURE 6. *Potential relations between previously unexposed cast iron and graphitized cast iron in puddled soil.*

●, Previously unexposed; △, previously unexposed; ○, graphitized, previously exposed for 13 years; ▲, graphitized, previously exposed for 13 years.

tized specimens. The data of figure 6 extend over a longer time period than the data obtained by these investigators. The large potential difference observed after initial exposure is of no particular significance, and for the period between 40 and 200 days it is questionable whether there is any significant potential difference. However, for the last 60 days of exposure both of the previously graphitized specimens were cathodic to the previously unexposed pieces, therefore, indicating that graphitization should be considered when replacing bolts on underground cast-iron structures.

4.2. Potentials of Low-Alloy Steels

Because of the tendency of cast iron and even plain steel, after long exposure, to assume potentials cathodic to similar materials previously unexposed, such as replaced bolts, made it desirable to measure the potentials of additional alloys that might be used for fabricating bolts. Potentials of 4 chromium steels and a cast iron containing 3.1 percent of nickel are tabulated in table 5. The average values are directly comparable with the average potentials recorded in table 1, being made in the same soil and under the same conditions. The average potential variation between the two specimens of each alloy was less than 2 millivolts. The effect of the amount of chromium on the potential is noteworthy. The steels containing 4.67, 5.02, and 5.76 percent of chromium are significantly cathodic to the steel containing only 2 percent of chromium and, of course, to plain steel and cast iron. The potential measurements were carried on for a considerably longer period than were most of the measurements shown in table 1. This was necessary because the potentials continued to get more cathodic as time went on, as will be noted by comparing the average and final readings (table 5). As shown by the data (tables 1 and 5), steel alloyed with about 5 percent of chromium is cathodic to plain steel or cast iron by at least 50 mv, and therefore might be a desirable material for use in the fabrication of bolts. The increase of nickel content in cast iron from 2 to 3.1 percent also seems to have a significant effect on the potential, as will be observed by comparing the potentials in tables 1 and 5.

TABLE 5. *Potentials of low-alloy ferrous materials in puddled soil*

Material		Exposure time	Potential, referred to saturated calomel		
Composition	Identification		Initial [a]	Final [a]	Average [b]
		Days	*v*	*v*	*v*
Steel (2 Cr, with Mo)	KK	45	−0.662	−0.666	−0.663
Steel (4.67 Cr, with Mo)	E	45	−.653	−.629	−.636
Steel (5.02 Cr)	D	45	−.650	−.616	−.623
Steel (5.76 Cr, with Mo)	H	45	−.653	−.609	−.623
Cast iron (3.1 Ni)	N	45	−.638	−.651	−.649

[a] Average of 2 specimens.
[b] Average of 19 measurements made on each pair of specimens throughout the exposure period.

5. Effect of Exposure on the Galvanized-Iron—Iron Couple

Long-time underground-exposure tests have shown, particularly in alkaline soils, that galvanized steel is superior to bare steel [11]. However, it cannot be concluded that galvanized bolts should be more corrosion resistant than plain-steel bolts on underground mechanical joints because in this application galvanic rather than local corrosion becomes predominant. Under such conditions the zinc coating would soon be completely corroded away and the alloy layer exposed to the soil.

While experimenting with iron–zinc-iron alloy couples in tap water, even at room temperature, Britten [12] found that the alloy layer became cathodic to the iron. Later, as a result of similar experiments, Gilbert [13] states, "the alloy remains cathodic to steel in the aerated supply water, whether hot or cold." Gilbert also found that zinc can become cathodic to iron under aerated conditions but that the alloy layer was always cathodic to zinc under similr conditions. In aerated solutions, Hoxeng [14] observed that the reversal of the zinc-iron couple was promoted by the addition of bicarbonates and nitrates but that chlorides and sulfates decreased the probability of reversal. Recently, Romanoff [15] measured the potentials of zinc, zinc-iron alloy layer, and steel in 12 soils by the method [7] previously described. The soils varied in pH from 3.1 to 8.0. The resistivities of eight of the soils were below 400 ohm-cm. In none of the soils was the zinc found to be cathodic to steel, but in 11 soils the zinc-iron alloy layer was observed to be cathodic to steel on the average by 100 mv. Romanoff prepared the zinc-iron alloy layer by electrolytic stripping. This must not be confused with the surface resulting from exposure of galvanized iron to soil corrosion which surface was observed to be anodic to steel in all the soils.

The findings of the above investigators suggest the possibility that galvanized bolts underground, at least in some soil environments, may actually become cathodic to the structure of which they are a part. To investigate such a possibility under somewhat extreme conditions, a couple was prepared for exposure to a 0.2-percent potassium chloride solution in the laboratory at room temperature. Such a solution is equivalent in resistivity (approximately 400 ohm-cm) to a very corrosive soil. As the area ratio of structure to bolt is relatively large on underground systems, this area relation was also carried out in the laboratory experiment. The low-carbon steel that formed one element of the galvanic couple was in the shape of a disk (1/32 in. thick by 11 in. diam). The other element (hot-dipped galvanized iron) of the couple was ring-shaped having an exposed area of 1.3 in.^{2} The ring was insulated from the disk and centrally mounted about 1 in. above it. Rubber-insulated copper wires were soldered to each of the elements and the solder and exposed copper coated with bituminous paint. The couple was placed into a glass jar (11.5 in. diam by 12 in. high)

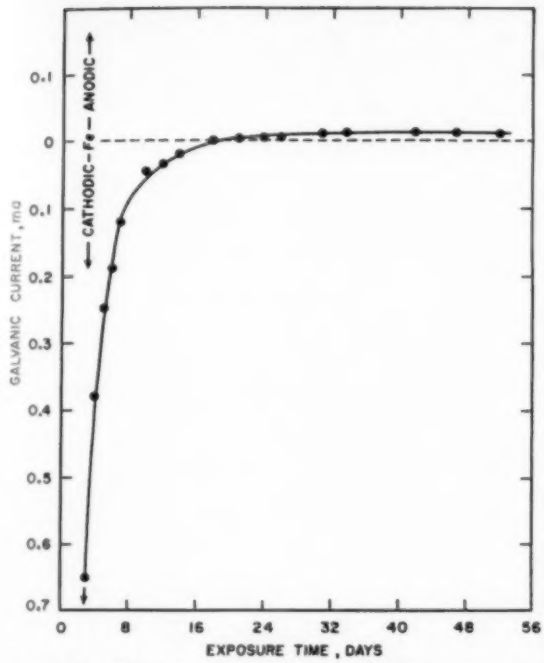

FIGURE 7. *Effect of exposure time on the galvanic current of a galvanized iron–iron couple exposed to a 0.2-percent potassium-chloride solution at room temperature.*

Galvanic current was initially 15 ma. After five additional months of exposure, the direction and magnitude of the galvanic current remained unchanged.

filled with the potassium-chloride solution and rested on insulators about 1 in. above the bottom of the jar, with the galvanized ring toward the top. The relation between the galvanic current, measured with a zero resistance milliameter, and time of exposure is shown in figure 7. The experiment showed that the zinc coating of itself offered no particular advantage, being removed rapidly, as indicated by the rapid decrease in current, but that the secondary effect of potential reversal must invariably result in some electrochemical protection of the exposed alloy layer. The experiment also suggests the likelihood of similar action underground, especially in soils of higher or perhaps even equivalent resistivity.

6. Summary

Galvanic couples consisting of cast-iron gland sections and bolts of steel and cast iron alloyed with small amounts of nickel and copper and bolts of high-alloy cast iron and nickel-copper alloy (70–30) were exposed to a corrosive soil in the laboratory for a period of 1 year. Even though galvanic current between a cathodic bolt and a structure will produce weight loss in accordance with Faraday's law, the laboratory data show that local action on the structure is reduced by the galvanic current and that the overall effect is apparently not detrimental. This should be particularly true if the structure is relatively large and fabricated of heavy material.

It is shown that the relative reduction of weight loss of the cathodic bolts can generally be predicted by potential changes of the bolts after placing the couples on open-circuit. The relative degrees of protection produced by the galvanic currents on the various bolts after exposure for 1 year were also indicated by cathodic polarization curves.

The effect of graphitization of cast iron as a result of 13 years of field exposure on the potential is shown by comparison with the potential of previously unexposed cast iron. The importance is brought out of the length of exposure time when making potential measurements.

Potentials of steels containing chromium in varying amounts between 2 and 5.76 percent were measured in a puddled soil. Steel alloyed with 5 percent of chromium was observed to be cathodic to unalloyed ferrous material by about 50 mv, indicating that it might be a desirable bolt material especially for bolt replacement purposes.

The behavior of galvanized bolts underground, at least in some soils, is suggested by an experiment in which it was observed that a potential reversal occurred in a couple consisting of galvanized iron and low-carbon steel. The electrolyte used was a solution of 2,000 ppm of potassium chloride in tap-water at room temperature. This chloride concentration is greater than that of many corrosive soils and considerably in excess of the amount heretofore believed sufficient to prevent a reversal.

The author gratefully acknowledges the cooperation of the United States Pipe & Foundry Co., American Cast Iron Pipe Co., Youngstown Sheet & Tube Co., and the Carnegie-Illinois Steel Corp. in supplying most of the materials for this study.

7. References

[1] M. R. Whitmore and J. Teres, Dissimilar metal couples, Ind. Eng. Chem. **31,** 608 (1939).
[2] F. L. LaQue and G. L. Cox, Some observations of the potentials of metals and alloys in sea water, Proc. ASTM **40,** 670 (1940).
[3] H. R. Copson, Distribution of galvanic corrosion, Trans. Electrochem. Soc. **84,** 71 (1943).
[4] W. J. Schwerdtfeger and O. N. McDorman, Measurement of the corrosion rate of a metal from its polarizing characteristics, J. Electrochem. Soc. **99,** 407 (1952).
[5] O. Gatty and E. C. R. Spooner, The electrode potential behavior of corroding metals in aqueous solutions, p. 283 (Oxford University Press, London, 1938).
[6] C. K. Donoho and J. T. MacKenzie, Control of galvanic corrosion of iron, Corrosion **2,** 20 (1946).
[7] W. J. Schwerdtfeger and O. N. McDorman, Potential and current requirements for the cathodic protection of steel in soils, J. Research NBS **47,** 104 (1951) RP2233.
[8] Ralph Landau and C. S. Oldach, Corrosion of Binary Alloys, Trans. Electrochem. Soc. **81,** 521 (1942).
[9] Robert B. Darnielle, Measurement of electrode potentials and polarization in soil-corrosion cells, J. Research NBS **25,** 421 (1940) RP1336.

[10] W. A. Wesley, H. R. Copson, and F. L. LaQue, Some consequences of graphitic corrosion of cast iron, Metals & Alloys **7,** 325 (1936).

[11] Irving A. Denison and Melvin Romanoff, Corrosion of galvanized steel in soils, J. Research NBS **49,** 299 (1952) RP2366.

[12] S. C. Britton, The resistance of galvanized iron to corrosion by domestic water supplies, J. Soc. Chem. Ind. **55,** 19T (1936).

[13] P. T. Gilbert, The corrosion of zinc and zinc-coated steel in hot waters, Pittsburgh International Conference on Surface Reactions, p. 21 (Corrosion Publishing Co., Pittsburgh, Pa., 1948).

[14] R. B. Hoxeng, Electrochemical behavior of zinc and steel in aqueous media—Part 2, Corrosion **6,** 308 (1950).

[15] Melvin Romanoff, National Bureau of Standards (unpublished).

WASHINGTON, January 8, 1954.

rnal of Research of the National Bureau of Standards Vol. 52, No. 5, May 1954 Research Paper 2500

Heat Capacity of Gaseous Perfluoropropane

Joseph F. Masi, Howard W. Flieger, Jr., and John S. Wicklund

An accurate flow calorimeter, previously described, has been used to measure the heat capacity of gaseous perfluoropropane (C_3F_8) at three pressures up to 1.5 atmospheres at each of the temperatures −30°, +10°, +50°, and +90° C. The results, believed accurate to 0.1 percent, have been extrapolated to zero pressure at each temperature, in order to obtain the ideal-gas heat capacity (C_p^o) and the pressure coefficient of heat capacity. Values of C_p^o are 31.10, 34.22, 37.02, and 39.49 calories mole^{-1} degree C^{-1}, respectively, at the four temperatures of measurement.

1. Introduction

Experimental gas heat capacities, obtained at several low pressures and over a range of temperatures, can be helpful in interpreting molecular structure and spectroscopic data and in studying equations of state at low pressure. The present investigation was undertaken as part of a comprehensive study of the thermodynamic and structural properties of fluorocarbons. The heat capacities of gaseous hexafluoroethane [1] and perfluorocyclobutane [2] have previously been reported.

2. Experimental Procedure

2.1. Material

A specially purified sample of perfluoropropane (C_3F_8) was very kindly furnished by the Minnesota Mining & Manufacturing Corp. The entire sample was evaporated in a closed system while surrounded with a mixture of carbon tetrachloride and chloroform, cooled with dry ice to about 2 deg below the normal boiling point of C_3F_8 (−38° C). The vapor was condensed in a trap at liquid-nitrogen temperature. During this distillation the system was continuously pumped with a high-vacuum apparatus. First and last portions (about 25 g each) of the distillate were discarded. There was obtained a sample of about 450 g for use in the experiments.

A mass-spectrograph analysis of the sample, performed after most of the heat-capacity data had been taken, showed only a trace (less than 0.1 percent) of CF_2Cl^+ and CF_2H^+ ions. A gravimetric determination of the amount of carbon dioxide and moisture present was made by passing the entire flow-calorimeter sample, as vapor, through tubes of Anhydrone and Ascarite. Absorption of less than 0.01 percent was obtained. It was indicated that impurities should affect the heat-capacity measurements by much less than 0.1 percent.

2.2. Apparatus and Method

The construction and operation of the flow calorimeter have been described in detail; [3] a résumé has also been published.[4]

[1] J. S. Wicklund, H. W. Flieger, Jr., and J. F. Masi, J. Research NBS 51, 91 (1953) RP2437.
[2] J. F. Masi, J. Am. Chem. Soc. 75, 5082 (1953).
[3] J. F. Masi and B. Petkof, J. Research NBS 48, 179 (1952) RP2303.
[4] J. F. Masi, J. Am. Chem. Soc. 74, 4738 (1952).

The heat capacity was determined at a number of different flow rates at each temperature and pressure, so that the effect of any residual heat leak could be eliminated by extrapolation to the zero of reciprocal rate. "Blank" determinations were made at several rates at each temperature and pressure to measure the amount of cooling, δT, experienced by the gas in passing through the calorimeter when no heat was applied. A total of 57 heat-capacity experiments and 67 blank experiments was made.

3. Results

The important data for all of the heat-capacity experiments are given in table 1. The values of heat capacity, C, (column 7) were calculated from the power, W; the flow rate, F; the rise in temperature, ΔT; and the temperature fall, δT, in the corresponding blank experiment, by the relation

$$C = \frac{W}{F(\Delta T + \delta T)}.$$

These have been corrected by the amounts in column 8 in order to bring all results to the nominal mean pressure, p_m, and mean temperature, T_m, to yield the values of "C_p (observed)" appearing in column 9.

The values of "C_p (observed)" were plotted against the reciprocal of flow rate, and straight lines were fitted by least squares. Typical plots are given in figure 1, which shows the results at 10° C. An analysis of variance, performed under the direction of W. J. Youden of the Bureau's Applied Mathematics Division, indicated that, for the data as a whole, the variation in slope of these lines was statistically significant. Consequently, the least-square intercepts have been retained in all cases as the desired value of heat capacity at each temperature and pressure, indicated as "extrapolated value" in table 1. The precision of the data is indicated by the value of σ, where $\sigma = \sqrt{\sum d^2/(n-1)}$, d is the deviation of each point from the appropriate line, and n is the number of experiments for each line. The average value of σ is equivalent to ±0.03 percent of the heat capacity.

Results are summarized in table 2, having been converted to calories mole^{-1} degree^{-1}. (The defined calorie, equal to 4.1840 j, is used here.) A slight correction has been made, where necessary, for the

TABLE 1. *Data on perfluoropropane*

Reciprocal of rate, P^{-1}	Mass of sample, m	Power, W	Pressure drop, Δp	Temperature rise, ΔT	Blank correction, δT	Heat capacity, C	Correction for T_m and p_m, ΔC	Heat capacity, C_p (observed)
				−30.00° C=243.16° K; 1.00 atm				
sec g^{-1}	*g*	*w*	*mm* Hg	° *K*	° *K*	*j g*$^{-1}$ *deg*$^{-1}$	*j g*$^{-1}$ *deg*$^{-1}$	*j g*$^{-1}$ *deg*$^{-1}$
9.1325	57.5097	0.753506	74.42	9.5427	0.1208	0.71210	+0.00038	0.71248
10.4708	71.9782	.612918	55.83	8.9149	.0933	.71243	+.00031	.71274
11.7710	65.1171	.615517	44.20	10.0930	.0757	.71250	+.00003	.71253
14.8430	88.1819	.491159	28.41	10.1797	.0517	.71254	−.00017	.71237
17.8982	46.0844	.413501	19.17	10.3433	.0367	.71300	−.00037	.71263
28.3768	44.6435	.248342	7.14	9.8719	.0150	.71278	−.00024	.71254
28.8342	38.2730	.247685	7.37	10.0048	.0162	.71268	−.00018	.71250
							Extrapolated value.....	0.71238
							σ.....	±0.00010
				0.67 atm				
9.2277	108.1488	0.750862	111.95	9.6622	0.1648	0.70506	+0.00043	0.70549
11.6910	104.6250	.614240	65.89	10.0704	.1036	.70583	−.00027	.70556
14.6602	43.3911	.491134	42.97	10.1400	.0733	.70498	−.00003	.70495
17.4329	50.1947	.411872	30.45	10.1267	.0567	.70508	−.00001	.70507
28.0026	41.4276	.247657	11.73	9.8091	.0318	.70471	−.00012	.70459
29.7293	38.4368	.248370	10.98	10.4511	.0305	.70446	−.00033	.70413
							Extrapolated value.....	0.70607
							σ.....	±0.00018
				0.33 atm				
12.0251	81.4694	0.614151	140.09	10.3706	0.1933	0.69910	−0.00018	0.69892
14.8191	62.4984	.491274	84.97	10.2924	.1287	.69861	−.00044	.69817
14.8249	58.9523	.489272	82.40	10.2445	.1254	.69947	−.00054	.69893
17.1889	55.1834	.412296	61.64	10.0468	.0987	.69857	−.00027	.69830
28.8417	30.3918	.246727	22.79	10.1415	.0425	.69874	−.00017	.69857
							Extrapolated value.....	0.69875
							σ.....	±0.00034
				+10.00° C=283.16° K; 1.50 atm				
7.6341	88.4219	0.964866	80.32	9.4063	0.0803	0.77645	+0.00060	0.77705
11.9426	63.3854	.616531	32.92	9.4435	.0345	.77685	+.00058	.77743
15.5622	38.0904	.494454	19.41	9.8831	.0226	.77680	+.00029	.77709
24.0445	39.9908	.328796	8.25	10.1606	.0150	.77693	+.00002	.77695
31.7895	32.1109	.247218	4.68	10.0937	.0133	.77758	+.00006	.77764
							Extrapolated value.....	0.77699
							σ.....	±0.00026
				1.00 atm				
7.8857	78.2654	0.963962	119.17	9.7483	0.1103	0.77106	+0.00043	0.77149
12.1578	44.1411	.616923	49.72	6.6800	.0489	.77094	+.00053	.77147
15.4957	51.0117	.493985	29.93	9.8900	.0270	.77187	+.00032	.77219
18.4080	47.5825	.414090	21.82	9.8584	.0194	.77169	+.00040	.77209
23.2923	43.5259	.328493	13.28	9.8988	.0131	.77194	+.00004	.77198
31.4505	35.7164	.247232	7.26	10.0655	.0094	.77178	+.00008	.77170
							Extrapolated value.....	0.77162
							σ.....	±0.00030
				0.50 atm				
9.5808	73.4262	0.617011	161.50	7.5868	0.1406	0.76500	+0.00186	0.76686
15.7018	41.9239	.493877	59.04	10.0547	.0580	.76683	−.00010	.76673
23.6735	38.3678	.329408	26.08	10.1422	.0269	.76686	−.00020	.76666
31.9499	33.6054	.246343	14.49	10.2447	.0175	.76695	−.00023	.76672
							Extrapolated value.....	0.76687
							σ.....	±0.00006

TABLE 1. *Data on perfluoropropane*—Continued

Reciprocal of rate, F^{-1}	Mass of sample, m	Power, W	Pressure drop, Δp	Temperature rise, ΔT	Blank correction, $(T$	Heat capacity, C	Correction for T_m and p_m, ΔC	Heat capacity, $C^\sim$ (observed)
				+50.00° C=323.16° K; 1.50 atm				
sec g^{-1}	*g*	*w*	*mm* Hg	° *K*	° *K*	*j g*$^{-1}$ *deg*$^{-1}$	*j g*$^{-1}$ *deg*$^{-1}$	*j g*$^{-1}$ *deg*$^{-1}$
8.3615	69.1872	0.973454	77.59	9.7307	0.0508	0.83214	+0.00034	0.83248
16.7869	52.7321	.481291	19.69	9.7010	.0146	.83159	+.00034	.83193
24.0516	28.5482	.345862	9.69	9.9928	.0076	.83211	+.00014	.83225
32.5992	22.6392	.243888	5.43	0.5597	.0045	.83128	+.00044	.83172
						Extrapolated value		0.83261
						σ		±0.00021
				1.00 atm				
8.5834	63.0260	0.973891	112.88	01.0070	0.0714	0.82943	+0.00008	0.82951
16.9441	27.7200	.481379	29.27	9.8184	.0209	.82897	+.00017	.82914
23.8000	33.9298	.345495	14.99	9.9039	.0125	.82921	+.00011	.82932
36.1370	35.5804	.244058	6.69	10.6325	.0070	.82894	−.00039	.82855
						Extrapolated value		0.82981
						σ		±0.00019
				0.50 atm				
12.1633	116.3520	0.687173	117.66	10.0371	0.0752	0.82654	+0.00011	0.82665
17.2428	82.3232	.481102	58.93	10.0040	.0407	.82586	+.00020	.82606
25.2559	31.9494	.345031	27.28	10.5514	.0205	.82570	−.00020	.82550
34.7789	21.7759	.243559	14.02	10.2411	.0114	.82621	−.00011	.82610
						Extrapolated value		0.82662
						σ		±0.00042
				+90.00° C=363.16° K; 1.50 atm				
8.2178	89.1452	1.088710	91.27	10.0689	0.0350	0.88548	+0.00015	0.88563
16.3840	56.9990	0.542204	23.18	10.0315	.0083	.88482	+.00009	.88491
23.8928	29.8241	.362959	11.04	9.8054	.0035	.88410	+.00024	.88434
35.7259	24.9024	.272077	5.53	10.9986	.0013	.88353	−.00048	.88305
						Extrapolated value		0.88644
						σ		±0.00009
				1.00 atm				
8.2735	79.4052	1.088739	137.93	10.1385	0.0563	0.88356	−0.00008	0.88348
17.0922	45.7350	0.542399	32.51	10.4810	.0108	.88362	−.00037	.88325
25.8957	40.1121	.363091	14.50	10.6396	.0028	.88349	−.00046	.88303
32.5131	24.8082	.272968	9.27	10.0527	.0006	.88290	−.00008	.88282
						Extrapolated value		0.88371
						σ		±0.00002
				0.50 atm				
11.8229	91.7568	0.768290	137.67	10.2451	0.0591	0.88152	−0.00022	0.88130
16.7215	61.3767	.540098	69.10	10.2177	.0303	.88127	−.00020	.88107
24.4192	34.9221	.362947	32.21	10.0491	.0094	.88113	−.00008	.88105
33.7577	28.0348	.272367	17.42	10.4279	.0055	.88125	−.00028	.88097
						Extrapolated value		0.88138
						σ		±0.00007

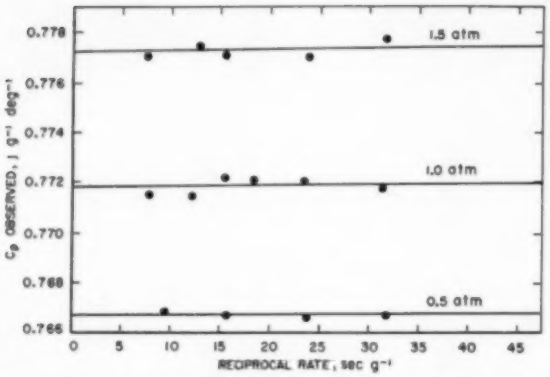

FIGURE 1. *Measured heat-capacity values for perfluoropropane at 10° C and three pressures.*

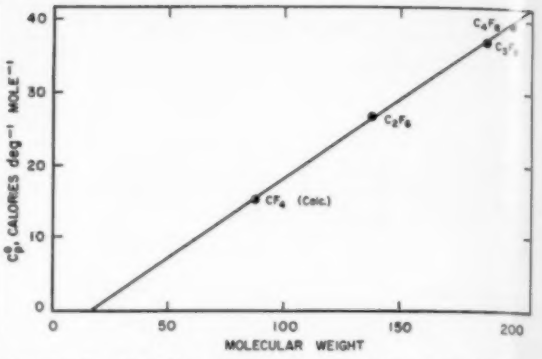

FIGURE 2. *Variation with molecular weight of the ideal-gas heat capacities at 50° C of four saturated fluorocarbons.*

effect of curvature of the heat capacity-temperature function. Values of the heat capacity of the ideal gas C_3F_8 were obtained by extrapolation of the results to zero pressure at each temperature of measurement, and are given as "C_p^0, observed" in table 2.

There has been no complete assignment of the vibration fundamentals of perfluoropropane, and consequently statistical calculation of the ideal-gas heat capacity cannot yet be made. Also, there are no density data available for C_3F_8 gas, so the values of the pressure coefficient of heat capacity, given in the last line of table 2, cannot yet be used in determining the constants of a low-pressure equation of state.

The experimental values of C_p^0 for hexafluoroethane (see footnote 1), perfluoropropane, and perfluorocyclobutane (see footnote 2), together with a calculated value [5] for carbon tetrafluoride, are compared at one temperature (50°) in figure 2 by plotting against molecular weight. Similar plots are obtained at other temperatures. It is seen that a nearly constant increment of heat capacity per mole (amounting to about 10.3 cal deg^{-1} $mole^{-1}$ at 25° C) may be indicated for each added CF_2 group, at least in the straight-chain series. In the case of paraffin hydrocarbons, constancy of heat-capacity increments per added CH_2 group occurs in the higher members of the series, beginning at about *n*-hexane.

TABLE 2. *Heat capacity of gaseous perfluoropropane* (C_3F_8)

Summary of results

Temperature, ° C	−30.00	+10.00	+50.00	+90.00
	Calories $mole^{-1}$ $degree^{-1}$			
C_p, 1.50 atm		34.93	37.42	39.84
1.00 atm	32.02	34.68	37.29	39.71
0.67 atm	31.73			
0.50 atm		34.45	37.15	39.61
0.33 atm	31.40			
C_p^0, observed	31.10	34.22	37.02	39.49
	Calories $mole^{-1}$ $degree^{-1}$ atm^{-1}			
$\Delta C_p/\Delta P$	0.93	0.47	0.27	0.23

[1] Rita M. Potocki and D. E. Mann (informal communication).

WASHINGTON, September 29, 1953.